DUDLEY KNOX LIBRARY
NAVAL POSTGRADUATE SCHOOL
MONTEREY CA 93943-5101

Modeling and Control of a Fish-Like Vehicle

by

Thomas Alan Trapp

B.S. Electrical Engineering, University of Wisconsin-Milwaukee, 1988

Submitted to the Departments of Ocean Engineering and Mechanical Engineering
in partial fulfillment of the requirements for the degrees of

Naval Engineer

and

Master of Science, Mechanical Engineering

at the

MASSACHUSETTS INSTITUTE OF TECHNOLOGY

June 1998

Modeling and Control of a Fish-Like Vehicle

by

Thomas Alan Trapp

Submitted to the Departments of Ocean Engineering and Mechanical Engineering
on May 22, 1998, in partial fulfillment of the
requirements for the degrees of
Naval Engineer
and
Master of Science, Mechanical Engineering

Abstract

To understand the extremely complex hydrodynamics of fish swimming, it is desirable to build a mechanical prototype. This allows better cooperation of the "vehicle" under study than would be allowed with a live specimen. Draper Laboratory has undertaken the design and construction of a free-swimming fish robot called the Vorticity Control Unmanned Undersea Vehicle (VCUUV), patterned and scaled after a yellowfin tuna. The mechanical and electronic design of the VCUUV is versatile to allow ready variation of swimming parameters. Tests can be performed that will reveal the importance of each swimming pattern and how it contributes to the potentially superior efficiency of fish propulsion and how, ultimately, this mode of propulsion can be adapted to man-made vehicles.

In this case of a mechanically complex and versatile robotic fish, a sophisticated control system algorithm is needed to ensure the motion closely approximates that of a live fish. Modeling and control of a hydrodynamic system is a difficult task, especially when the exact hydrodynamics have not yet been captured in a mathematical model. Based on some simplifying assumptions, a linear system model for the VCUUV is derived. Using state-space methods, a simulated controller is designed to govern this model. The ability of the controller to produce the desired system response is demonstrated, as well as robustness of the control algorithm in the presence of environmental disturbances and system model errors.

Thesis Supervisor: Jamie M. Anderson
Title: Senior Member Technical Staff, Charles Stark Draper Laboratory

Thesis Supervisor: Michael S. Triantafyllou
Title: Professor of Hydrodynamics and Ocean Engineering

Reader: David L. Trumper
Title: Rockwell International Professor of Mechanical Engineering

Acknowledgments

There is no doubt that the greatest contributor to this work was my wife, Karen, who has taken such good care of everything (including me) during my time of "concentration;" I thank her and I thank God for her. My dear children, Mimi, David, Michaela, Lydia and Sarah also deserve much credit for putting up with my short attention span while they have been about the best example of unconditional love I have ever seen on earth.

I would also like to thank Jamie Anderson, Michael Triantafyllou, and David Trumper for those things they have taught me. Thanks also to Peter Kerrebrock, the greatest engineer at Draper Lab, who never failed to give patient answers to all my dumb questions.

I owe much gratitude to my shipmates: Chris Levesque, Kurt Crake, Tom Laverghetta, Casey Moton, Allan Andrew and Mark Welsh. It's been a privilege to work with them and I know full well they had a big part in helping me through this place.

And to the guys I have spent the last $1\frac{1}{2}$ years with in the Robot Lab, and some not so long; Alan DiPietro, Joseph Paul Marquardt, Mohan Gurunathan, Will McFarland, ENS Ryan Norris, Mark Little, Bill Kaliardos, Jonah Peskin, Chris Gadda, John Hoctor, Jamie Cho, and others...let's go for a dunk in the tank!

To my church: Pastor John Saxton, Kate Saxton, Kim Desjardin and Steph Rogers: thanks for all your support and prayers.

And my parents, Tom and Karen Trapp, who "always knew I could do it."

Overall credit for anything insightful (if anything) in this thesis belongs to God who, according to the Bible, created all things and, from time to time for His glory, allows us to catch a tiny glimpse into the mechanisms of the universe. If my MIT degree or even this thesis (though doubtful) should bring me any honor, I will accept, but only temporarily, as some day I will lay it at the feet of Jesus Christ.

> But as it is written, Eye hath not seen, nor ear heard, neither have entered into the heart of man, the things which God hath prepared for them that love him. (1 Corinthians 2:9)

Contents

1 Introduction **12**

1.1 Background 12

1.2 Thesis Motivation and Goal 16

1.3 Mechanical Summary 17

1.4 Hydrodynamic Summary 19

2 System Modeling **22**

2.1 Approach to Model Derivation 22

2.2 Tail Free-Flood Dynamics Model 25

2.3 Hydrodynamics Model 35

2.3.1 Lighthill's Theory Applied to a Swimming Fish 36

2.3.2 Lighthill's Theory Applied to the Tail System 38

2.4 Hydraulic Plant Model 42

2.5 Conclusions 51

3 Controller Design **60**

3.1 Approach 60

3.2 LQR Feedback Control 62

3.3 Cost Function 63

3.4 Development of the State Space System 64
3.5 LQR Approach 68
3.6 "Computed Torque" Approach 76
3.6.1 Disturbance and Noise Rejection 84
3.6.2 Model Error Sensitivity 92

4 Conclusions **101**

4.1 Controller Performance and Robustness 101
4.2 Summary 102
4.3 Future Work 102

A Development of Dynamics Equations in Maple V **104**

A.1 Define the Linear Jacobian Matrices 104
A.2 Define the Angular Jacobian Matrices 105
A.3 Construct the H Matrix: Inertia Tensor 105
A.4 Construct the h Matrix: Centrifugal and Coriolis Effects 107

B Lighthill EBT Derivation in Maple V **111**

B.1 Define the Arrays. 111
B.2 Define the Geometry of the Linkage. 111
B.3 Displacement of Links 1 Through 4. 112
B.4 Torque for Link 1 115
B.5 Torque for Link 2 117
B.6 Torque for Link 3 118
B.7 Torque for Link 4. 120

C VCUUV Hydraulic Propulsion Plant Simulation 122

C.1 Introduction 122

C.2 Component Selection 122

C.3 Development of the Model 123

C.4 Development of the System 127

C.5 Conclusions 132

List of Figures

1-1 Vorticity Control Unmanned Undersea Vehicle (VCUUV) 14

1-2 Modes of swimming in fishes: (a) "angulliform"; (b) "carangiform"; (c) "thunniform" (From *Life in Moving Fluids*, Vogel [14]) 19

1-3 Profile View of a Carangiform Swimmer (Skipjack Tuna) 21

2-1 General Carangiform Swimming Motion 23

2-2 Motion of Tail Over One Period, T (Vectors Represent Instantaneous Velocity). Parameters used from Table 2.1 26

2-3 System Model Derivation Approach 27

2-4 VCUUV Tail Linkage Assembly 30

2-5 VCUUV Tail Mass Ascribed to Each Link 32

2-6 Lighthill EBT Theory Applied to a Swimming Fish 37

2-7 Lighthill EBT Theory Applied to the VCUUV Linkage 39

2-8 Hydrodynamic Torques on the Caudal Fin 41

2-9 VCUUV Hydraulic Plant Schematic 43

2-10 VCUUV Tail Linkage Assembly With Dimensions 44

2-11 Piston Linear, s, and Link Angular, q, Position 48

2-12 Piston Linear, ds/dt, and Link Angular, dq/dt, Velocity 49

2-13 Servovalve Schematic (HR Textron) 50

2-14 Relative Joint Angles During Swimming Cycle (swimming parameters from Table 2.1) 52
2-15 Torque Outputs From the Lagrange Nonlinear Model, ("A" in Figure 2-3), Top and From the Linearized Model ("B" in Figure 2-3), Bottom 54
2-16 Torque Outputs Due to Nonlinear Corioulis and Centrifugal Forces . 55
2-17 Torque Outputs From the Lighthill Continuous EBT Model ("C" in Figure 2-3), Top and From the Lighthill Discrete EBT Model ("D" in Figure 2-3), Bottom 56
2-18 Torque Outputs From the Full Nonlinear VCUUV System Model ("E" in Figure 2-3), Top and From the Linearized VCUUV System Model ("F" in Figure 2-3), Bottom 57

3-1 Controller With Integrator 66
3-2 Response of Linkage to a Step Input of 0.1 Radians to Link #1. . . . 70
3-3 Actual Position Plotted With Desired Position For the Initial LQR Control Design 71
3-4 Actual Velocity Plotted With Desired Velocity For the LQR Control Method 72
3-5 Control Effort Signal For the Initial LQR Control Design 74
3-6 Position and Velocity Errors For the Initial LQR Control Design . . . 75
3-7 Computed Torque Controller Design 78
3-8 Desired and Actual Positions of Links 1-4 for Computed Torque Controller 80
3-9 Desired and Actual Velocities of Links 1-4 for Computed Torque Controller 81

3-10 Position and Velocity Errors for the Computed Torque Controller . . 82
3-11 Control Efforts for Computed Torque Controller 83
3-12 Noise Applied to Position Sensor and Velocity Sensor 85
3-13 Input Disturbance Applied to Computed Torque Control System . . . 86
3-14 Desired and Actual Positions of Links in the Presence of Noise and Input Disturbance 87
3-15 Desired and Actual Velocities of Links in the Presence of Noise and Input Disturbance 88
3-16 Position and Velocity Errors of the System in the Presence of Noise and Input Disturbance 89
3-17 Proportional and Derivative Control Effort Signals in the Presence of Noise and Input Disturbances 90
3-18 Total Control Effort Signal in the Presence of Noise and Input Disturbances 91
3-19 Noise Applied to the Position Sensor, top, and Velocity Sensor, bottom 92
3-20 Desired and Actual Positions of Links in the Presence of Increased Noise 93
3-21 Desired and Actual Velocities of Links in the Presence of Increased Noise 94
3-22 Desired and Actual Positions of Links in the Presence of 25% Overestimation of Model Dynamic Parameters 95
3-23 Desired and Actual Positions of Links in the Presence of 25% Overestimation of Model Dynamic Parameters 96
3-24 Position and Velocity Errors of Links in the Presence of 25% Overestimation of Model Dynamic Parameters 97

3-25 Desired and Actual Positions of Links in the Presence of 25% Underestimation of Model Dynamic Parameters 98

3-26 Desired and Actual Positions of Links in the Presence of 25% Underestimation of Model Dynamic Parameters 99

3-27 Position and Velocity Errors of Links in the Presence of 25% Underestimation of Model Dynamic Parameters 100

C-1 Piston Displacement And Velocity 125

C-2 Pressure Drop Across Servovalve and Piston 126

C-3 Fluid Flow And Servovalve Current 128

C-4 Piston Force And Joint Moment 129

C-5 Total System Power And Efficiency 130

C-6 Total Flowrate and Total Servovalve Current 131

List of Tables

2.1 Optimal Swimming Parameters Derived by Barrett [2] 24

2.2 Parameters of the VCUUV Tail Free-Flood Water Ascribed to Each Link 32

2.3 Linkage Dimensions From Figure 2-10 43

C.1 Hydraulic Plant Concept Component Summary 123

C.2 Hydraulic Plant Final Summary 133

Chapter 1

Introduction

1.1 Background

Almost 30 years ago, M.J. Lighthill published a study of the superior hydrodynamic efficiency of aquatic animal propulsion [9]. Since that time, there has been a growing effort to capture the benefits of fish-like modes of propulsion for use in man-made vehicles. Most recently, the effort has intensified with the achievement of a robotic fish ("RoboTuna") at MIT by M. S. Triantafyllou, et al [12]. It is generally undisputed that the fish-like propulsive motion is possibly superior in efficiency relative to propellers, yet it has not been attempted in the design of large scale submersible vehicles. In fact, modern submarine design has focused on reducing the disturbance of the flow around the hull, whereas fish create large disturbances in the water. This incredible, unintuitive design demands our attention and makes the study of fish-like propulsion very interesting and worthwhile studying. If the essence of the propulsive motion that achieves this high efficiency in fish can be captured and understood, then it can be implemented in vehicles such as manned and unmanned submarines or even surface ships. There is a growing need for higher efficiency, longer range ocean-going vessels.

In order to study the motion of fish in a scientific scientific, where variables in the swimming motion can be controlled, it is necessary that a fish-like robot be built. This way, the motions essential to efficient propulsion can be isolated and their effects understood. Building a robot for the study also demonstrates that the swimming motion can be implemented in a man-made vehicle. Simulating the motion of a fish requires a sophisticated mechanical design and control system algorithm.

The Vorticity Control Unmanned Undersea Vehicle (VCUUV) Project at Draper Laboratory is attempting to find answers to the questions raised about the superior performance of "fish-like," or biological propulsion. An eight-foot autonomous mechanical yellowfin tuna has been designed and constructed for testing. The following thesis describes the system modeling and controller design for the VCUUV. A picture of the VCUUV is shown in Figure 1-1. Due to the complex nature of the mechanical system, the thesis focuses on developing a linear system model using robot dynamics derivation and then adding nonlinear effects in a logical manner to the model while in simulation. The simulation method is Simulink, in which I also implemented my control algorithm. The control algorithm was derived using state space methods. The general approach that I used to complete my thesis is the following:

- Developed a linear system model of the robot fish based on physical data, dynamics analysis and engineering assumptions.
- Implemented the model in Simulink.
- Used state space and nonlinear methods to design a controller.
- Implemented the controller in the Simulink model.
- Modeled and include significant nonlinear effects such as friction, deadband and

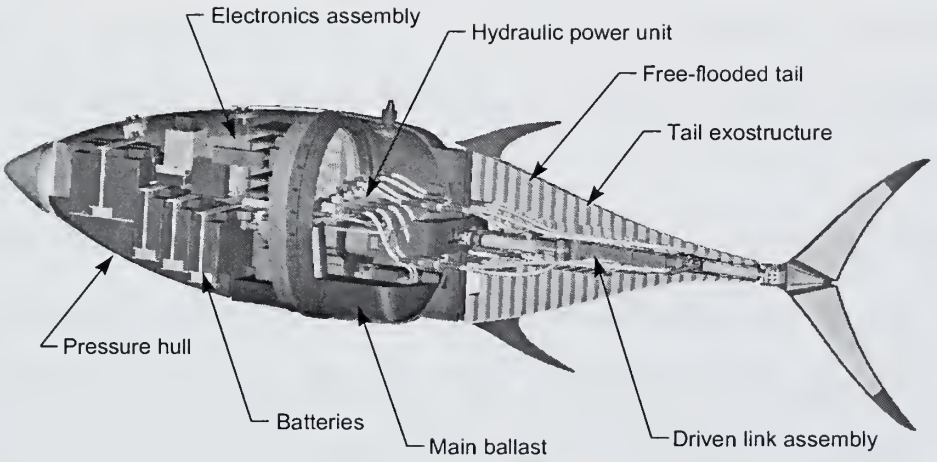

Figure 1-1: Vorticity Control Unmanned Undersea Vehicle (VCUUV)

actuator saturation.

- Tested the controller for robustness by varying model parameters.
- Optimized the controller.
- Described a method to implement the controller.

In order to implement a control system, it is useful to develop a system model in the form of equations of motion (i.e., inertia, spring, damping and input forces). I developed my model by defining the dynamics of the tail portion of the VCUUV as a hydraulically powered robot arm [3, 8]. The model includes my estimates, using Lighthill's Elongated Body Theory (EBT) [9], of the inertia due to the added mass, and the damping and spring forces.

I used a state space approach for the controller design. The format of the first controller design attempt is a linear quadratic regulator (LQR). "Linear", because the system is linearized, "quadratic" due to the quadratic cost function used for optimization, and "regulator" since the system is set up to regulate to a reference input. The quadratic cost function is discussed in Section 3.3. The cost function is an optimization tool for developing a controller that best meets the design specifications. The second design attempt is a "computed torque" controller which uses the same state space system model, but a different approach altogether. The input torques are calculated from the state space system equations and input directly into the system while position and velocity errors are used for feedback. The controller commands joint positions to mimic the configuration of the tail at each swimming instant. The objective is simply to match the biological fish's swimming motion and produce an accurate trajectory whenever swimming parameters are changed for testing. Vehi-

cle heading control will be left to a next-generation controller due to the extremely complex relationship between the tail motion and the heading.

1.2 Thesis Motivation and Goal

The motivation for this thesis comes from the now widespread desire to unlock the secrets of biologic propulsion, namely the mechanisms by which fish can swim so fast, both in spurts and for distances with relatively small power input. In his famous study, Sir James Gray determined that the power density of a dolphin's muscles would have to be seven times that of measured land mammals' muscles in order to explain the superior efficiency of an assumed "dead body" drag resistance for the swimming dolphin (commonly referred to as "Gray's Paradox") [7]. Due to the unlikelihood of such superior muscle power density, it is hypothesized that the swimming action is responsible for a significant drag reduction. As will be explained later in Section 1.4, the majority of body motion of a swimming carangiform , under which category the tuna falls, is in the aft $\frac{1}{2}$ to $\frac{2}{3}$ of the fish. Therefore, the VCUUV was designed with the linkages in the aft $\frac{1}{2}$ of the body, and the system model of the propulsion system addressed in this thesis deals with the activated portion of the fish - the tail linkage, which is shown in Figure 2.2.

My goal in this thesis is to explain the derivation of the system model, asssumptions and simplification in a manner that will aid future work in the area of fish-like propulsion and control of multiple degree-of-freedom systems. I will also demonstrate the use of several computer programs that are useful in this work.

1.3 Mechanical Summary

The vehicle design is approximately 2.4m (8ft) in length, scaled and modeled after an actual yellowfin tuna. In order to closely approximate the curve followed by the spine of the biological fish as the tail undulates, it was determined that three joints would be required, plus an independent caudal fin. The linkage is shown in Figure 2.2. The tail spine is an upper and lower support made of G-10 fiberglass. The G-10 spine is able to help support, along with the pin joints, the large weight of the tail structure, but flexes in the yaw plane to allow the undulatory swimming motion. The tail joints are powered by servovalve controlled hydraulic pistons, and a hydraulic power unit consisting of a DC motor powering a hydraulic pump is employed. The tail has a number of "ribs" connected to the spine, each made of a sturdy PVC foam. Fiberglass "scales" are attached to the ribs to keep the nylon outer "skin" from collapsing between ribs, which would cause flow-disturbing pockets on the tail surface. The body forward of the tail is a pressure hull made of carbon fiber, which houses the electronics, inertial measurement unit (IMU) and the hydraulic power plant in a dry environment. The major components that make up the VCUUV are:

- Composite Pressure Hull
  - Hydraulic Power Unit (HPU)
  - Computer
  - Lead-Acid batteries
  - Inertial Measurement Unit (IMU)
- Tail Mechanical Linkage
  - Three Aluminum Links
  - Composite Caudal Fin

Hydraulic Power Pistons

Bridge-attaches tail linkage to pressure hull

- Tail Exostructure

  G-10 flexible spine

  Ribs

  Scales

  Neoprene Skin

The tail linkage is made up of three aluminum links and the caudal fin making a four degree-of-freedom robot arm. The aluminum links attach as a unit to the VCUUV pressure hull by a rigid connector called the "bridge." Power to the tail links is supplied by hydraulic pistons as shown in Figure 2.2. To move the fish tail "envelope" while maintaining it's correct shape, ribs surround the tail linkage and attach to the thin G-10 fiberglass (upper and lower) "spine." The G-10 fiberglass supports most of the weight of the tail system when the VCUUV is out of water, but while submerged, the structure, including the linkage and actuators, is nearly neutrally bouyant. This is due to the low density PVC foam used for the ribs. Finally, the rib structure attaches to the tail linkage at four points to transfer the force from the linkage to the ribs, the skin, and ultimately to the water.

For the purposes of feedback control, sensors that have been included in the design or that were present in commercial systems are: DC motor speed, hydraulic system pressure, joint angular position and speed, and leak detection. Additionally, load cells have been incorporated in the design to gather propulsion efficiency data for analysis.

The tail mechanical system must be modeled due to the inertial forces the actuators must overcome to properly position the tail linkage. The inertial forces are mainly due to the free-flood mass of water contained within the tail exostructure. To be

used in a state-space control system, the final mechanical linkage dynamics model must be both linear and a function of the state variables and torque inputs. First, a Lagrangian dynamics approach [1] was used to develop the equations of motion for the four link system. Then, following several simplifying assumptions, the model was linearized and the results were compared to determine if the assumptions were acceptable. The derivation is explained in Section 2.2.

1.4 Hydrodynamic Summary

The approach taken for hydrodynamics in the system model was a discretized version of Lighthill's Elongated Body Theory (EBT) [9]. C.M. Breder [4] describes three different types of biological swimming motions, categorized by the relative length of the portion of the body involved in the undulatory motion. The basic types are *anguilliform*, *carangiform* and *thunniform*, in order of decreasing fraction of body in motion (illustrated in Figure 1-2).

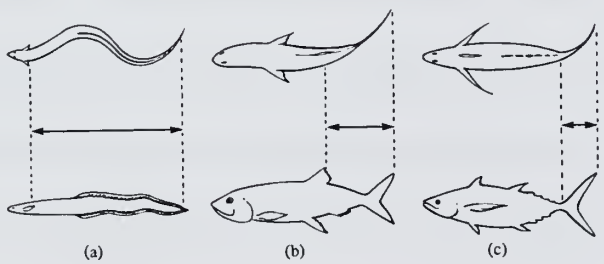

Figure 1-2: Modes of swimming in fishes: (a) "angulliform"; (b) "carangiform"; (c) "thunniform" (From *Life in Moving Fluids*, Vogel [14])

Anguilliform, or eel-like motion involves almost the entire body length in the propulsion, carangiform, about half the body length, and thunniform one-third or less. The VCUUV most closely resembles the carangiform since approximately half of the body is involved in the undulatory motion. The VCUUV may, however, be optionally operated as thunniform as it is really a subset of carangiform motion. It should be noted that most live tuna more closely resemble the thunniform mode. The mode of swimming assumed is important in the development of my system model only to the extent that Lighthill's assumptions will be either obeyed or violated, which I explain further in Section 2.3.

Lighthill refers to the very elegant design of the carangiform swimming body [9]. Refer to Figure 1-3. This swimming mode and body form work closely together to produce extremely efficient propulsion. Although the complete hydrodynamic mechanism is not completely understood, three well recognized hydrodynamic characteristics can be summarized here:

1. A carangiform has a deep, massive anterior. The inertia of the forebody plus its added mass prevent excessive yawing motion while the tail undulates.

2. The posterior decreases dramatically in depth toward the caudal fin in order to reduce inertia the tail must overcome as undulatory amplitude increases. Immediately before the caudal fin, the depth of the body reaches a minimum.

3. The tall lunate caudal fin extends into the body wake and may react with vortex sheets shed from the body to recapture wake momentum and produce propulsion "jets."

To be used in a state-space control system, the final hydrodynamic model must be

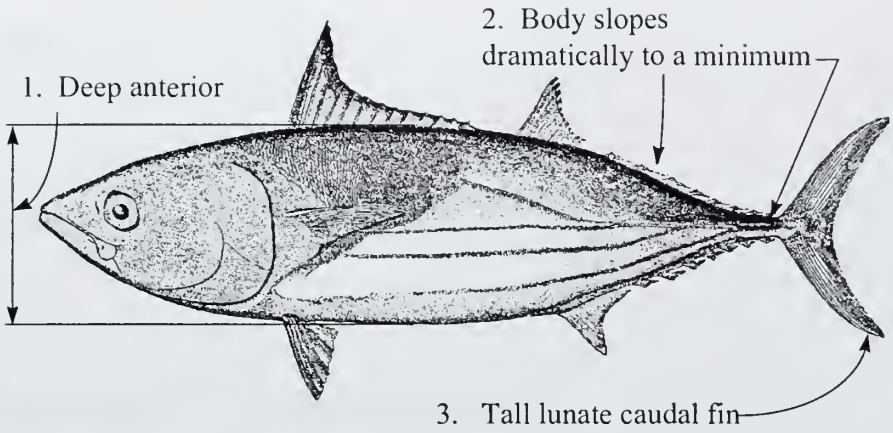

Figure 1-3: Profile View of a Carangiform Swimmer (Skipjack Tuna)

both linear and a function of the state variables and torque inputs. First, Lighthill's EBT was used to estimate the torques on each joint during swimming motion. This model was not in a form that was compatible with linearization, nor was it a function of the state variables. The purpose of developing this model was to use it to compare torques with a linearized model of the tail system, which was developed separately using a discrete application of Lighthill's EBT [9]. The derivation is explained in Section 2.3.2.

Chapter 2

System Modeling

2.1 Approach to Model Derivation

In general, the spine displacement, $y(x,t)$ from a neutral (straight-body) position of a carangiform swimmer can be described by the following equation given by Barrett [2]:

$$y(x,t) = a(x)sin(kx - \omega t) \tag{2.1}$$

as shown in Figure 2-1, where $a(x)$ is given by:

$$a(x) = c_1 x + c_2 x^2 \tag{2.2}$$

The caudal fin motion is extremely important, as it has been theorized that most of the thrust is produced by it. The angular motion of the caudal fin has a special phase relationship with the body motion described by:

$$\theta_{tail}(t) = \theta_0 sin(\omega t + \phi) \tag{2.3}$$

David Barrett derived self-propelled optimal values for "RoboTuna" at MIT [2] for the kinematic variables in the above equations. The values are listed in Table 2.1. Using

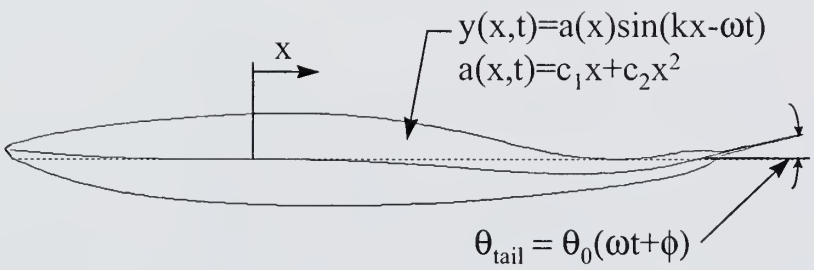

Figure 2-1: General Carangiform Swimming Motion

Variable	Description	Value
U	Swimming Speed (Body Lengths/Second)	0.65
St	Strouhal Number: $\frac{f\,A_{TIP}}{U}$	0.156
$\mathbf{A}_{TIP}$	Peak-to-Peak Amplitude of Caudal Fin Tip (Body Lengths)	0.115
α	Maximum Angle of Attack of Caudal Fin	16.2°
ϕ	Phase of Caudal Fin Motion With Respect to Body Motion	$75 - 95°$
λ	Propulsive Wavelength (Body Lengths)	1.27
$\mathbf{c_1}$	Coefficient of Linear Term	.00372
$\mathbf{c_2}$	Coefficient of Quadratic Term	.002

Table 2.1: Optimal Swimming Parameters Derived by Barrett [2]

the parameters given in Table 2.1, the motion of the VCUUV tail over one period is shown in Figure 2-2. My approach to developing a linearized dynamic model of the VCUUV tail system was to first derive the full nonlinear model, then linearize it and compare the results to see if the difference between them was negligible. The two major sections of my model are:

1. **Lagrangian Dynamics Model**: The dynamics due to inertia of the free-flood water entrained in the VCUUV tail exostructure.

2. **Lighthill Hydrodynamics Model**: The dynamics due to hydrodynamic forces on the exterior of the VCUUV tail exostructure.

Figure 2-3 summarizes my approach.

2.2 Tail Free-Flood Dynamics Model

The dynamics of any rigid body can be completely described by the translation of the centroid and the rotation of the body about its centroid. The dynamics equations for the four link system described in Section 1.3 are derived by defining the inertia torques of each link and the reaction torques from the connecting links. This leads to the ability to derive the actuator torques necessary to produce the tail motion that is desired. The links are interdependent in two major respects:

- The torque produced on or by a link produces a reaction torque on the other links.

- The motion of the links changes the shape of the linkage, which changes the inertia seen by previous links (links closer to the bridge).

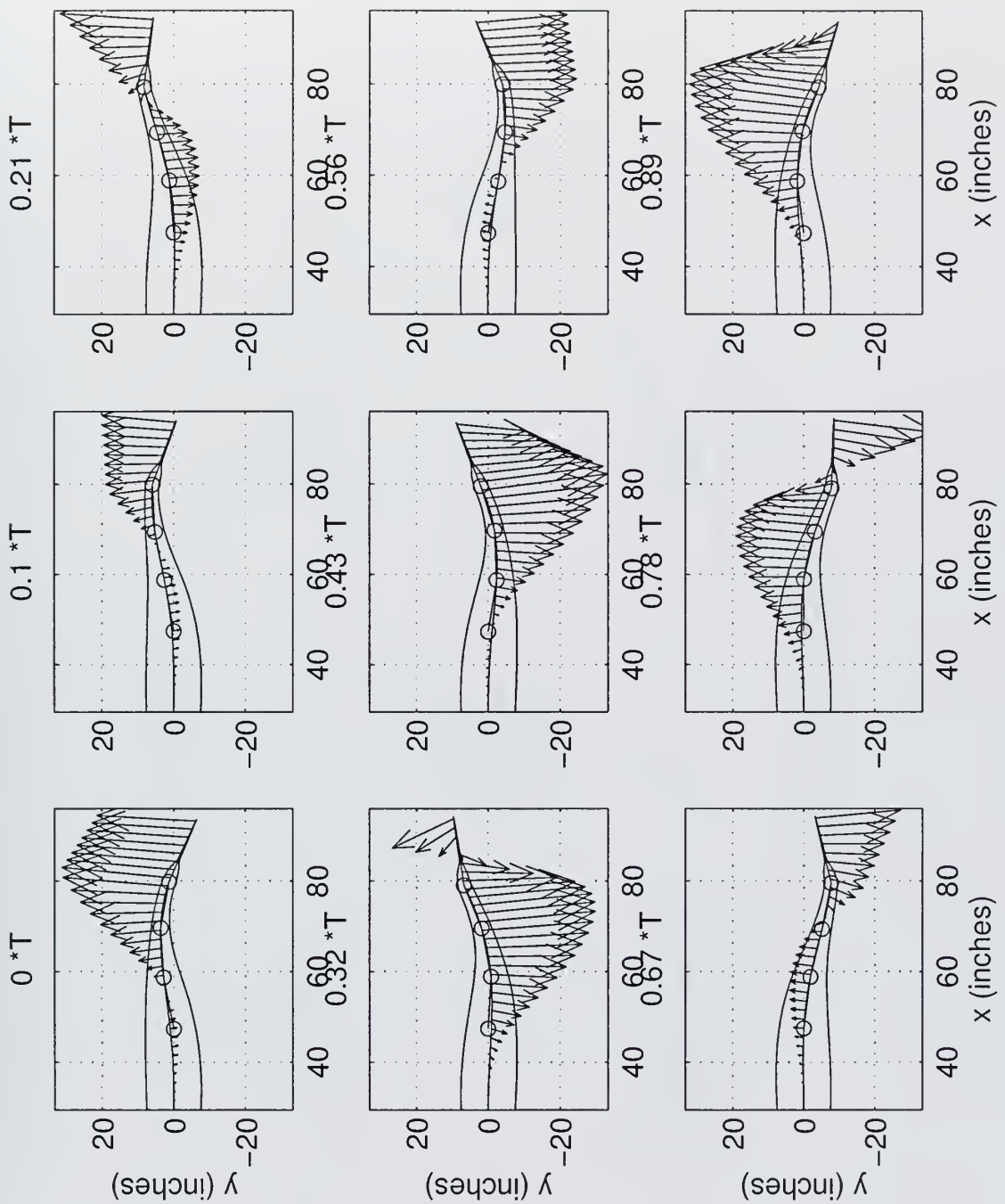

Figure 2-2: Motion of Tail Over One Period, T (Vectors Represent Instantaneous Velocity). Parameters used from Table 2.1

Figure 2-3: System Model Derivation Approach

Therefore, the result for the four link system is a rather complicated interdependent set of dynamics equations. There are two basic approaches to deriving the dynamics equations, the Newton-Euler and the Lagrangian approach, each having its advantages and disadvantages listed below:

Method	Advantages	Disadvantages
Newton-Euler	Uses intuitive concepts of torque balance and free-body diagram	Resultant set of equations not in "closed form"
Lagrangian	Resultant set of equations in "closed form"	Energy method approach not as intuitive as Newton-Euler

In the Newton-Euler formulation, a "free-body" approach is taken in the classical dynamics sense where the linkage is conceptually disassembled and torques are balanced about each joint pivot, taking into account the torques caused by inertia, centrifugal and Coriolis forces. External forces such as reactions from other joints, gravity, and actuator forces are also accounted for. The resultant intermediate equations are not in a useful form, however, as they do not involve the actuator torques explicitly, but instead contain the forces of constraint between joints. These must be eliminated by back-substitution to arrive at the useful form called the "closed form" dynamics equations.

Due to the shortcomings in this case for the Newton-Euler approach, the Lagrangian approach was used according to Asada and Slotine [1]. The Lagrangian approach to dynamics involves energy methods; namely, the system is first described by the work and energy stored therein. Deriving the work and energy of the system as

a whole is a relatively simple undertaking and although the dynamics equations are still complicated, the closed form dynamics equations are quickly produced without having to back-substitute to eliminate the constraint forces.

Figure 2-4 is a schematic of the VCUUV tail linkage, showing the relative angular displacement between each link, q_i and the length of each link, l_i. These parameters, along with those of the free-flood water parameters in Table 2.1 will be used in the system model derivation. The state variables in the system are the angular positions and velocities of each link relative to the previous link. In terms of the global variable (θi):

$$\theta_1 = q_1; \theta_2 = q_1 + q_2; \theta_3 = q_1 + q_2 + q_3; \theta_4 = q_1 + q_2 + q_3 + q_4 \tag{2.4}$$

The purpose of the derivation of the dynamics equations is to obtain a system model that can be used to design a controller in computer simulation, leading to control of the actual VCUUV prototype. The first hurdle to overcome was modeling the inertia of the mass of water within the skin and tail exostructure, and also the inertia of the caudal fin, which is not free-flood. The second hurdle to overcome was modeling the hydrodynamics of the surrounding water as the tail moves in an undulatory motion. The first part is addressed here and the second part is addressed in Section 2.3.2.

To derive the dynamics of the water entrained in the tail free-flood volume, the general form of the VCUUV tail dynamics equations must be derived. Then, the mass and moment of inertia of specific sections of the tail can be ascribed to each link. There are two major assumptions that have gone into this derivation:

- The section of the tail surrounding each link moves rigidly with its corresponding

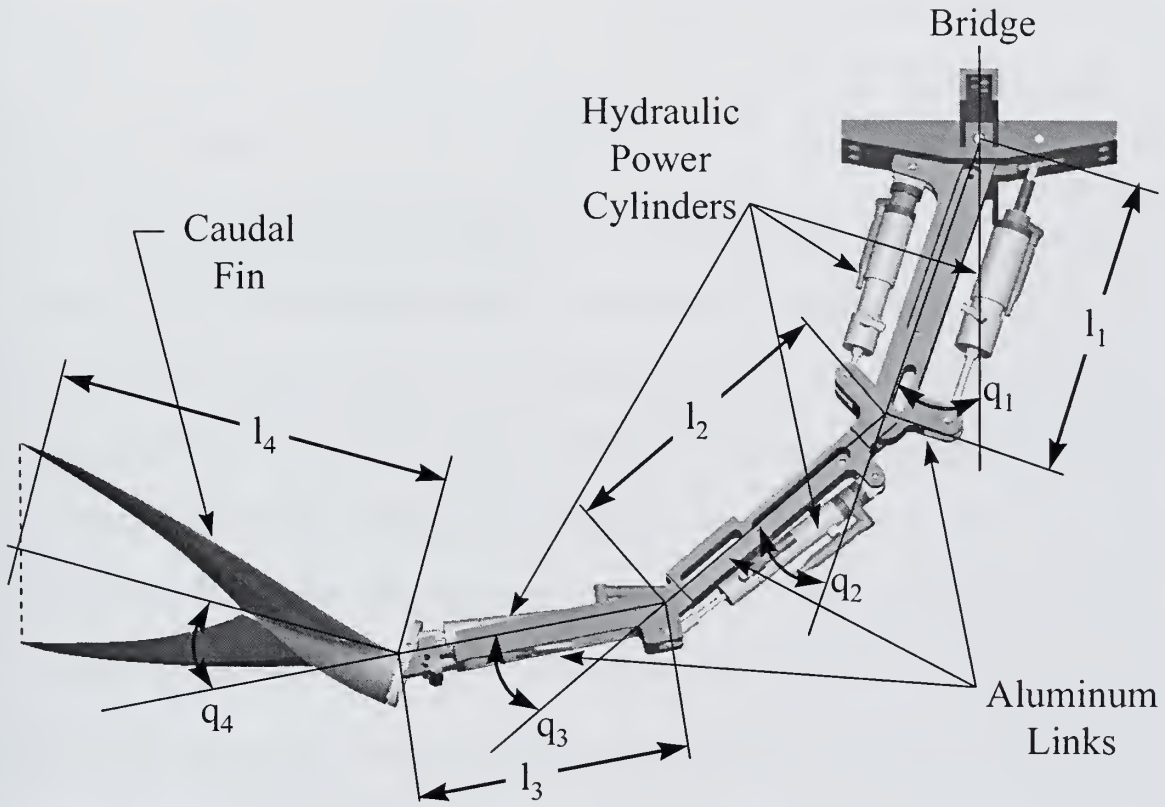

Figure 2-4: VCUUV Tail Linkage Assembly

link and the effect of any curvature of the spine on the dynamics is negligible.

In the initial design stages of the VCUUV, three links were determined to closely approximate the ideal curvature of the spine, so the very slight deviation from ideal can be neglected. Also, slight curvature of the tail sections will have no effect on the mass of those sections and very little effect on the moment-of-inertia with respect to each joint pivot.

- For the purposes of mass and moment-of-inertia calculations, the tail free-flood water, actuators, rib structure, and spine mass can be lumped, thus approximating the entire tail volume as water mass.

  Since the VCUUV was designed for neutral bouancy and zero trim, the complete tail assembly is essentially the same density as water. The tail actuators are relatively small, but quite a bit denser than water, while the rib structures are quite large and slightly bouyant. Overall, the tail is neutrally bouyant and the mass is relatively homogeneous; therefore, the mass can be lumped. Also, circulation flows inside the tail structure, if any, will have a net force on the linkage of approximately zero and will be damped considerably by the internals.

The masses, moments of inertia and centroid distances were derived by a numerical calculation using the VCUUV hull envelope data. Figure 2-5 illustrates the four sections of the tail that are ascribed to each of the four links. The values for each parameter of the tail linkage are listed in Table 2.2.

To derive the Lagrangian dynamics equations, the geometry of the linkage must be defined by the Jacobian relationships. The linear velocities of the centroids of each link in the global reference frame (the stationary reference frame attached to the

[1] Inertia is taken about a vertical axis at the centroid of each link

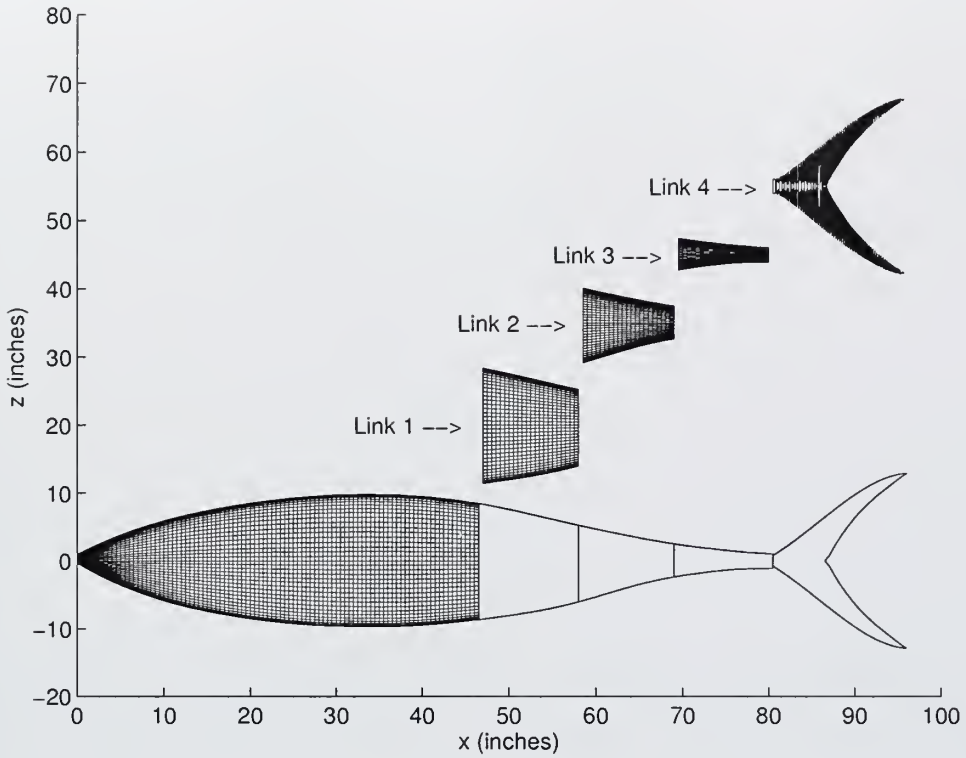

Figure 2-5: VCUUV Tail Mass Ascribed to Each Link

	Link 1	**Link 2**	**Link 3**	**Link 4**
Mass, m (lbm)	58.6	18.2	4.32	1.69
Inertia[1], (I_c lbm ·in^2)	787	185	44.0	8.00
Length, L (in)	11.45	11.20	10.33	15.50
Centroid, L_c (in)	5.01	4.18	4.47	4.72

Table 2.2: Parameters of the VCUUV Tail Free-Flood Water Ascribed to Each Link

bridge) can be described by the linear Jacobian relationship shown in the following equations:

$$\mathbf{v}_{c1} = \mathbf{J}_L^{(1)}\dot{\mathbf{q}} \tag{2.5}$$

$$\mathbf{v}_{c2} = \mathbf{J}_L^{(2)}\dot{\mathbf{q}} \tag{2.6}$$

$$\mathbf{v}_{c3} = \mathbf{J}_L^{(3)}\dot{\mathbf{q}} \tag{2.7}$$

$$\mathbf{v}_{c4} = \mathbf{J}_L^{(4)}\dot{\mathbf{q}} \tag{2.8}$$

Where $\mathbf{J}_L^{(1)}$, $\mathbf{J}_L^{(2)}$, $\mathbf{J}_L^{(3)}$, and $\mathbf{J}_L^{(4)}$ are defined in Appendix A. The somewhat complex derivation of these matrices is confined to Appendix A for the reader's convenience.

Likewise, the angular velocities of each link in the global reference frame are simply:

$$\omega_1 = \mathbf{J}_A^{(1)}\dot{\mathbf{q}} \tag{2.9}$$

$$\omega_2 = \mathbf{J}_A^{(2)}\dot{\mathbf{q}} \tag{2.10}$$

$$\omega_3 = \mathbf{J}_A^{(3)}\dot{\mathbf{q}} \tag{2.11}$$

$$\omega_4 = \mathbf{J}_A^{(4)}\dot{\mathbf{q}} \tag{2.12}$$

Appendix A also defines $\mathbf{J}_A^{(1)}$, $\mathbf{J}_A^{(2)}$, $\mathbf{J}_A^{(3)}$, and $\mathbf{J}_A^{(4)}$.

The above Jacobian relationships simply describe the velocity (either linear or angular) of each link with respect to the global reference frame as a function of the relative (local) angular velocities ($\dot{\mathbf{q}}_i$) of the other links.

With the linear and angular velocity relationships of the links now derived, the energy stored in each link in the form of translational kinetic ($\frac{1}{2}\mathbf{m}\dot{\mathbf{q}}^T\mathbf{J}_L^T\mathbf{J}_L\dot{\mathbf{q}}$) and rotational kinetic ($\frac{1}{2}\dot{\mathbf{q}}^T\mathbf{J}_A^T\mathbf{I}\mathbf{J}_A\dot{\mathbf{q}}$) to determine the total energy of the four arm linkage:

$$T = \frac{1}{2}\sum_{i=1}^{4}\left(m_i\dot{\mathbf{q}}^T\mathbf{J}_L^{(i)T}\mathbf{J}_L^{(i)}\dot{\mathbf{q}} + \dot{\mathbf{q}}^T\mathbf{J}_A^{(i)T}I_i\mathbf{J}_A^{(i)}\dot{\mathbf{q}}\right) \tag{2.13}$$

From the total energy equation, the inertia tensor 4 x 4 matrix can be extracted by removing the $\frac{1}{2}\dot{\mathbf{q}}^T\dot{\mathbf{q}}$ from the elements, leaving only the inertia:

$$H = \sum_{i=1}^{4}\left(m_i\mathbf{J}_L^{(i)T}\mathbf{J}_L^{(i)} + \mathbf{J}_A^{(i)T}I_i\mathbf{J}_A^{(i)}\right) \tag{2.14}$$

The Jacobian matrices in the formula account for the change in the moment of inertia the linkage experiences as it changes shape (i.e. as $\mathbf{q}$ changes).

The Coriolis and centrifugal effect inertia elements can be derived by the following relation [1]:

$$h_{ijk} = \frac{\partial H_{ij}}{\partial q_k} - \frac{1}{2}\frac{\partial H_{jk}}{\partial q_i} \tag{2.15}$$

As can easily be observed, the Coriolis and centrifugal effects are nonlinear, being products of the velocity terms. The dynamics equations become the summation of the inertia terms and the Coriolis and centrifugal terms, as shown in Equation 2.16.

$$\tau_i = \sum_{j=1}^{4}H_{ij}\ddot{q}_j + \sum_{j=1}^{4}\sum_{k=1}^{4}h_{ijk}\dot{q}_j\dot{q}_k + G_i \tag{2.16}$$

Where G_i, the torque due to gravity on the links, is zero in the VCUUV horizontal planar linkage. The complete derivation of the closed form dynamics equations using the Lagrangian method is shown in Appendix A.

2.3 Hydrodynamics Model

M.J. Lighthill has done extensive work in capturing an expression to estimate the efficiency of the fish propulsion motion. In his work, he describes a "first principles" approach that incorporates basic dynamics with some well-known hydrodynamics assumptions to derive an equation for output power into the water. In doing so, he derives an expression for momentum of the water adjacent to the body as the tail undulates. According to Newton's Law, the derivative of the momentum gives the force, and torque on the body can be calculated knowing the moment arm of the force. Since the fish has forward velocity, the relative velocity between the free stream and the angled fish body must be accounted for in the momentum expression. Similarly, the time derivative of momentum of the water must account for the change experienced as the changing fish body travels past the water slice in question. This is known as the "substantial derivative" and is described in Section 2.3.2. In order to derive a useful hydrodynamics model for my control algorithm, the VCUUV continous, flexible tail system must be discretized into a four link model that is in terms of the state variables.

Two major assumptions made in EBT are as follows:

1. The body slope ($\frac{\partial z}{\partial x}$) from fore to aft is negligible.

2. The added mass of fish sections are approximately the same for a rigid cylinder of the same cross-section if the undulation wavelength λ is at least 5 times

the section depth (s). This assumes that (1) the effect of different sections pushing the fluid at different velocities and (2) the cross-sections being non-uniform produces negligible differences from the rigid cylinder case as long as $\lambda < 5s$.

The following is a description of adherence (or lack thereof) in my model to Lighthill's EBT. The body of the VCUUV has considerable slope compared to an eel-like body (anguilliform) and would fail Lighthill's assumptions. The assumption is based on the spatial derivative of the added mass being too large and the body, instead of pushing the fluid, will allow some to pass over and under the body as it propels forward while undulating. The VCUUV body slope is not extreme, however, and the added mass will be slightly overestimated rather than underestimated, which is conservative. Overall, this is a good engineering approximation.

The undulation wavelength is, indeed, 5 times the section depth (s). The VCUUV λ at a swimming frequency of .93 Hz is 109.2 inches. The maximum depth (s) of the VCUUV is 19.54 inches. 5s is 97.7 inches, less than the undulation wavelength, so the rigid cylinder approximation (discussed above) is good.

2.3.1 Lighthill's Theory Applied to a Swimming Fish

Lighthill's theory is a very solid first principles approach to this extremely complicated hydrodynamic problem. If energy stored in vortex sheets can be neglected, and the added mass can be treated as that due to a rigid cylinder, the substantial derivative of the momentum of the fluid along the body can be integrated to determine the total force on the body. For the interest of the VCUUV tail actuation system, the torques at each joint can be calculated by integrating the force ($\frac{D}{Dt}\{m_a(x,t)\omega(x,t)\}$) times

the moment arm (x) over the body. Where $\frac{D}{Dt}$, the substantial derivative operator, is denoted by:

$$\frac{D}{Dt} = \frac{\partial}{\partial t} + U\frac{\partial}{\partial x}$$

A flexible, undulating fish body has local spine lateral displacement, $y(x,t)$ as shown in Figure 2-6, and it is swimming into undisturbed water with forward velocity U. The lateral velocity of a cross-section of the tail with respect to the water slice it is pushing, denoted by $\omega_n(x,t)$ can be written:

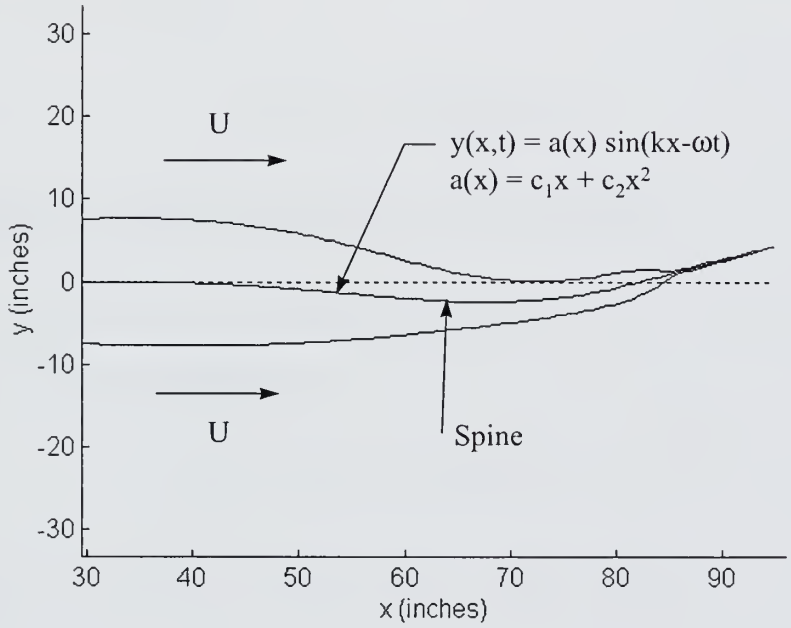

Figure 2-6: Lighthill EBT Theory Applied to a Swimming Fish

$$\omega_n(x,t) = \frac{\partial y(x,t)}{\partial t} + U\frac{\partial y(x,t)}{\partial x} \tag{2.17}$$

The momentum in the lateral direction of each water slice is simply the added mass of each fish section multiplied by the relative velocity of the tail:

$$\mathcal{M}(x,t) = m_a(x)\omega(x,t) \tag{2.18}$$

where

$$m_a(x) = \frac{1}{4}\rho\pi s(x)^2,$$

wher s is the body depth at section x. Now, calculate the change in momentum of each water "slice" as it passes by with velocity U. Integrating xdF over link "i" gives the total torque on that link:

$$\tau(x,t) = \int_0^l x\frac{D}{Dt}\mathcal{M}(x,t) \tag{2.19}$$

2.3.2 Lighthill's Theory Applied to the Tail System

Referring to Figure 2-7, the kinematics of a particular link "i" can be described as a function of x_i and time as follows:

$$y_i(x_i,t) = \frac{Y_i(t) - Y_{i-1}(t)}{l_i}x_i + Y_{i-1}(t) \tag{2.20}$$

Assuming small displacements, this can be linearized as follows:

$$y_i(x_i,t) = \theta_i(t)x_i + Y_{i-1}(t) \tag{2.21}$$

The lateral velocity of a cross-section of the tail with respect to the water slice it is pushing, denoted by $\omega_{n_i}(x_i,t)$ can be written:

$$\omega_{n_i}(x_i,t) = \frac{\partial y_i(x_i,t)}{\partial t} + U\frac{\partial y_i(x_i,t)}{\partial x_i} \tag{2.22}$$

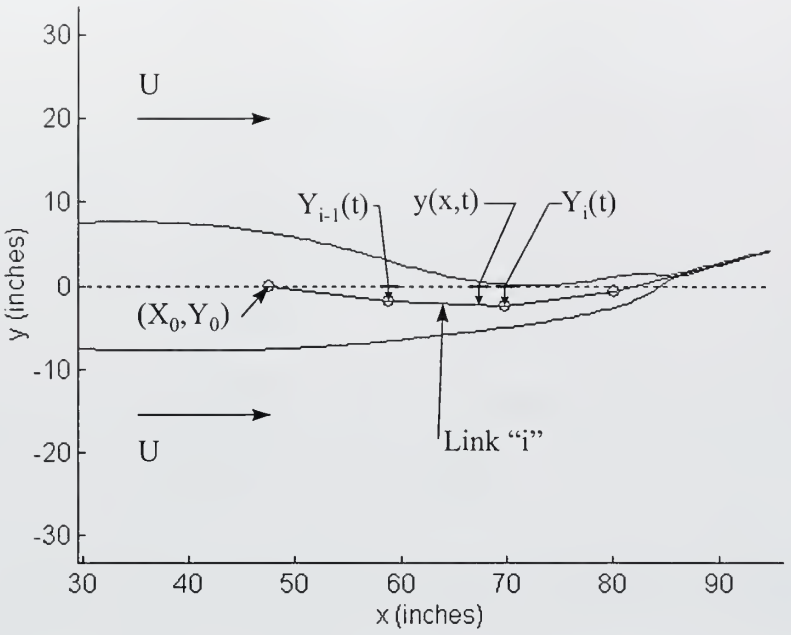

Figure 2-7: Lighthill EBT Theory Applied to the VCUUV Linkage

The fish is traveling at speed U which Dewar and Graham [5] have shown, is strongly dependent on tail undualation frequency. For a frequency of 1.0 Hz, an estimate of U is 0.656 body lengths/second. Substituting Equation (2.21) and expanding:

$$\omega_{n_i}(x_i,t) = \dot{\theta}_i(t)x_i + \dot{Y}_{i-1}(t) + U\theta_i(t) \tag{2.23}$$

Now, calculate the differential force on each water "slice" as it passes by with velocity U:

$$dF_i(x_i,t) = \frac{D}{Dt}\left(m_a(x_i)\omega_{n_i}(x_i,t)\right)dx_i \tag{2.24}$$

Where

$$\frac{D}{Dt} = \left(\frac{\partial}{\partial t} + U\frac{\partial}{\partial x_i}\right)$$

Now, expand out to view all the terms:

$$\begin{aligned} dF_i(x_i,t) &= -\Big\{ m_a(x_i)\left(\ddot{\theta}_i x_i + \ddot{Y}_{i-1}(t) + U\dot{\theta}_i\right) \\ &\quad + U\frac{\partial m_a(x_i)}{\partial x_i} x_i \left(\dot{\theta}_i x_i + \dot{Y}_{i-1}(t) + U\theta_i\right) \\ &\quad + m_a(x_i)\dot{\theta}_i \Big\} dx_i \end{aligned} \tag{2.25}$$

$$\begin{aligned} \tau_1(t) = &- \int_0^{l_1} x_1 dF_1 - \int_0^{l_2} (x_2 + l_1) dF_2 - \int_0^{l_3} (x_3 + l_2 + l_1) dF_3 \\ &- \int_0^{l_4} (x_4 + l_3 + l_2 + l_1) dF_4 \end{aligned} \tag{2.26}$$

$$\tau_2(t) = -\int_0^{l_2} x_2 dF_2 - \int_0^{l_3} (x_3 + l_2) dF_3 - \int_0^{l_4} (x_4 + l_3 + l_2) dF_4 \tag{2.27}$$

$$\tau_3(t) = -\int_0^{l_3} x_3 dF_3 - \int_0^{l_4} (x_4 + l_4) dF_4 \tag{2.28}$$

$$\tau_4(t) = -\int_0^{l_4} x_4 dF_4 \tag{2.29}$$

To illustrate the derivation of the hydrodynamics of the links, I will work through the torque on the fourth link (caudal fin). My approach is taken from Triantafyllou [13], where the integration of EBT forces over a rigid body results in distinct hydrodynamic coefficients. The tail fin (looking from above) is shown in Figure 2-8. First of all, the torque on the joint for link 4 is shown in Equation 2.29. Expanding the equation:

$$\begin{aligned} \tau_4(t) &= \int_0^{l_4} x_4 \Big\{ m_{a_4}(x_4)\left(\ddot{\theta}_4 x_4 + \ddot{Y}_3 + U\dot{\theta}_4\right) \\ &+ U\frac{\partial m_{a_4}(x_4)}{\partial x_4}\left(\dot{\theta}_4 x_4 + \dot{Y}_3 + U\theta_4\right) \\ &+ m_{a_4}(x_4)\dot{\theta}_4 \Big\} dx_4 \end{aligned} \tag{2.30}$$

Expanding this out:

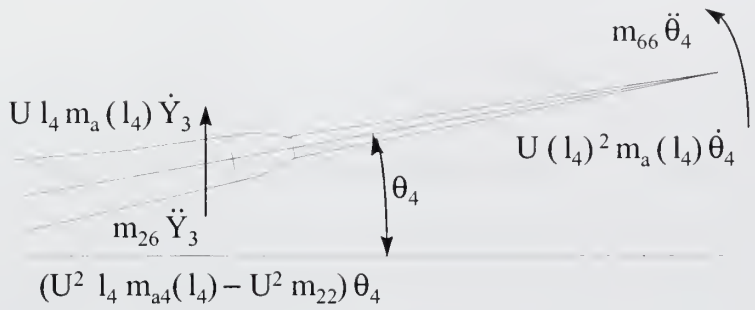

Figure 2-8: Hydrodynamic Torques on the Caudal Fin

Variable		Coefficient	Simplified (Refer to Newman [10])
$\ddot{\theta}_4$	$\Rightarrow$	$\int_0^{l_4} x_4^2 m_{a_4} dx_4$	$= m_{66_4}$
$\dot{\theta}_4$	$\Rightarrow$	$\int_0^{l_4} U x_4 \left(2m_a(x_4) + \frac{\partial m_{a_4}(x_4)}{\partial x_4} x_4\right) dx_4$	$= U l_4^2 m_{a_4}(l_4)$
θ_4	$\Rightarrow$	$\int_0^{l_4} U^2 x_4 \left(\frac{\partial m_{a_4}(x_4)}{\partial x_4}\right) dx_4$	$= U^2 l_4 m_{a_4}(l_4) - U^2 m_{22_4}$
$\ddot{Y}_3$	$\Rightarrow$	$\int_0^{l_4} x_4 m_{a_4}(x_4) dx$	$= m_{26_4}$
$\dot{Y}_3$	$\Rightarrow$	$\int_0^{l_4} U x_4 \left(\frac{\partial m_{a_4}(x_4)}{\partial x_4}\right) dx_4$	$= U l_4 m_{a_4}(l_4)$

Substitution must now be made with the state variables, given in Equation 2.4 and assuming small angular displacements such that $\sin(\theta_i) \approx \theta i$:

$$Y_0 = 0; \dot{Y}_0 = 0; \ddot{Y}_0 = 0$$

$$Y_1 \approx l_1\theta_1; \dot{Y}_1 \approx l_1\dot{\theta}_1; \ddot{Y}_1 \approx l_1\ddot{\theta}_1$$

$$Y_2 \approx l_1\theta_1 + l_2\theta_2; \dot{Y}_2 \approx l_1\dot{\theta}_1 + l_2\dot{\theta}_2; \ddot{Y}_2 \approx l_1\ddot{\theta}_1 + l_2\ddot{\theta}_2$$

$$Y_3 \approx l_1\theta_1 + l_2\theta_2 + l_3\theta_3; \dot{Y}_3 \approx l_1\dot{\theta}_1 + l_2\dot{\theta}_2 + l_3\dot{\theta}_3; \ddot{Y}_3 \approx l_1\ddot{\theta}_1 + l_2\ddot{\theta}_2 + l_3\ddot{\theta}_3$$

$$Y_4 \approx l_1\theta_1 + l_2\theta_2 + l_3\theta_3 + l_4\theta_4; \dot{Y}_4 \approx l_1\dot{\theta}_1 + l_2\dot{\theta}_2 + l_3\dot{\theta}_3 + l_4\dot{\theta}_4; \ddot{Y}_4 \approx l_1\ddot{\theta}_1 + l_2\ddot{\theta}_2 + l_3\ddot{\theta}_3 + l_4\ddot{\theta}_4$$

The complete derivation of the four link system is shown in Appendix B.

2.4 Hydraulic Plant Model

The state space VCUUV tail model has torque input with angular position and velocity output. In the VCUUV prototype, however, the input to the system is electrical current to the hydraulic servovalves and the outputs are linear position and velocity of the hydraulic pistons. Therefore, for implementation, the torque control signal must be converted to a servovalve current input. The relationship between desired torque and servovalve current is a nonlinear relationship that can not be modeled in a state-space system without large linearization error. A schematic of the VCUUV hydraulic system is shown in Figure 2-9; the link system is shown with dimensions in Figure 2-4. To calculate the linear position and velocity of each piston, the positions of the attachment points must be known. From the figure, the following dimensions can be taken: The change in piston end points can be defined by the following geometric relationships:

$$x_A = x_{A_0}$$

$$y_A = y_{A_0}$$

$$x_B = x_{B_0}\cos(\theta_1) - y_{B_0}\sin(\theta_1)$$

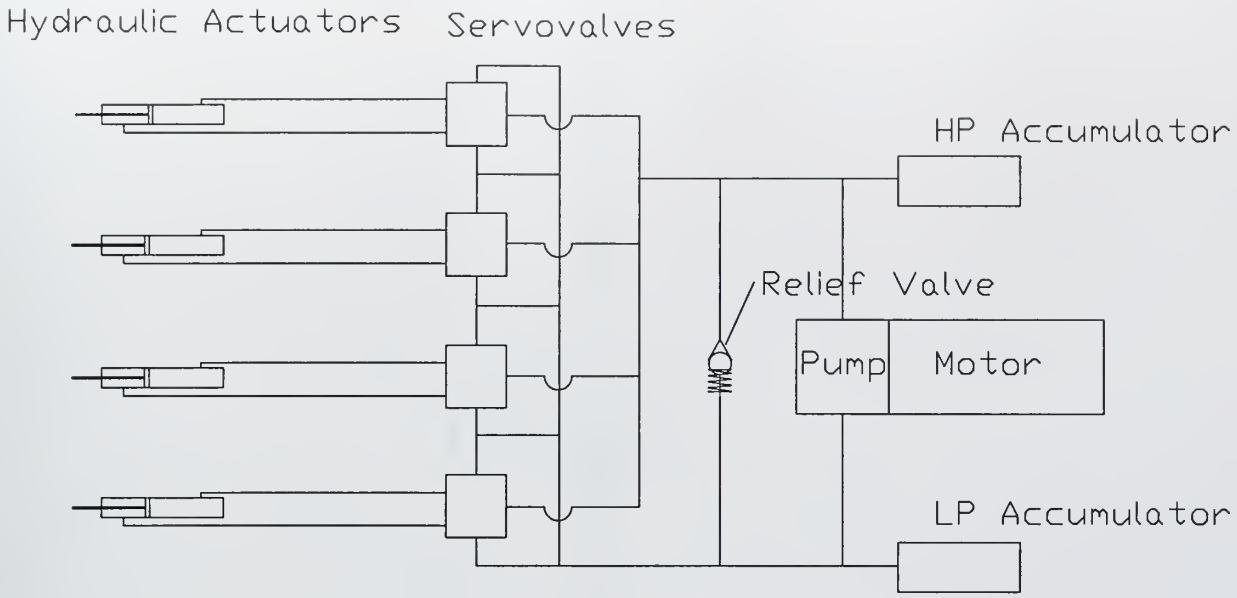

Figure 2-9: VCUUV Hydraulic Plant Schematic

Point	x_0 **(in) (measured from previous joint)**	y_0 **(in)**
A	0.0	2.3
B	10.75	2.3
C	1.54	-2.144
D	0.0	-2.144
E	1.85	1.5
F	0.0	1.19
G	1.10	0
H	0	.953

Table 2.3: Linkage Dimensions From Figure 2-10

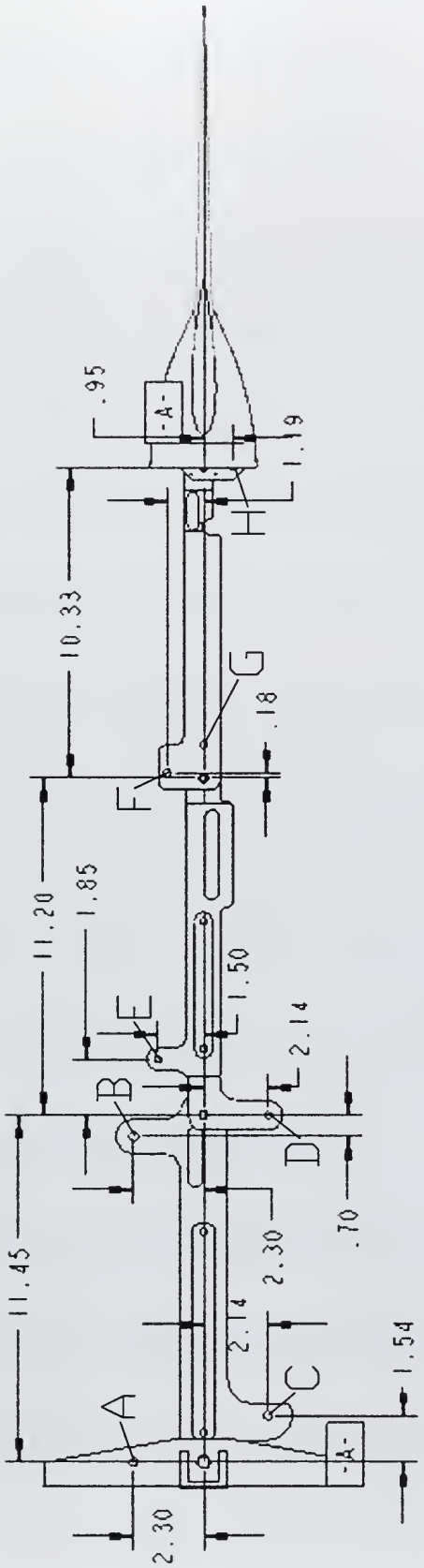

Figure 2-10: VCUUV Tail Linkage Assembly With Dimensions

$$y_B = x_{B_0}\sin(\theta_1) + y_{B_0}\cos(\theta_1)$$

$$x_C = x_{C_0}\cos(\theta_1) - y_{C_0}\sin(\theta_1)$$

$$y_C = x_{C_0}\sin(\theta_1) + y_{C_0}\cos(\theta_1)$$

$$x_D = L_1\cos(\theta_1) + x_{D_0}\cos(\theta_1) - y_{D_0}\sin(\theta_1)$$

$$y_D = L_1\sin(\theta_1) + x_{D_0}\sin(\theta_1) + y_{D_0}\cos(\theta_1)$$

$$x_E = L_1\cos(\theta_1) + x_{E_0}\cos(\theta_1) - y_{E_0}\sin(\theta_1)$$

$$y_E = L_1\sin(\theta_1) + x_{E_0}\sin(\theta_1) + y_{E_0}\cos(\theta_1)$$

$$x_F = L_1\cos(\theta_1) + L_2\cos(\theta_2) + x_{F_0}\cos(\theta_1) - y_{F_0}\sin(\theta_1)$$

$$y_F = L_1\sin(\theta_1) + L_2\sin(\theta_2) + x_{F_0}\sin(\theta_1) + y_{F_0}\cos(\theta_1)$$

$$x_G = L_1\cos(\theta_1) + L_2\cos(\theta_2) + x_{G_0}\cos(\theta_1) - y_{G_0}\sin(\theta_1)$$

$$y_G = L_1\sin(\theta_1) + L_2\sin(\theta_2) + x_{G_0}\sin(\theta_1) + y_{G_0}\cos(\theta_1)$$

$$x_H = L_1\cos(\theta_1) + L_2\cos(\theta_2) + L_3\cos(\theta_3) + x_{H_0}\cos(\theta_1) - y_{H_0}\sin(\theta_1)$$

$$y_H = L_1\sin(\theta_1) + L_2\sin(\theta_2) + L_3\sin(\theta_3) + x_{H_0}\sin(\theta_1) + y_{H_0}\cos(\theta_1)$$

The linear position for each piston is then simply:

$$s_1 = \sqrt{(x_B - x_A)^2 + (y_B - y_A)^2} - \sqrt{(x_{B_0} - x_{A_0})^2 + (y_{B_0} - y_{A_0})^2}$$

$$s_2 = \sqrt{(x_C - x_B)^2 + (y_C - y_B)^2} - \sqrt{(x_{C_0} - x_{B_0})^2 + (y_{C_0} - y_{B_0})^2}$$

$$s_3 = \sqrt{(x_E - x_D)^2 + (y_E - y_D)^2} - \sqrt{(x_{E_0} - x_{D_0})^2 + (y_{E_0} - y_{D_0})^2}$$

$$s_4 = \sqrt{(x_H - x_G)^2 + (y_H - y_G)^2} - \sqrt{(x_{H_0} - x_{G_0})^2 + (y_{H_0} - y_{G_0})^2}$$

Linear velocity can be obtained by taking the derivative of the positions:

$$v_{A_x} = \frac{\partial x_A}{\partial t} = 0$$

$$v_{A_y} = \frac{\partial y_A}{\partial t} = 0$$

$$v_{B_x} = \frac{\partial x_B}{\partial t} = -x_{B_0}\sin(\theta_1)\dot{\theta}_1 - y_{B_0}\cos(\theta)\dot{\theta}_1$$

$$v_{B_y} = \frac{\partial y_B}{\partial t} = x_{B_0}\cos(\theta_1)\dot{\theta}_1 - y_{B_0}\sin(\theta)\dot{\theta}_1$$

$$v_{C_x} = \frac{\partial x_C}{\partial t} = -x_{C_0}\sin(\theta_1)\dot{\theta}_1 - y_{C_0}\cos(\theta)\dot{\theta}_1$$

$$v_{C_y} = \frac{\partial y_C}{\partial t} = x_{C_0}\cos(\theta_1)\dot{\theta}_1 - y_{C_0}\sin(\theta)\dot{\theta}_1$$

$$v_{D_x} = \frac{\partial x_D}{\partial t} = -L_1\sin(\theta_1)\dot{\theta}_1 - x_{D_0}\sin(\theta_1)\dot{\theta}_1 - y_{D_0}\cos(\theta)\dot{\theta}_1$$

$$v_{D_y} = \frac{\partial y_D}{\partial t} = L_1\cos(\theta_1)\dot{\theta}_1 x_{D_0}\cos(\theta_1)\dot{\theta}_1 - y_{D_0}\sin(\theta)\dot{\theta}_1$$

$$v_{E_x} = \frac{\partial x_E}{\partial t} = -L_1\sin(\theta_1)\dot{\theta}_1 - x_{E_0}\sin(\theta_1)\dot{\theta}_1 - y_{E_0}\cos(\theta)\dot{\theta}_1$$

$$v_{E_y} = \frac{\partial y_E}{\partial t} = L_1\cos(\theta_1)\dot{\theta}_1 x_{E_0}\cos(\theta_1)\dot{\theta}_1 - y_{E_0}\sin(\theta)\dot{\theta}_1$$

$$v_{F_x} = \frac{\partial x_F}{\partial t} = -L_1\sin(\theta_1)\dot{\theta}_1 - L_2\sin(\theta_2)\dot{\theta}_2 - x_{F_0}\sin(\theta_1)\dot{\theta}_1 - y_{F_0}\cos(\theta)\dot{\theta}_1$$

$$v_{F_y} = \frac{\partial y_F}{\partial t} = L_1\cos(\theta_1)\dot{\theta}_1 + L_2\cos(\theta_2)\dot{\theta}_2 + x_{F_0}\cos(\theta_1)\dot{\theta}_1 - y_{F_0}\sin(\theta)\dot{\theta}_1$$

$$v_{G_x} = \frac{\partial x_G}{\partial t} = -L_1\sin(\theta_1)\dot{\theta}_1 - L_2\sin(\theta_2)\dot{\theta}_2 - x_{G_0}\sin(\theta_1)\dot{\theta}_1 - y_{G_0}\cos(\theta)\dot{\theta}_1$$

$$v_{G_y} = \frac{\partial y_G}{\partial t} = L_1\cos(\theta_1)\dot{\theta}_1 + L_2\cos(\theta_2)\dot{\theta}_2 + x_{G_0}\cos(\theta_1)\dot{\theta}_1 - y_{G_0}\sin(\theta)\dot{\theta}_1$$

$$v_{H_x} = \frac{\partial x_H}{\partial t} = -L_1\sin(\theta_1)\dot{\theta}_1 - L_2\sin(\theta_2)\dot{\theta}_2 - L_3\sin(\theta_3)\dot{\theta}_3 - x_{H_0}\sin(\theta_1)\dot{\theta}_1 - y_{H_0}\cos(\theta)\dot{\theta}_1$$

$$v_{H_y} = \frac{\partial y_H}{\partial t} = L_1\cos(\theta_1)\dot{\theta}_1 + L_2\cos(\theta_2)\dot{\theta}_2 + L_3\cos(\theta_3)\dot{\theta}_3 + x_{H_0}\cos(\theta_1)\dot{\theta}_1 - y_{H_0}\sin(\theta)\dot{\theta}_1$$

To determine the linear velocity numerically, the dot product was taken between each position velocity vector and the vector defined by the two points and the difference calculated:

$$\dot{s}_1 = (\mathbf{v_B}, \vec{AB}) - (\mathbf{v_A}, \vec{AB})$$

$$\dot{s}_2 = (\mathbf{v_D}, \vec{CD}) - (\mathbf{v_C}, \vec{CD})$$

$$\dot{s}_3 = (\mathbf{v_F}, \vec{EF}) - (\mathbf{v_E}, \vec{EF})$$

$$\dot{s}_4 = (\mathbf{v_H}, \vec{GH}) - (\mathbf{v_G}, \vec{GH})$$

The results for the swimming motion, again with parameters from Table 2-1 is shown in Figures 2-11 and 2-12. Now that the linear positions and velocities of the pistons have been calculated, the flowrate, f_i for each the cylinder can be determined at any time by multiplying the piston area, A_{pist_i} by the linear velocity, $\dot{s}_i$:

$$f_i = \dot{s}_i A_{pist_i}$$

The pressure, P_i, necessary to produce the desired torque, τ_i, can be calculated as follows:

- Calculate force, F_i by dividing the torque by the moment arm, d_i:

$$F_i = \frac{\tau_i}{d_i}$$

- Calculate pressure by dividing force by dividing force by piston area:

$$\Delta P_i = \frac{F_i}{A_{pist_i}}$$

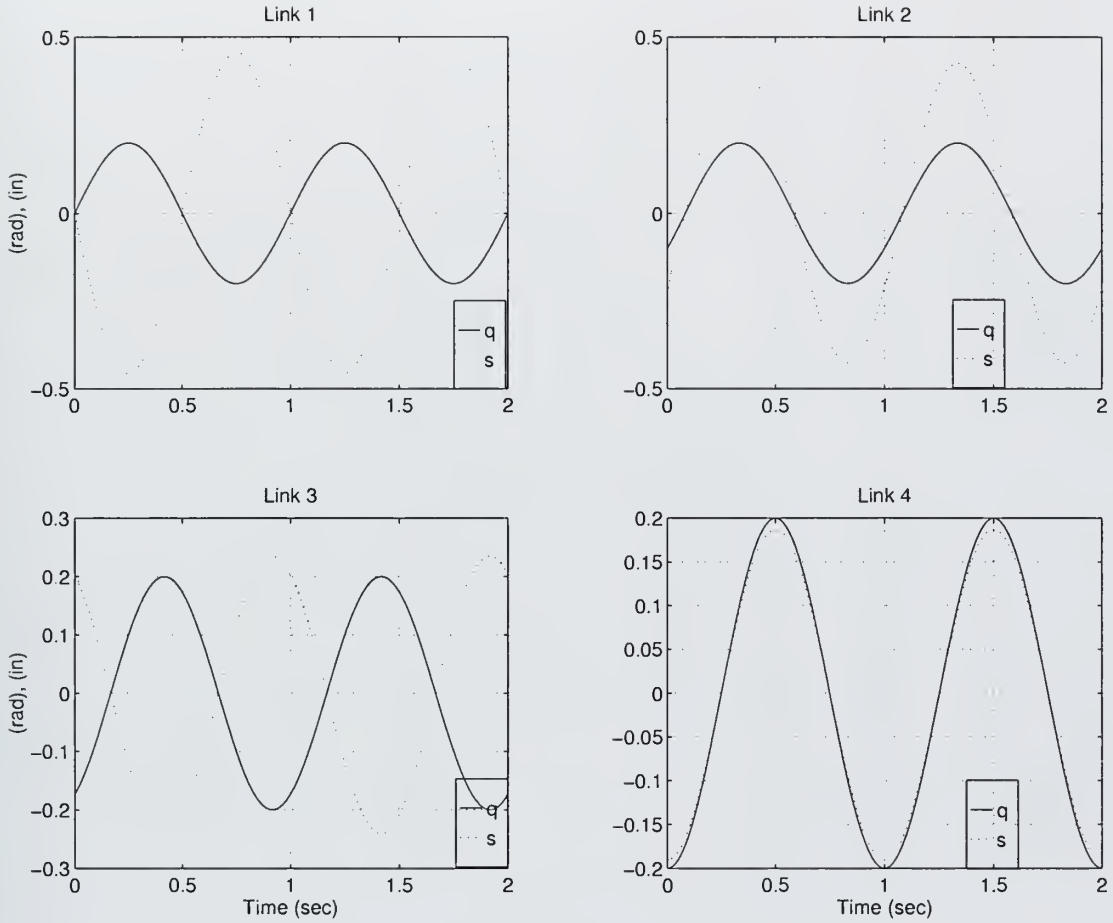

Figure 2-11: Piston Linear, s, and Link Angular, q, Position

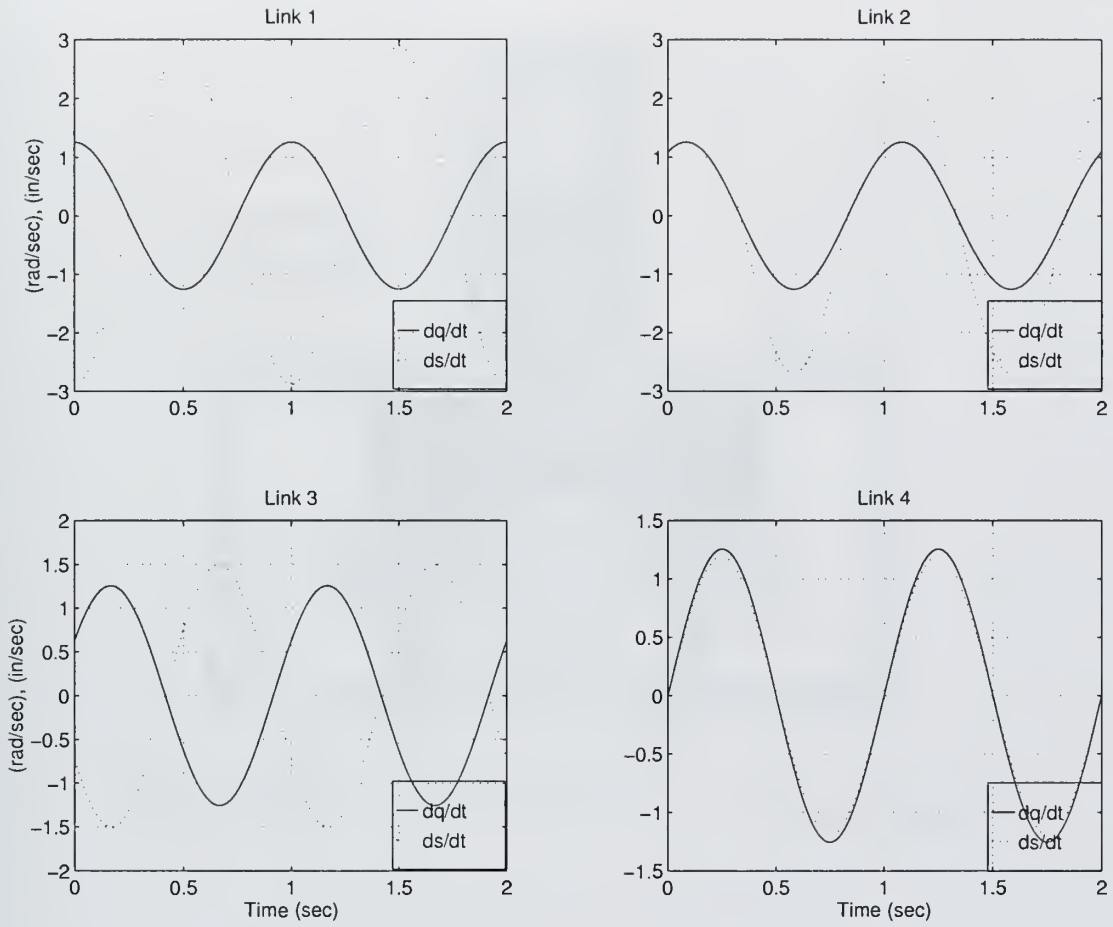

Figure 2-12: Piston Linear, ds/dt, and Link Angular, dq/dt, Velocity

The flowrate through the servovalve is driven by the differential pressure across it, along with the valve spool position, which is current controlled. The servovalve "gain," K, is defined by the current required to produce a flow, f_i at the reference pressure, P_{ref}; $K = f_i/I_i$. A schematic of one of the servovalves used in the VCUUV is shown in Figure 2-13. For flow through an orifice, Darcy's formula gives a good

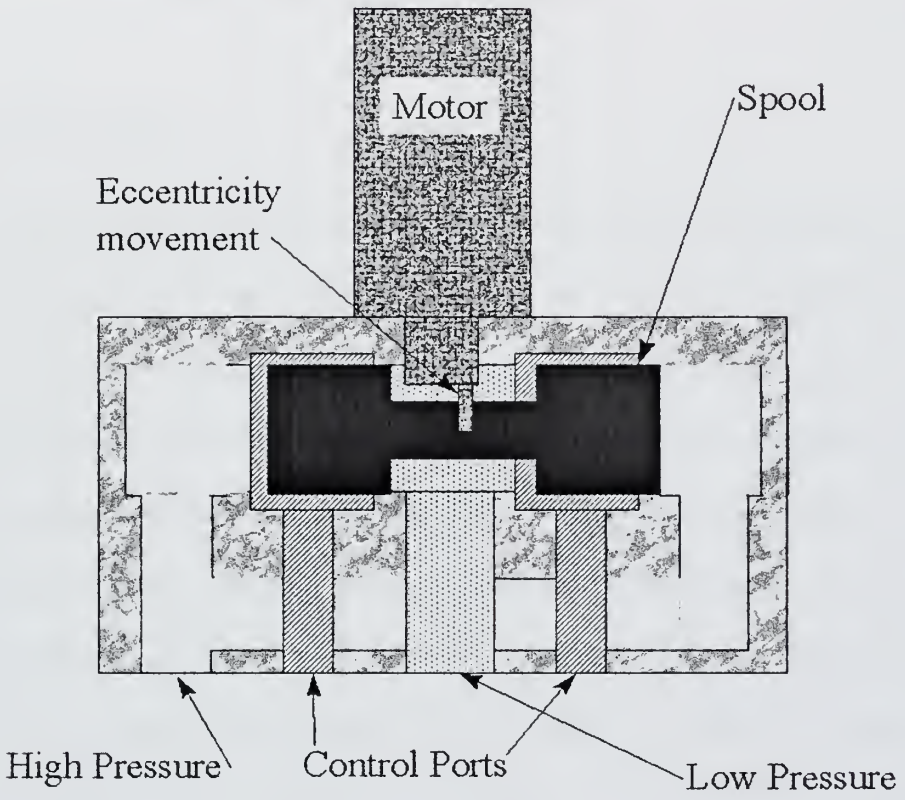

Figure 2-13: Servovalve Schematic (HR Textron)

estimate of the pressure drop:

$$\Delta P \propto f^2$$

. With this relation, the pressure drop can be scaled if the flow is known. The required current, I_{sv}, can then be calculated for each servovalve by the following relation:

$$I_{sv_i} = K_i \sqrt{\frac{\Delta P_i}{\Delta P_{ref_i}}}$$

Where $\Delta P_i = P_{system} - P_i$. This current command can be fed to the servovalves, giving the required spool position that will produce the required torque on the link.

2.5 Conclusions

For the models to be compared, there must be a given swimming motion to follow; then torques will be generated (numerically) by the models and the differences compared. I chose to use link angular positions and velocities that will give the motion using parameters from Table 2.1 and I also chose 1.0 Hz as the undulation frequency. The link angular displacements over one cycle used for the comparison are plotted in Figure 2-14. Figure 2-15, top, shows the estimated torque on each joint over two cycles of swimming motion at 1.0 Hz for the Lagrange Dynamics Model represented by block "A" in Figure 2-3. Compare with Figure 2-15, bottom, in which the Lagrange Linearized Model (represented by block "B" in Figure 2-3) is run with the same input parameters. As can be seen, there is no detectable difference between the ouputs of the two models. The nonlinear effects are due to the Coriolis and centrifigal forces, and those terms which are products of joint angular velocities, are very low in the swimming motion. The torques produced by the nonlinear terms are shown in Figure 2-16. Note how small the magnitude is compared to the linearized torque model output in Figure 2-15, bottom.

The parameters used for the motion in all of the outputs shown here are those of

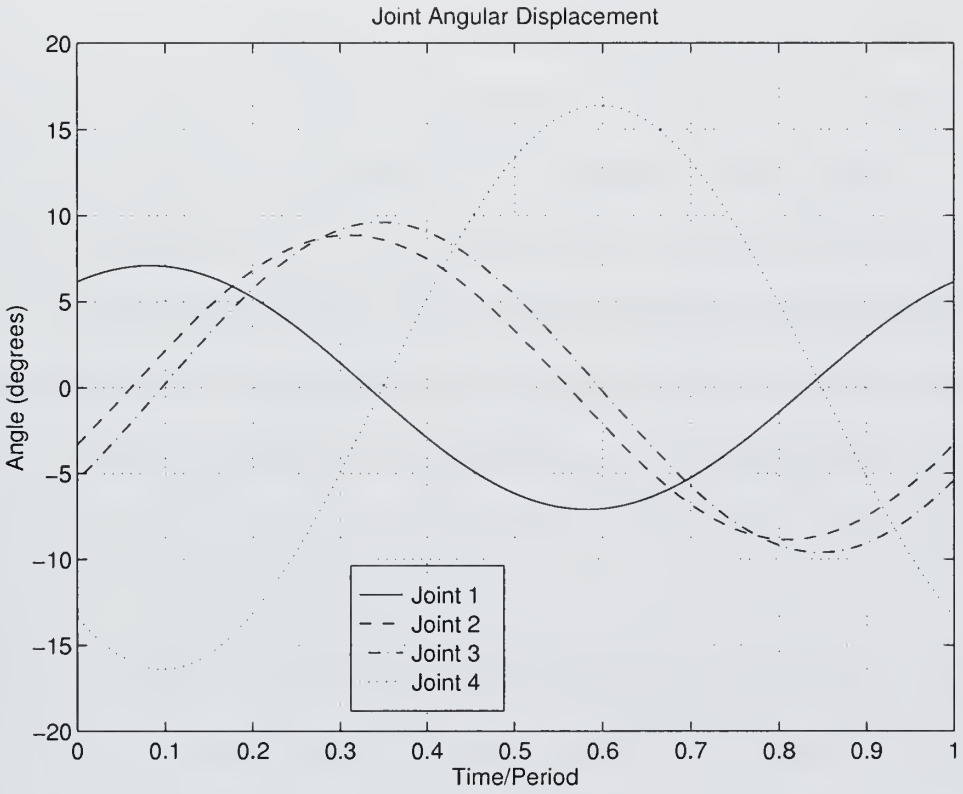

Figure 2-14: Relative Joint Angles During Swimming Cycle (swimming parameters from Table 2.1)

Table 2.1. The undulation frequency of 1.0 Hz is considered near maximum speed and therefore, a case where the differences between the non-linear and linearized models would become apparent.

Shown in Figure 2-17, top, are the estimated torques on the joints for the Lighthill EBT Continous Model represented by block "C" in Figure 2-3. Figure 2-17, bottom, is the output of the Discretized Lighthill Hydrodynamics Model represented by block "D" of Figure 2-3. The difference can be seen in joint 1 since force errors in the model will be magnified to torque on the hip joint (#1) by the distance to the force error. The discretized model is a reasonably good approximation and is useful in that it has allowed the representation of the hydrodynamics in terms of the state variables, which the continuous model would not do. The differences in the EBT discrete and continuous models are mitigated somewhat when the free-flood dynamic inertias are added to produce the overall system model. Because of the slight phase differences between the hydrodynamics models, the addition of the free-flood inertia brings the two models closer (see Figure 2-18).

Finally, the combined linear and combined nonlinear models can be compared. Since the tail is a linear system, the torque outputs can be added to produce the total torque on each joint at a given time instant. Figure 2-18, top, representing block "E" in Figure 2-3 shows the combined torques from blocks "A" (Figure 2-15), top and "C" (Figure 2-15), bottom. These torque outputs from the nonlinear models can be compared with Figure 2-18, bottom, which represents block "F" in Figure 2-3.

The results show that the linearized system model is a reasonably good approximation of the full nonlinear model. However, the assumptions made in the full nonlinear model must not soon be forgotten:

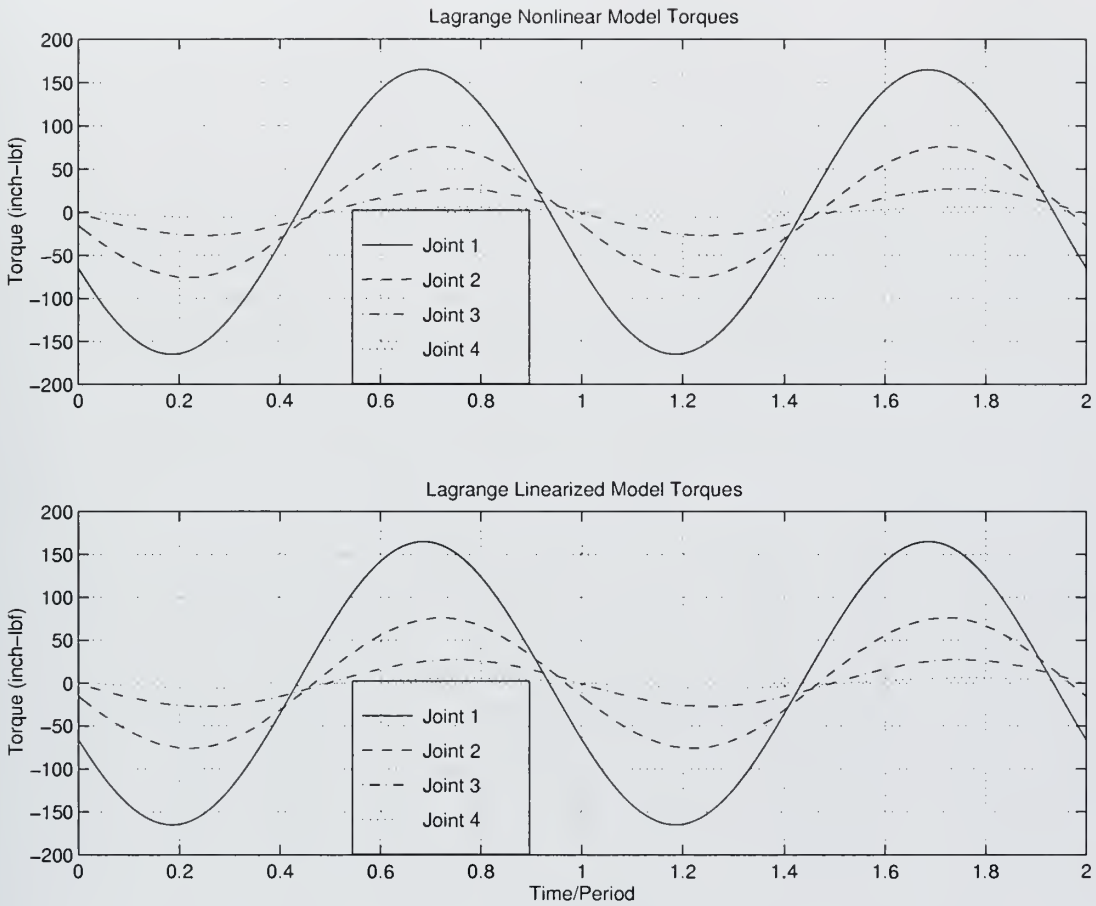

Figure 2-15: Torque Outputs From the Lagrange Nonlinear Model, ("A" in Figure 2-3), Top and From the Linearized Model ("B" in Figure 2-3), Bottom

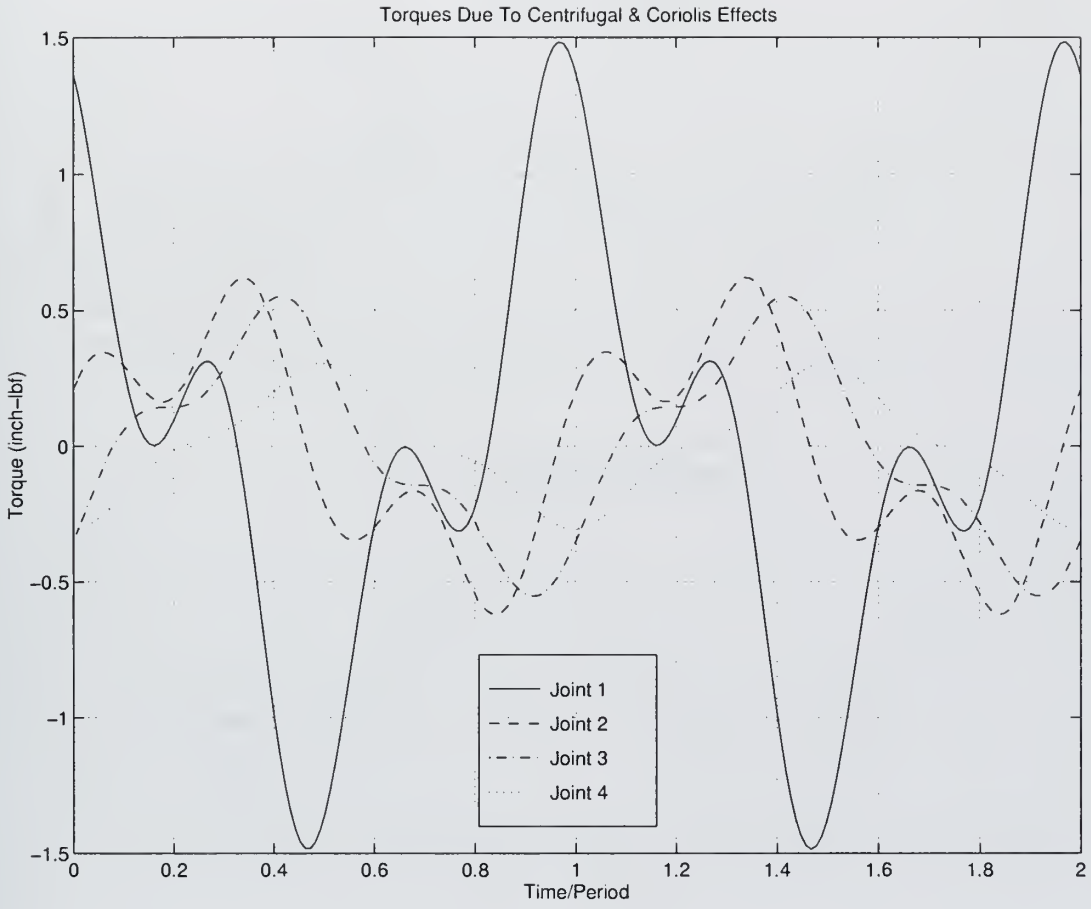

Figure 2-16: Torque Outputs Due to Nonlinear Corioulis and Centrifugal Forces

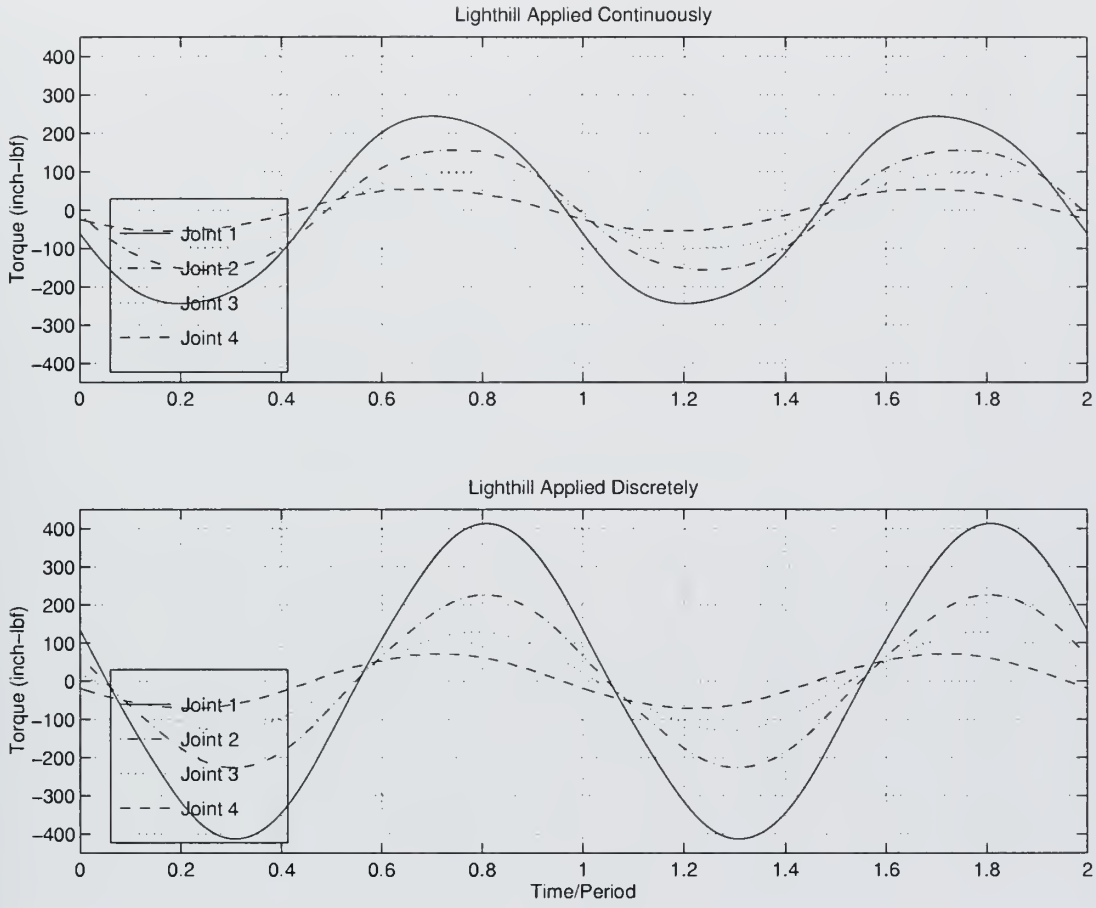

Figure 2-17: Torque Outputs From the Lighthill Continuous EBT Model ("C" in Figure 2-3), Top and From the Lighthill Discrete EBT Model ("D" in Figure 2-3), Bottom

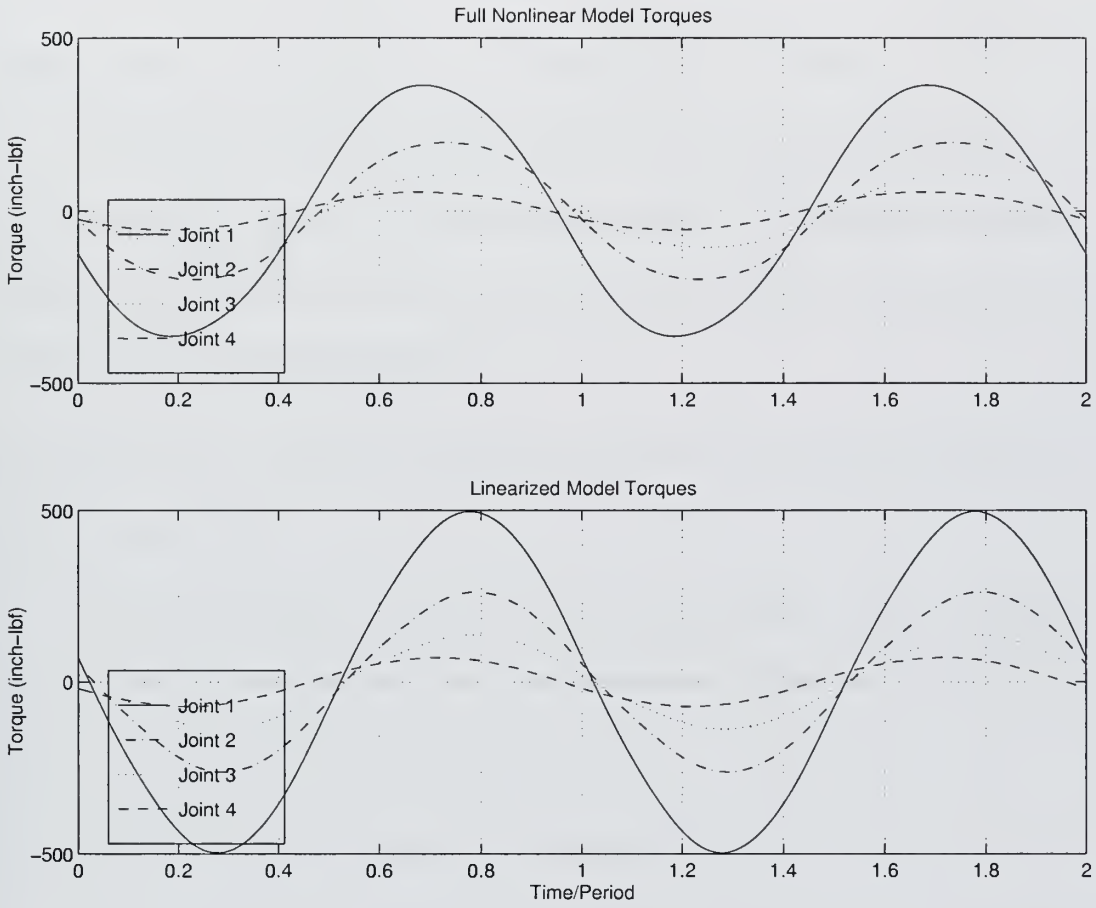

Figure 2-18: Torque Outputs From the Full Nonlinear VCUUV System Model ("E" in Figure 2-3), Top and From the Linearized VCUUV System Model ("F" in Figure 2-3), Bottom

- Neglects the effect of VCUUV anterior yawing.

  Due to the effects discussed in Section 1.4, the yawing motion should be very small, anyway. Also, initial testing of the VCUUV has shown that the yawing motion is extremely small at 1.0 Hz swimming frequency, which is considered to be near maximum speed for our design.

- Neglects energy stored in wake vortex sheets shed by the body.

  The vortices shed have an unknown effect on the body and caudal fin, and modeling unsteady forces would be extremely complex. The controller simulation demonstrates that the controller is robust enough to handle the unsteady forces, which are modeled as disturbances.

- Assumes VCUUV sections surrounding each link are homogeneous masses that move as rigid bodies.

  The water entrained in the tail by the nylon/neoprene skin is essentially trapped and will not exchange with the free-stream. Therefore, modeling the water as a rigid mass is a good approximation.

- Assumes VCUUV spine motion follows Equation 2.1.

  Early in the design, it was determined that three body links would closely approximate the continuous motion described by Equation 2.1. Furthermore, the tail exostructure is able to flex between the attachment points to form a splined curve that even more closely approximates the desired shape.

- Assumes small angular displacements (i.e. $\cos(q) \approx 1$ and $\sin(q) \approx 0$).

  The carangiform motion used for normal swimming motion only requires the relative joint angles to reach $7 - 10°$ and the caudal fin relative angle to reach

16° maximum (see Figure 2-14). The caudal fin relative angle amplitude, which is necessary for the proper phase relationship to the body motion, reaches a maximum of $\approx 16°$. Although this angle seems rather large, the error associated with the small angle approximation is only:

$$\frac{16\frac{\pi}{180} - \sin(16\frac{pi}{180})}{\sin(16\frac{pi}{180})}100\% = 1.3\%$$

The approximation will break down for larger displacements, such as motions used for starting or turning, but it is not as crucial for this motion to be exact, as it does not affect efficiency over a mission.

- Neglects tail fin circulation dependent forces.

  The tail fin hydrodynamics as well as circulatory forces associated with the generation of lift include the tail's (possible) reaction with vortices shed by the VCUUV body. This reaction will serve to create greater forces than have been modeled in the linear system model. The forces will also be unsteady and acting far from the center of gravity, will cause possible cause problems with control. Once again, however, in my simulation, I modeled the unsteady forces as torque disturbances and have shown sufficient robustness.

Chapter 3

Controller Design

The controller design was done in two approaches, both following a general state space format. The first approach, in which the system gains are calculated using the LQR method, defined in Section 1.1 results in a controller that commands the links with reference inputs each sample time to new desired positions along the desired link trajectories. The feedback signal is composed of a proportional, derivative and integral signal driven by the respective errors in the outputs. The second approach, in which the system gains are calculated in the same way as the first approach, uses the system model to "back-calculate" the desired input from the known desired states. The system is then driven by the calculated inputs, while the gains operate on the errors of the system. Although the first approach was abandoned and not fully developed, it can be seen that the second approach is more intuitive, gives tighter control, more robustness, is well suited to the application, and is easier to implement.

3.1 Approach

The controller design process proceeded as follows:

1. Develop state-space system of equations of the form

$$\dot{\mathbf{x}} = \mathbf{A}\mathbf{x} + \mathbf{B}\mathbf{u} \tag{3.1}$$

$$\mathbf{y} = \mathbf{C}\mathbf{x} \tag{3.2}$$

2. Augment the system with integrator states

$$\dot{\mathbf{x}}_{aug} = \mathbf{A}_{aug}\mathbf{x}_{aug} + \mathbf{B}_{aug}\mathbf{u} \tag{3.3}$$

$$\mathbf{y}_{aug} = \mathbf{C}_{aug}\mathbf{x}_{aug} \tag{3.4}$$

3. Solve for gains using LQR method

4. Demonstrate phase lag, attenuation with LQR method

5. Develop "computed torque" controller

6. Demonstrate satisfactory tracking with computed torque method

State space methods require a linear system model, which I have derived in Chapter 2. The VCUUV tail system model is a multiple-input, multiple-output (MIMO) system. The techniques for control system design can be more challenging than for single-input, single-output (SISO) systems due to coupling between degrees of freedom, which complicates the problem in several ways. First, the system has gain matrices, rather than simply scalars. Link#1 will receive a command signal based upon errors in link#2, link#3, and link#4 in addition to it's own errors. This makes the closed loop dynamics hard to comprehend. Second, the as will be explained below, the system of equations for calculating gains in MIMO systems is indeterminate and minimization principles must be used. As difficult as MIMO systems can be to understand, with

an accurate system model, they can be controlled much more accurately, since they account for the coupling between state variables.

3.2 LQR Feedback Control

For SISO system control, the proper gain can be easily chosen by pole-placement techniques. With the SISO system given as

$$\dot{\mathbf{x}} = \mathbf{A}\mathbf{x} + \mathbf{B}u$$

$$y = \mathbf{C}\mathbf{x}$$

and using Ackerman's formula, Equation 3.5, poles can be chosen for the system, giving the gain (K) necessary to achieve the desired response. The "desired response" can mean the system meets system step response maximum rise times, settling times, overshoots, or it can mean keeping the system output errors within some maximum specified values in the case of trajectory following. Both these types of system specifications are considered in this design, but the one more applicable to the tail system model is the trajectory following one.

$$K = [0 \ldots 0 \ 1] \underbrace{\left[\mathbf{B} \ \mathbf{AB} \ \mathbf{A}^2\mathbf{B} \ldots \mathbf{A}^{n-1}\mathbf{B}\right]}_{Controllability\ Matrix}^{-1} \alpha_c(\mathbf{A}) \tag{3.5}$$

Where

$$\alpha_c(\mathbf{A}) = \mathbf{A}^n + \alpha_1\mathbf{A}^{n-1} + \alpha_2\mathbf{A}^{n-2} + \cdots + \alpha_n\mathbf{I},$$

n is the number of state elements, and the α_i's are the coefficients of the characteristic equation.

However, for a MIMO system, the system of equations derived for pole placement will be indeterminate. In other words, there will be multiple gain matrix solutions that will satisfy the system equations, but will not necessarily meet the system response specifications. Therefore, Lagrangian minimization principles are used to find the optimum gains [6].

3.3 Cost Function

The Lagrangian minimization function $\mathcal{J}$ or "cost" function includes two "weighting functions," Q and R, with the following form:

$$\mathcal{J} = \frac{1}{2}\int (\mathbf{x^T Q x} + \mathbf{u^T R u})dt \tag{3.6}$$

subject to the constraint that

$$-\dot{\mathbf{x}} + \mathbf{A x} + \mathbf{B u} = 0 \tag{3.7}$$

The Q matrix weights the state variables, and the R matrix weights the actuation. In this way, the optimum tradeoff can be made between actuator saturation prevention and fast system response. The solution to the "Ricatti" equations is the steady-state answer to the minimization problem [6]:

$$\mathbf{A^T P + P A + Q - P B R^{-1} B^T P = 0} \tag{3.8}$$

and

$$\mathbf{K = -P B R^{-1}} \tag{3.9}$$

3.4 Development of the State Space System

To develop the state-space equations, I combined the dynamic system models derived in Sections 2.2 and 2.3.2

$$\tau_{\mathbf{hd}} = \mathbf{\Lambda}\ddot{\mathbf{q}} + \mathbf{\Omega}\dot{\mathbf{q}} + \mathbf{\Theta}\mathbf{q} \tag{3.10}$$

which is the linearized hydrodynamic system model using the Lighthill EBT approach, where $\mathbf{\Lambda}$ is the inertia coefficient matrix, $\mathbf{\Omega}$ is the damping coefficient matrix and $\mathbf{\Theta}$ is the spring coefficient matrix. Since the system is linear, it can be added to

$$\tau_{\mathbf{ff}} = \mathbf{H}\ddot{\mathbf{q}} \tag{3.11}$$

which is the linearized inertia dynamics equations due to the free flood water mass entrained in the tail. H is the inertia coefficient matrix. Adding equations 3.10 and 3.11 together, the total linearized system is:

$$\tau_{\mathbf{total}} = \tau_{\mathbf{hd}} + \tau_{\mathbf{ff}} = (\mathbf{\Lambda} + \mathbf{H})\ddot{\mathbf{q}} + \mathbf{\Omega}\dot{\mathbf{q}} + \mathbf{\Theta}\mathbf{q} \tag{3.12}$$

Separating the state variables,

$$\ddot{\mathbf{q}} \;=\; -(\mathbf{\Lambda} + \mathbf{H})^{-1}\mathbf{\Omega}\dot{\mathbf{q}} + -(\mathbf{\Lambda} + \mathbf{H})^{-1}\mathbf{\Theta}\mathbf{q} + (\mathbf{\Lambda} + \mathbf{H})^{-1}\tau_{\mathbf{total}}$$

Overall, the state-space system looks like:

$$\frac{d}{dt}\begin{bmatrix} q_1 \\ q_2 \\ q_3 \\ q_4 \\ \dot{q}_1 \\ \dot{q}_2 \\ \dot{q}_3 \\ \dot{q}_4 \end{bmatrix} = \begin{bmatrix} 0 & 0 & 0 & 0 & 1 & 0 & 0 & 0 \\ 0 & 0 & 0 & 0 & 0 & 1 & 0 & 0 \\ 0 & 0 & 0 & 0 & 0 & 0 & 1 & 0 \\ 0 & 0 & 0 & 0 & 0 & 0 & 0 & 1 \\ & & & & & & & \\ -(\mathbf{\Lambda}+\mathbf{H})^{-1}\mathbf{\Theta} & & & & -(\mathbf{\Lambda}+\mathbf{H})^{-1}\mathbf{\Omega} & & & \end{bmatrix} \begin{bmatrix} q_1 \\ q_2 \\ q_3 \\ q_4 \\ \dot{q}_1 \\ \dot{q}_2 \\ \dot{q}_3 \\ \dot{q}_4 \end{bmatrix} + \begin{bmatrix} 0 & 0 & 0 & 0 \\ 0 & 0 & 0 & 0 \\ 0 & 0 & 0 & 0 \\ 0 & 0 & 0 & 0 \\ & & & \\ & -(\mathbf{\Lambda}+\mathbf{H})^{-1} & & \end{bmatrix} \begin{bmatrix} \tau_1 \\ \tau_2 \\ \tau_3 \\ \tau_4 \end{bmatrix}$$

Therefore, the A and B matrices are:

$$A = \begin{bmatrix} \mathbf{0}_{(4\times4)} & \mathbf{I}_{(4\times4)} \\ -(\mathbf{\Lambda}+\mathbf{H})^{-1}\mathbf{\Theta} & -(\mathbf{\Lambda}+\mathbf{H})^{-1}\mathbf{\Omega} \end{bmatrix} \tag{3.13}$$

$$B = \begin{bmatrix} \mathbf{0}_{(4\times4)} \\ -(\mathbf{\Lambda}+\mathbf{H})^{-1} \end{bmatrix} \tag{3.14}$$

In a system with no integrator control, there will be steady state error present when the system reaches equilibrium with the external forces. To avoid any steady state error, I have implemented an integrator into the system as shown in Figure 3-1. To design an LQR optimized controller, the system must be augmented to include the integrator. This is done by adding states that correspond to the integral terms. For example, the integrator will sum the error between the reference input, $\mathbf{q_r}$, and the

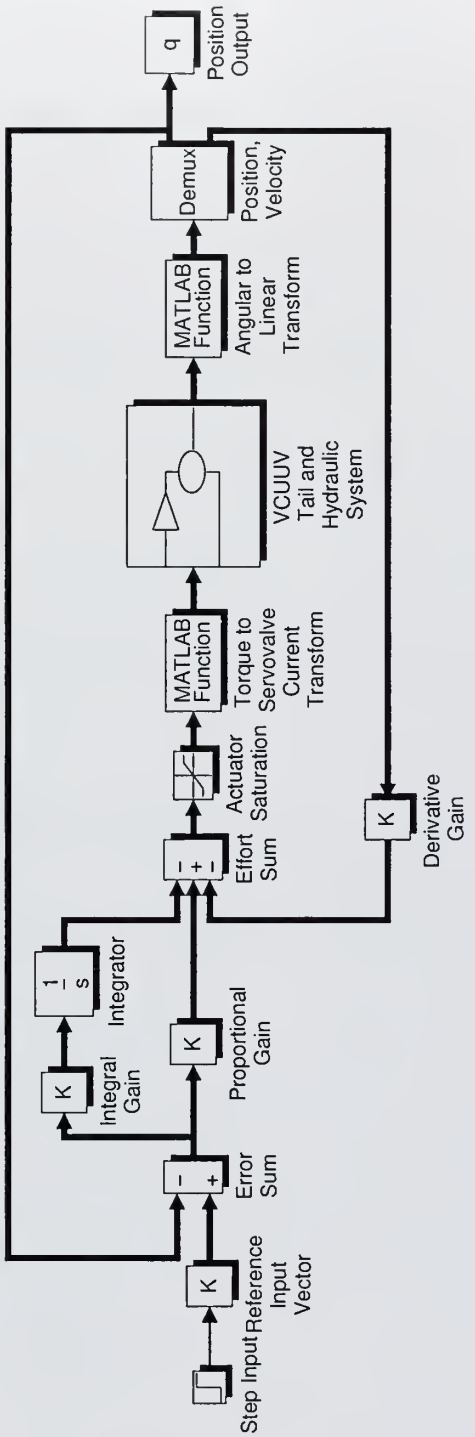

Figure 3-1: Controller With Integrator

actual position state $\mathbf{q(t)}$.

$$\mathbf{q_i(t)} = \int_0^{\mathbf{t}} (\mathbf{q_r} - \mathbf{q(t)})\mathbf{dt}$$

The derivative of the $\mathbf{q_i}$ state neglects the reference input, which is considered unchanging with time.

$$\frac{d}{dt}\mathbf{q}_i\mathbf{(t)} = -\mathbf{q(t)}$$

Overall, the augmented state-space system looks like:

$$\frac{d}{dt}\begin{bmatrix} q_1 \\ q_2 \\ q_3 \\ q_4 \\ \dot{q}_1 \\ \dot{q}_2 \\ \dot{q}_3 \\ \dot{q}_4 \\ q_1^i \\ q_2^i \\ q_3^i \\ q_4^i \end{bmatrix} = \begin{bmatrix} 0 & 0 & 0 & 0 & 1 & 0 & 0 & 0 & 0 & 0 & 0 & 0 \\ 0 & 0 & 0 & 0 & 0 & 1 & 0 & 0 & 0 & 0 & 0 & 0 \\ 0 & 0 & 0 & 0 & 0 & 0 & 1 & 0 & 0 & 0 & 0 & 0 \\ 0 & 0 & 0 & 0 & 0 & 0 & 0 & 1 & 0 & 0 & 0 & 0 \\ & & & & & & & & 0 & 0 & 0 & 0 \\ -(\mathbf{\Lambda}+\mathbf{H})^{-1}\mathbf{\Theta} & & & & & -(\mathbf{\Lambda}+\mathbf{H})^{-1}\mathbf{\Omega} & & & 0 & 0 & 0 & 0 \\ & & & & & & & & 0 & 0 & 0 & 0 \\ & & & & & & & & 0 & 0 & 0 & 0 \\ -1 & 0 & 0 & 0 & 0 & 0 & 0 & 0 & 0 & 0 & 0 & 0 \\ 0 & -1 & 0 & 0 & 0 & 0 & 0 & 0 & 0 & 0 & 0 & 0 \\ 0 & 0 & -1 & 0 & 0 & 0 & 0 & 0 & 0 & 0 & 0 & 0 \\ 0 & 0 & 0 & -1 & 0 & 0 & 0 & 0 & 0 & 0 & 0 & 0 \end{bmatrix} \begin{bmatrix} q_1 \\ q_2 \\ q_3 \\ q_4 \\ \dot{q}_1 \\ \dot{q}_2 \\ \dot{q}_3 \\ \dot{q}_4 \\ q_1^i \\ q_2^i \\ q_3^i \\ q_4^i \end{bmatrix} + \begin{bmatrix} 0 & 0 & 0 & 0 \\ 0 & 0 & 0 & 0 \\ 0 & 0 & 0 & 0 \\ 0 & 0 & 0 & 0 \\ & & & \\ & -(\mathbf{\Lambda}+\mathbf{H})^{-1} & & \\ & & & \\ & & & \\ 0 & 0 & 0 & 0 \\ 0 & 0 & 0 & 0 \\ 0 & 0 & 0 & 0 \\ 0 & 0 & 0 & 0 \end{bmatrix} \begin{bmatrix} \tau_1 \\ \tau_2 \\ \tau_3 \\ \tau_4 \end{bmatrix}$$

The augmented A and B matrices are:

$$\mathbf{A}_{aug} = \begin{bmatrix} \mathbf{0}_{(4\times4)} & \mathbf{I}_{(4\times4)} & \mathbf{0}_{(4\times4)} \\ -(\mathbf{\Lambda}+\mathbf{H})^{-1}\mathbf{\Theta} & -(\mathbf{\Lambda}+\mathbf{H})^{-1}\mathbf{\Omega} & \mathbf{0}_{(4\times4)} \\ -\mathbf{I}_{(4\times4)} & \mathbf{0}_{(4\times4)} & \mathbf{0}_{(4\times4)} \end{bmatrix} \tag{3.15}$$

$$\mathbf{B}_{aug} = \begin{bmatrix} \mathbf{0}_{(4\times4)} \\ -(\mathbf{\Lambda} + \mathbf{H})^{-1} \\ \mathbf{0}_{(4\times4)} \end{bmatrix} \tag{3.16}$$

3.5 LQR Approach

Now, the proper gains must be chosen. For a MIMO system, the selection of optimum gains is difficult, since the system has many interdependencies. For example, the system shown in Equations 3.15 and 3.16 has 4 inputs and 12 outputs. This leads to $4 \times 12 = 48$ dynamic relationships, 48 Bode plots, 48 root locus plots, etc. The optimal solution is not clear. A good place to start is given by the "Bryson" rule [6], where the **Q** weighting matrix is given diagonal values equal to the square of the inverse of the maximum actuation effort available:

$$Q_{i,i} = \frac{1}{u_{i_{max}}^2}$$

Likewise, the **R** weighting matrix diagonals are given by the maximum allowable state error:

$$R_{i,i} = \frac{1}{m_i^2}$$

Once determined, these values can be used in the cost function, Equation 3.6 and solve for the near-optimum gains using the Matlab LQR function. Matlab solves the Ricatti equations given the system dynamics matrices and the Lagrangian weighting matrices. The maximum effort the actuators in the VCUUV tail system are able to apply at a system pressure of 700 psi is given by the following: The analog-to-digital converter for the linkage sensors has 12 bits available, which makes for a $1/2^{12} = .000244$ resolution. Therefore, I made a reasonable estimate of the maximum allowable error

Actuator	Piston Diameter (inches)	u_{max} (inch-lbf)
1	1.0	1265
2	0.75	661.8
3	0.5	163.6
4	0.5	131.0

in position of 0.01 radians and 0.1 radians/second for the velocity states, allowing for noise and quantization effects. For the integral state, I used 0.01 radians also, since it is a position measure. After some experimentation, I found that 0.1 radians for position, velocity, and integral maximum allowed error was optimum. For a first check of the system response, I ran the Simulink simulation of the model in Figure 3-1 with a step input. The results are shown in Figure 3-2; The system has a fair step response using just the Bryson thumbrule. The plot shows the step input of 0.1 radians has been applied to joint#1, the hip joint. The rise time is about .35 seconds and the overshoot is 22%, which gives a natural frequency of approximately 10 radians/second and a damping ratio of $\zeta = .43$, which is somewhat low. These results are not exact, as the integrator is the cause for some of the overshoot. The three remaining links can be seen attempting to regulate their relative angles at zero. The tail fin initially tries to follow the hip joint, rather than the expected reaction force, but this is simply a function of the controller gains and the command signal's dependence on the errors of all the joints. Before beginning to optimize this controller, it was checked with a sinusoidal input to see how it tracks an actual VCUUV command. Figures 3-3 and 3-4 show the positions and velocities, respectively of the joints plotted with the desired positions and velocities. The desired positions and velocities in every case lead in phase and have greater magnitude, which is expected, as this is simply a time

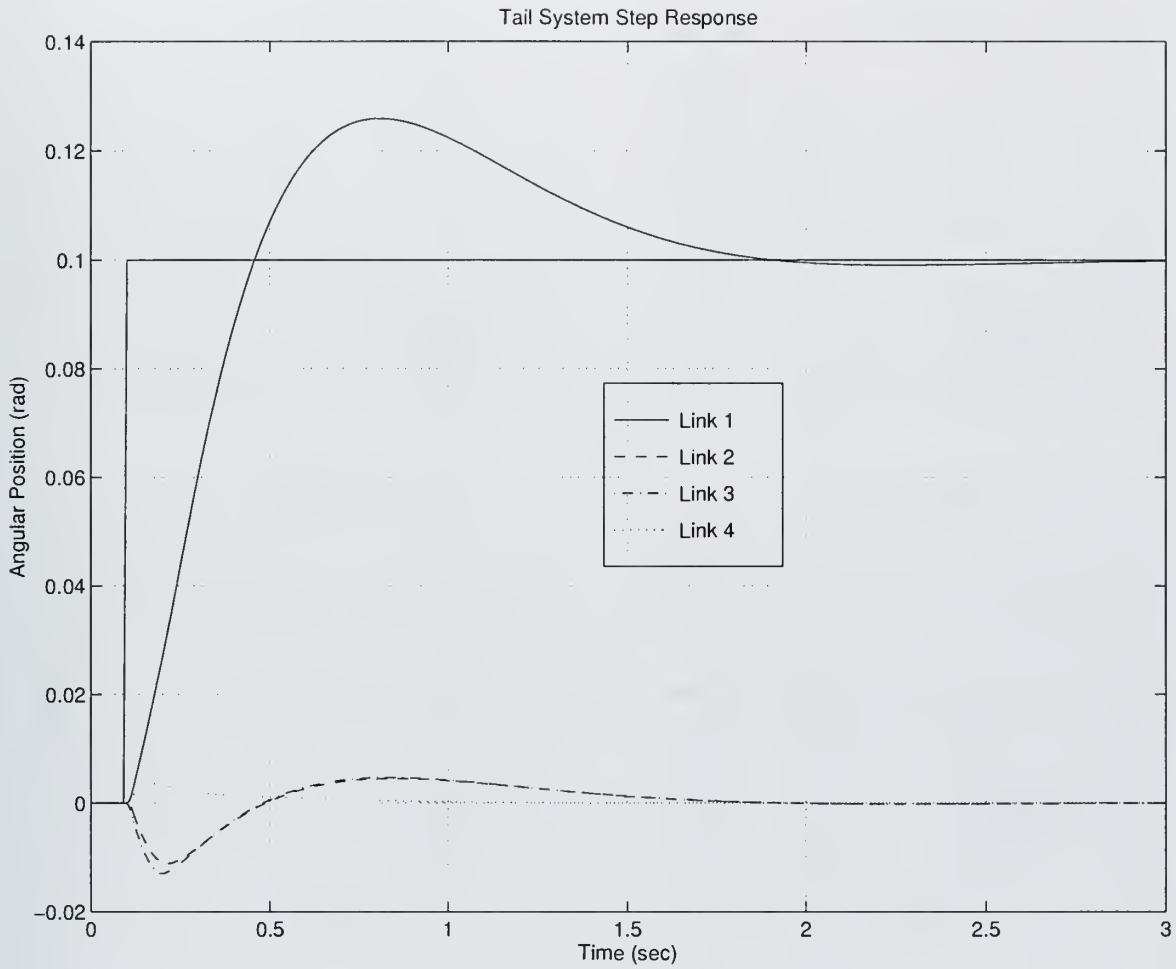

Figure 3-2: Response of Linkage to a Step Input of 0.1 Radians to Link #1.

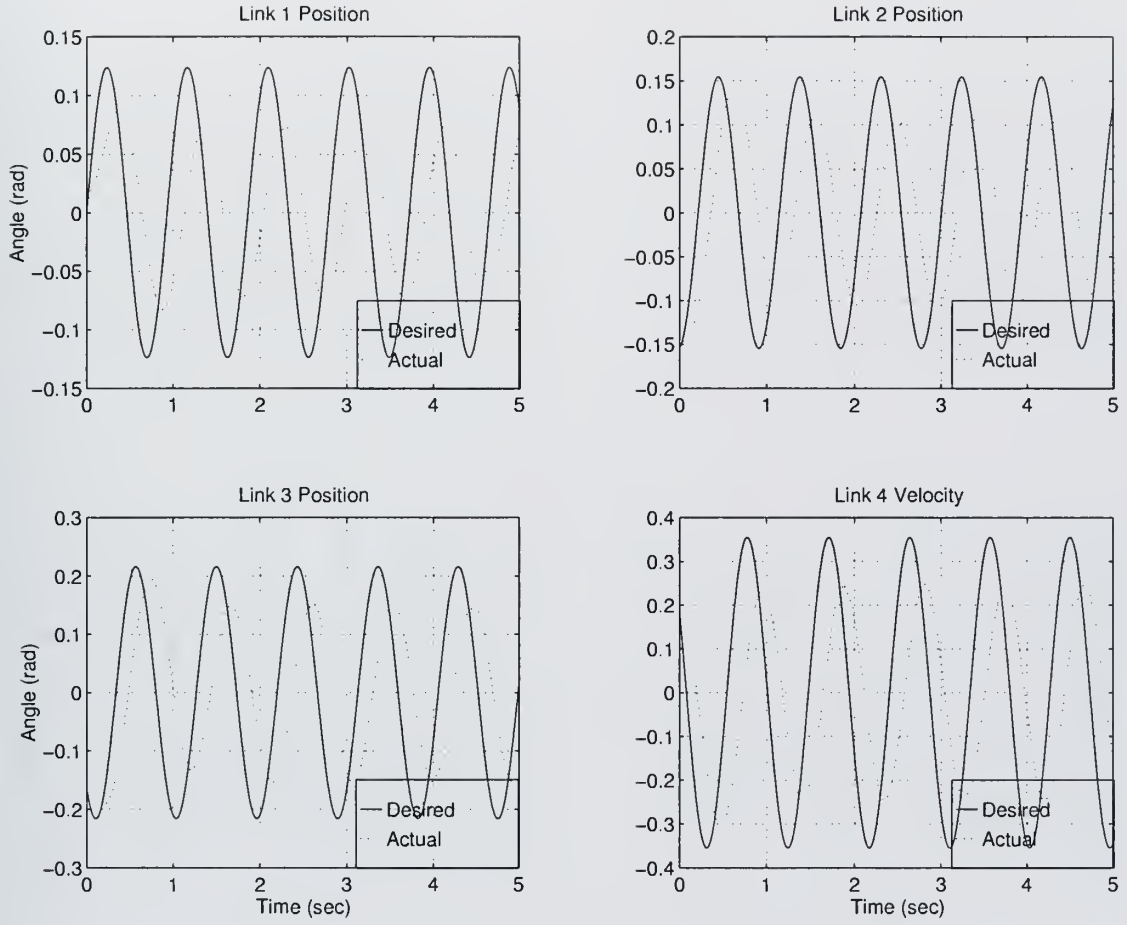

Figure 3-3: Actual Position Plotted With Desired Position For the Initial LQR Control Design

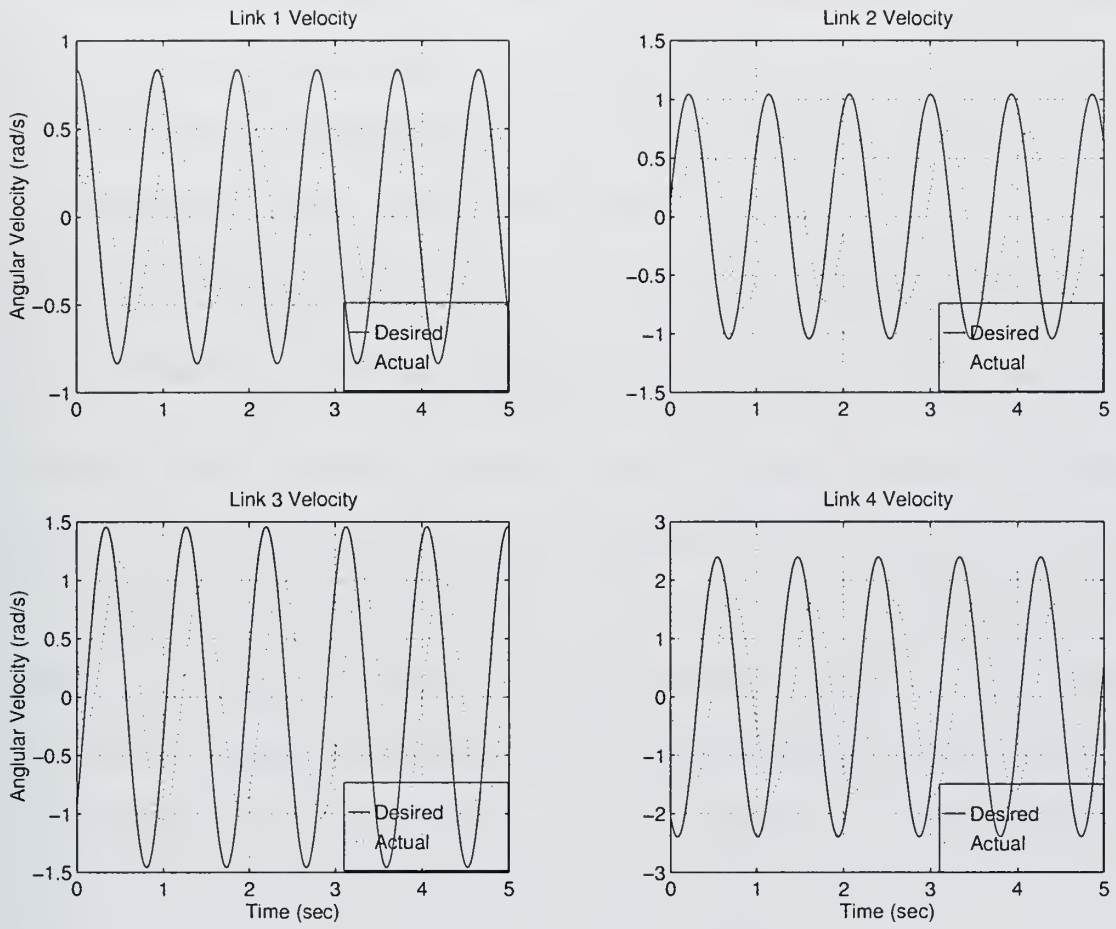

Figure 3-4: Actual Velocity Plotted With Desired Velocity For the LQR Control Method

domain illustration of a Bode plot, where attenuation and phase lag are visible in the output. The initial results are unacceptable for two reasons:

- The output magnitude must equal the desired magnitude in order to precisely place the robot linkage. Since the state variables are relative angular positions and velocities, the errors in the global position of the links add to produce large errors at the caudal fin. These errors in heave and angle of attack of the caudal fin, where it is hypothesized most of the thrust is produced, could destroy the hydrodynamic benefit of the desired motion.
- The phase shift, although it appears to be equal for each link, will change as undulating frequency changes and therefore will be unpredictable and inaccurate.

The control effort for the links is plotted in Figure 3-5, and it can be seen that the maximums are less than expected to move the linkage. There is still much actuator effort available to tune the controller with; as it stands it is very badly tuned. The output errors are plotted in Figure 3-6 and appear at first glance to be very large. The error is somewhat deceiving, however, in that the controller might be acceptable if phase shift was not important (i.e. most of the error is due to the phase shift, not attenuation). There was some effort made to optimize this controller, but the resulting difference between the optimal and the results presented was negligible. There are other methods that could be used to tune the controller, none of which are very intuitive. However, there are also other control design methods altogether. In the next section I discuss a different approach that is easier, more intuitive, gives more accurate results, and is more robust.

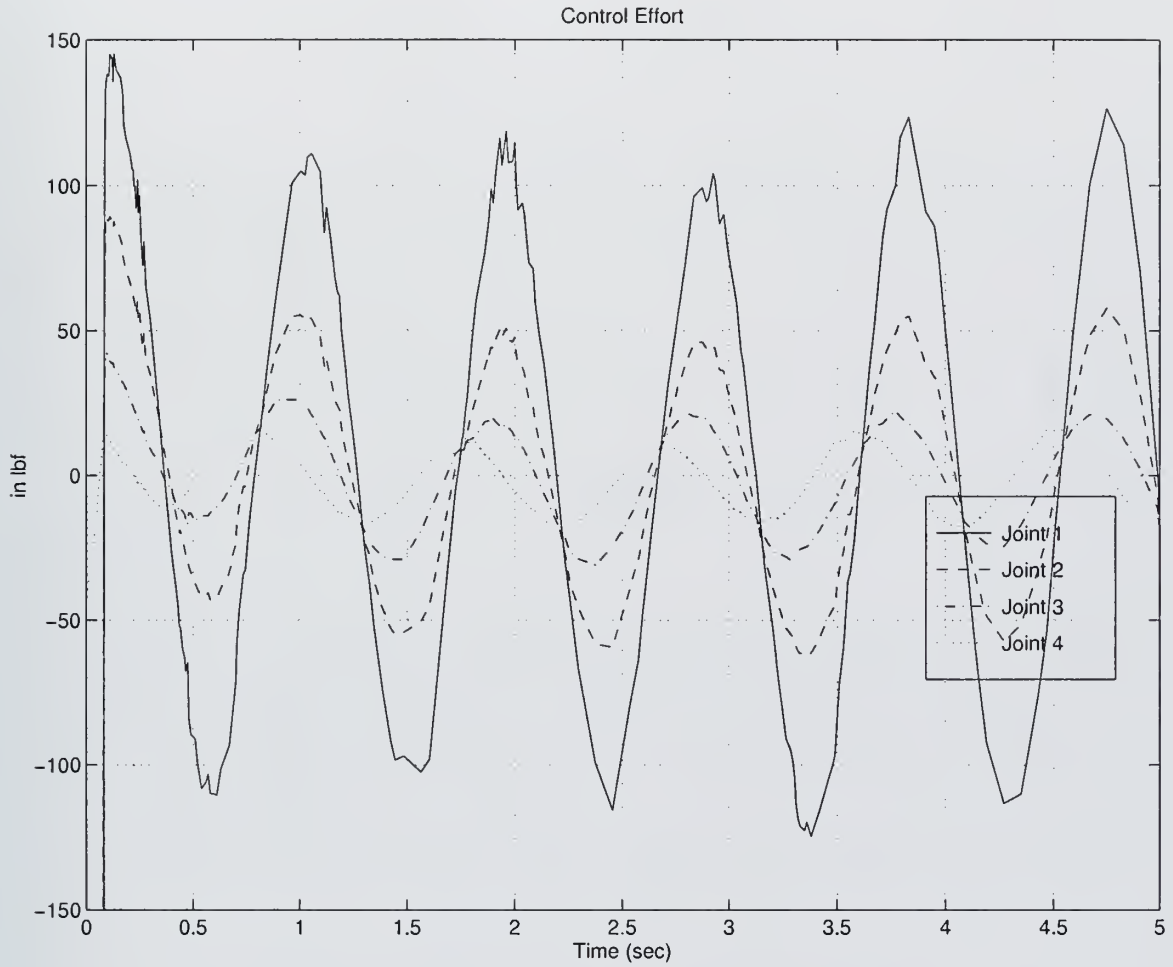

Figure 3-5: Control Effort Signal For the Initial LQR Control Design

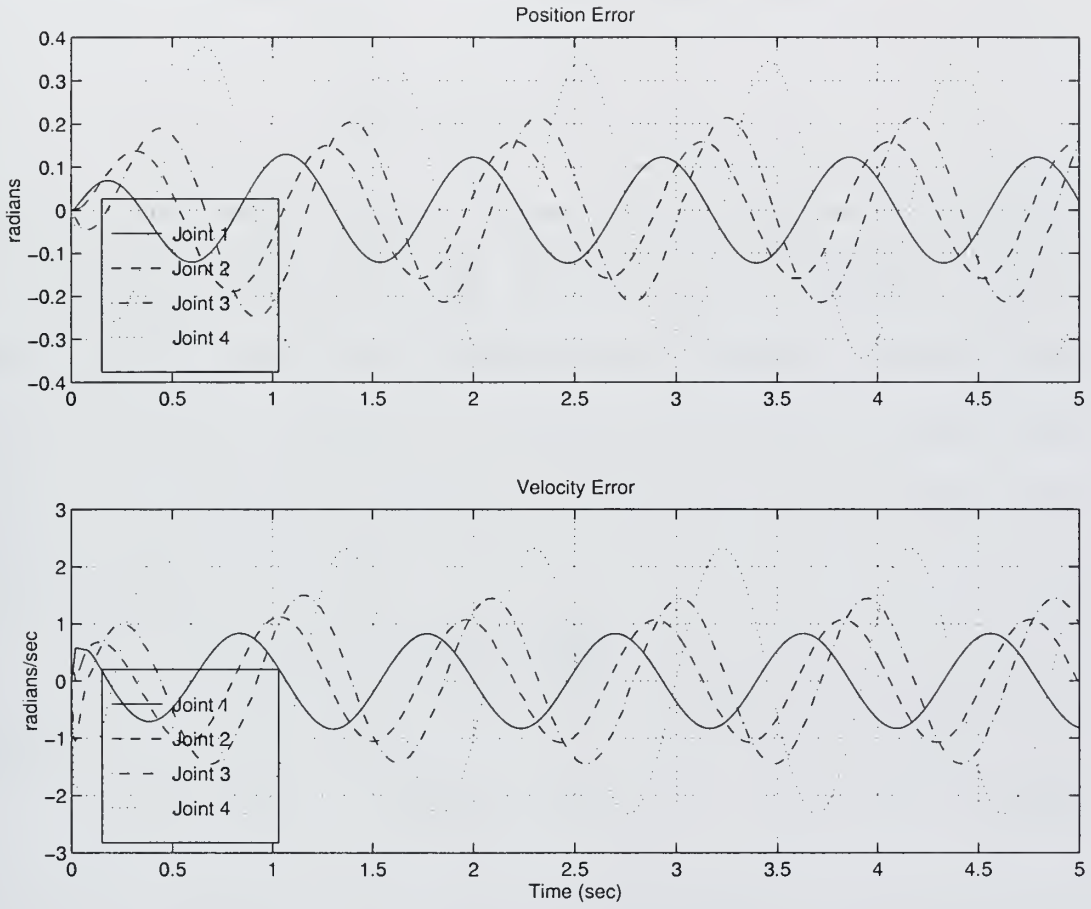

Figure 3-6: Position and Velocity Errors For the Initial LQR Control Design

3.6 "Computed Torque" Approach

Another method of control system design more suitable for this application is outlined by Slotine in *Applied Nonlinear Control* [11]. Although Slotine presents the concept as a nonlinear technique, it is also well suited for linear system applications. It is clear that for the prescribed motion of the spine to follow Equation 2.1,

$$y(x,t) = a(x)sin(kx - \omega t)$$

the links must also follow sinusoidal motions that can be solved for analytically, but are most easily derived numerically by calculating the amplitudes and phase differences between them. Since the links do follow sinusoids, the derivatives are smooth and continuous. Therefore, for normal swimming motion, the state vector is known for all time and the input can be solved for in the state space system (Equation 3.13):

$$\dot{\mathbf{x}} = \mathbf{A}\mathbf{x} + \mathbf{B}\mathbf{u}$$

as follows:

$$\mathbf{B}\mathbf{u} = \dot{\mathbf{x}} - \mathbf{A}\mathbf{x} \tag{3.17}$$

using Gaussian elimination or any other method. The $\mathbf{u}$ that is calculated, if input to the system, should give exactly the desired state output at every time instant. The problem, however, is that the plant is second order, acting as a double integrator. Therefore, the open loop system cannot track position or velocity, which are unknown integration constants. Proportional/derivative (PD) control can be used to provide position and velocity tracking control. It is appropriate now to declare some controller performance specifications. Certainly, the most important specification for

this system is that it mimic the live fish motion accurately enough so as to make the difference negligible in the testing environment. A challenging tracking specification would be 1% in position and velocity error magnitude, which is approximately 0.3 radians (caudal fin maximum) $\times 1\% = .003$ radians of average error. The velocity specification is similar: 0.3 (radians) $\times 2\pi$ (radians/sec) $\times 1\% = .019$ radians/sec of average velocity error. Admittedly, I would not have chosen such ambitious control specifications if I had not seen the results of this design approach, but as will be shown, the specifications are met. The final controller design in shown in Figure 3-7. The input is $\mathbf{u}$, computed using Equation 3.17 and the desired position, Pd and velocity, Vd are fed into the system as infinitely fast observers. The error signals are multiplied by the gains calculated using the LQR method outlined in Section 3.2. The actual gains calculated are displayed here for curiosity's sake:

$$K_{prop} = \begin{bmatrix} 11591 & -5561 & -1613 & 385 \\ 2241 & 5209 & -3828 & 596 \\ 899 & 1068 & 1520 & 252 \\ 175 & 161 & 248 & 1519 \end{bmatrix}$$

$$K_{deriv} = \begin{bmatrix} 11026 & -5938 & -1972 & 38 \\ 1991 & 4859 & -4130 & 246 \\ 767 & 874 & 1266 & -35 \\ 87 & 30 & 75 & 1308 \end{bmatrix}$$

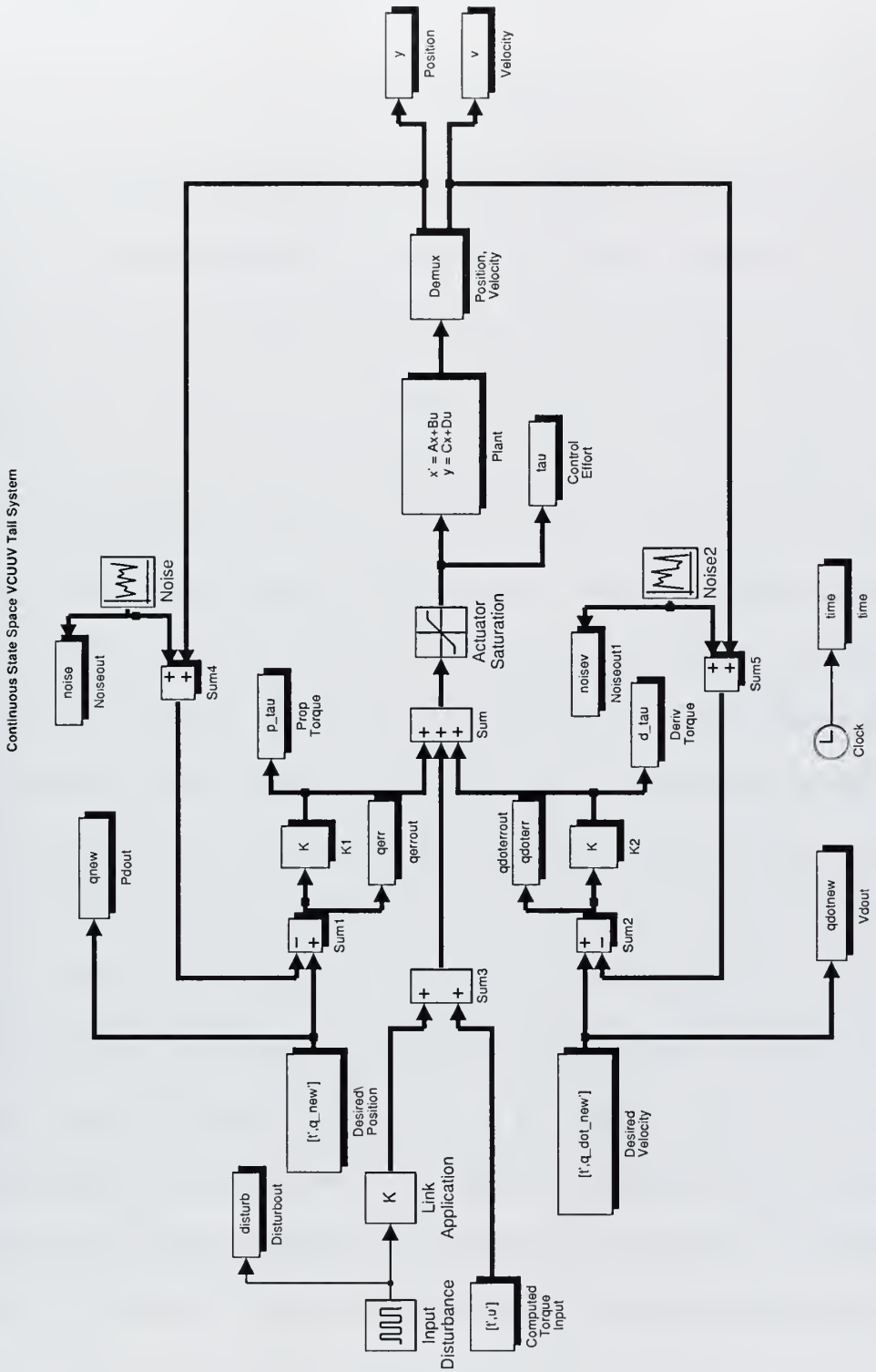

Figure 3-7: Computed Torque Controller Design

After receiving the calculated torque input, the controller is now using the error in the control law for the error as a disturbance on the system:

$$\dot{\tilde{\mathbf{x}}} = \mathbf{A}\tilde{\mathbf{x}} + \mathbf{B}\tilde{\mathbf{u}}$$

and since the system matrices $(\mathbf{A}, \mathbf{B})$ do not change, the dynamics of the system of course, do not change and the controller gains can be calculated the same way as in Section 3.2. No integral term is desired, in the controller since the system is following a sinusoidal input and an integral will just add unwanted dynamics. Steady-state error does not need to be minimized, as the system is not intended to actually regulate for any length of time to a reference input. Figures 3-8 and 3-9 show the system outputs plotted with the desired outputs. shows the excellent performance of the controller. The actual and desired positions are plotting very nearly on top of one another. In order to view the error, it is plotted separately in Figure 3-10. The error is so small as to be insignificant in this application. The total control efforts are plotted in Figure 3-11. and it can be seen that they fall easily within the available actuator efforts in Table 3.5. The testing that I have done to my model is all at 1.0Hz, which is near maximum frequency for the system and considered to be a good metric value for stressing the system. Also, the system diagram does not include transforms between linear and angular positions, etc., or servovalve current to torque since the former transform has been shown to be easily linearized to a simply scalar function and the latter transformation is simply algebraic with no dynamics. The performance results are not affected, and it is a simple matter to code the transformation along with the control algorithm when implementing it in the VCUUV.

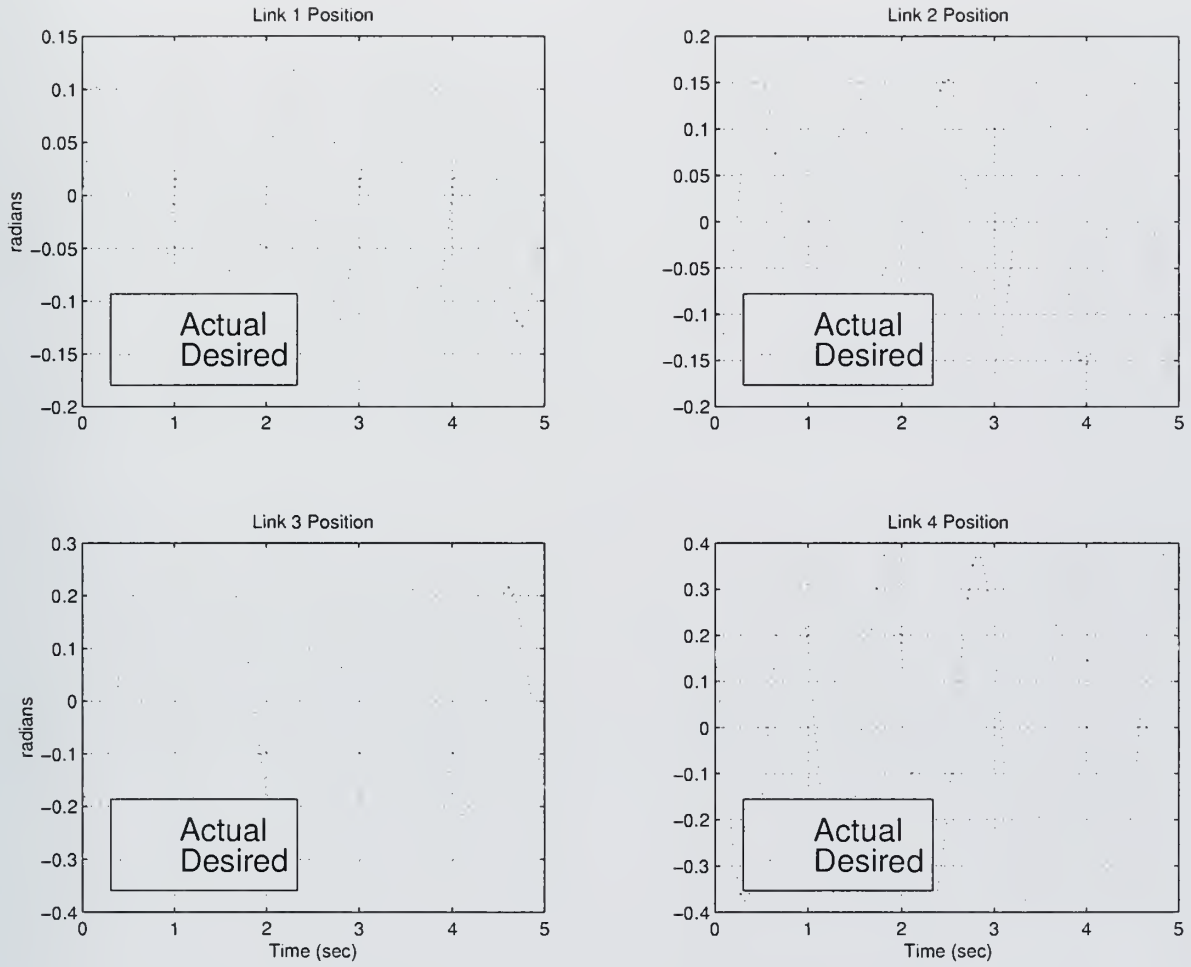

Figure 3-8: Desired and Actual Positions of Links 1-4 for Computed Torque Controller

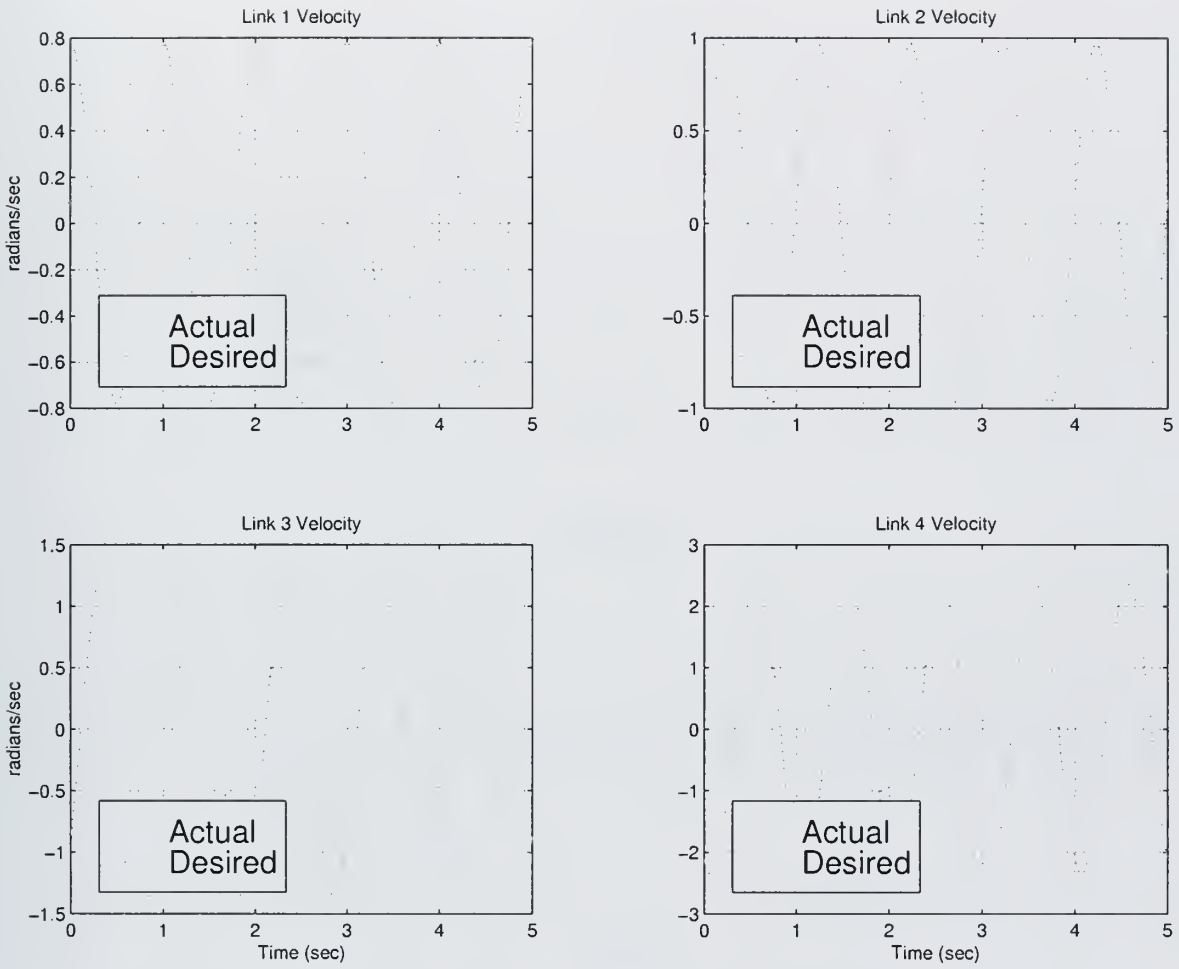

Figure 3-9: Desired and Actual Velocities of Links 1-4 for Computed Torque Controller

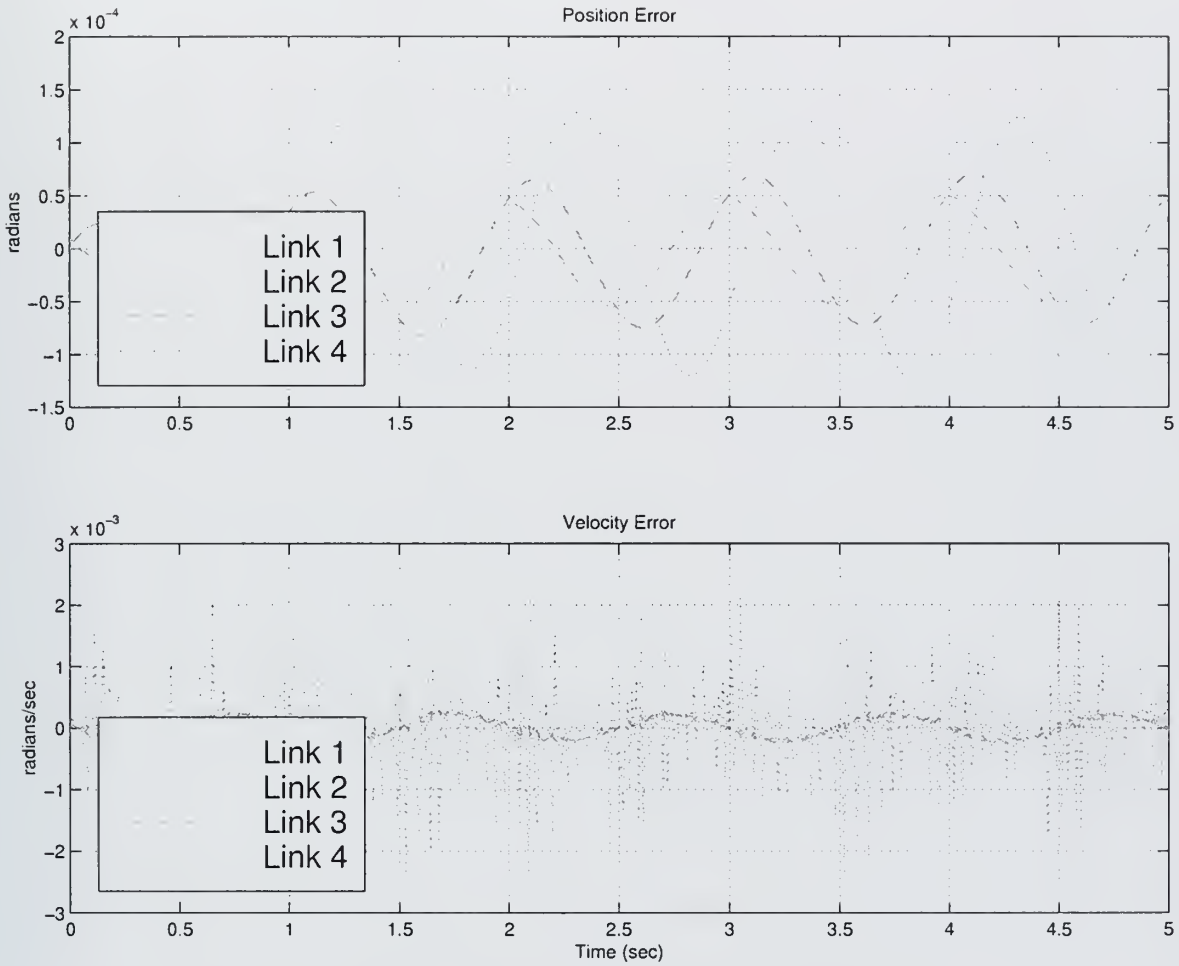

Figure 3-10: Position and Velocity Errors for the Computed Torque Controller

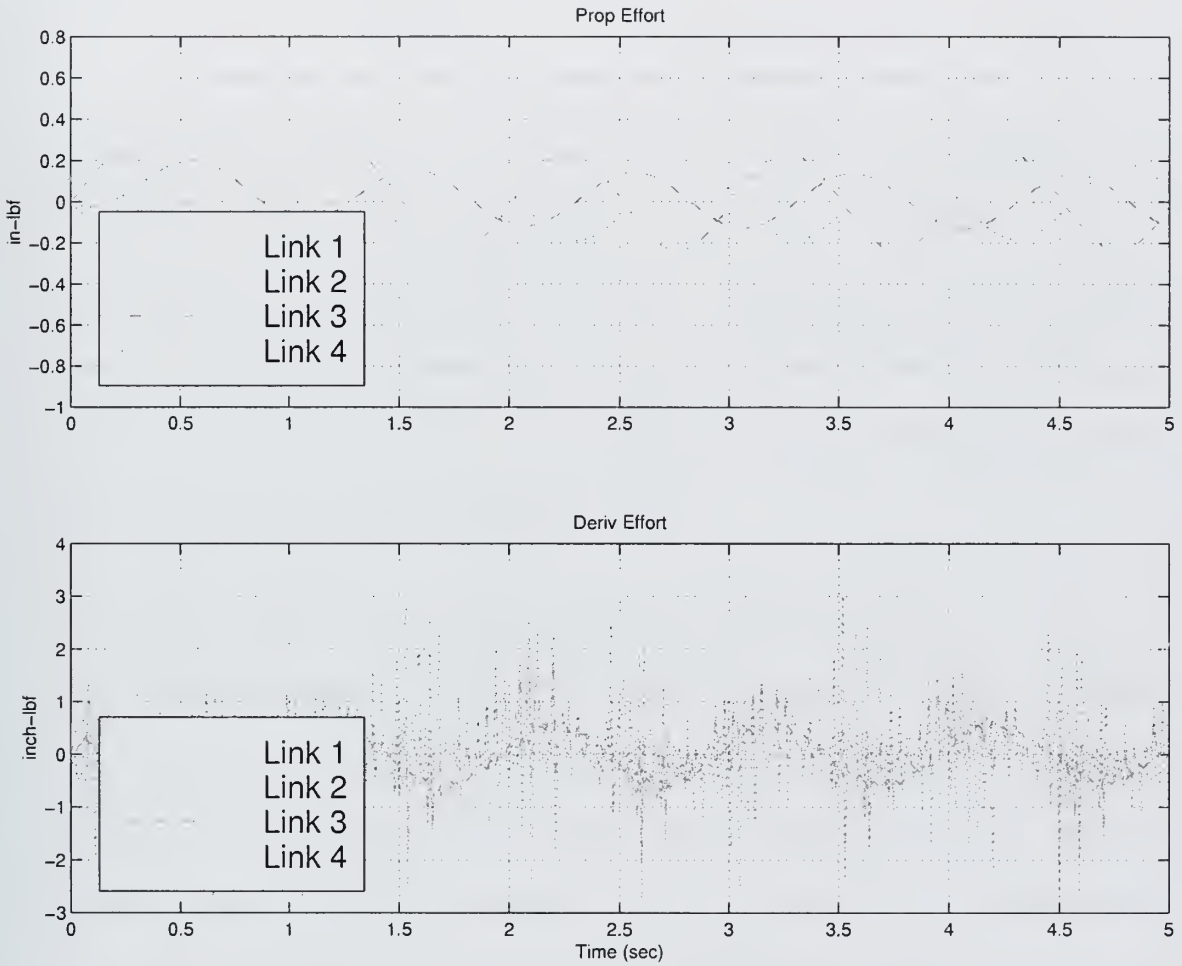

Figure 3-11: Control Efforts for Computed Torque Controller

3.6.1 Disturbance and Noise Rejection

The computed torque control method can be shown to be excellent at disturbance and noise rejection. The actual VCUUV prototype has additional sources of nonlinear effects that are neglected here:

- Sensor quantization and zero order hold

  The quantization is small and will pose no serious consequence to the system by itself; however, the zero order hold of the digital sampling system at a sample frequency of 100 Hz, which is low, may have a significant effect. This was not looked at in this study due to time constraints and available analysis tools. Simulink did not handle the zero order hold well in the model using any integration method. In order to show some robustness at the sensors, I placed noise appropriately, and I discuss this later.

- The derivative taken at the position sensor to calculate velocity

  Once again, Simulink did not handle the derivative well. Noise was applied to the sensors to determine the ability of the system to reject noise. Shown in Figure 3-12 is the noise applied to the position sensor in Figure 3-7 and the velocity sensor. The noise represents, as best as possible, the quantization error, zero order hold effect, and the derivative applied to the position in the actual prototype to obtain velocity.

Further justification for my assumptions listed above is the fact that the VCUUV prototype has operated with a decoupled (SISO for each link) PD control that has shown little problem with zero order hold or noise. In this simulation, I have placed a 150 inch-lbf torque disturbance on the caudal fin to investigate the effect of the

fin's possible reaction with shed vortices from the body. In order for the VCUUV to properly simulate the live tuna, the tail must not have a significant deviation from these torque disturbances. The disturbance was also tested on other links which always resulted in lesser effects. As can be seen by the output in Figures 3-14 and 3-

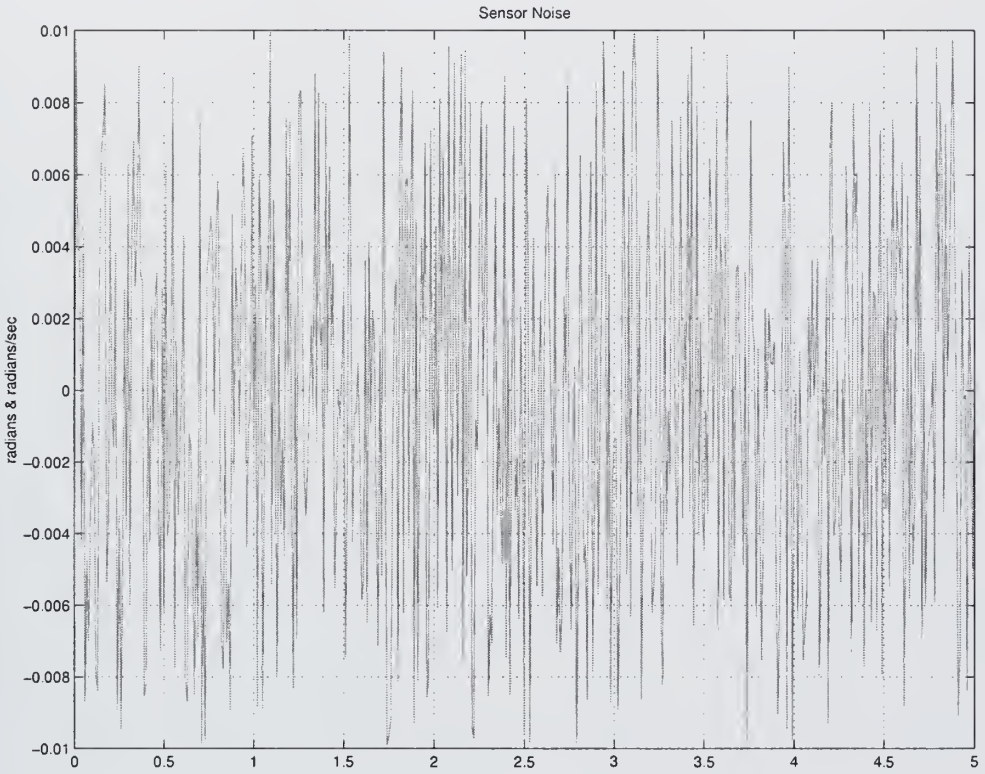

Figure 3-12: Noise Applied to Position Sensor and Velocity Sensor

15, the system responds well to the noise and disturbance with errors on the order of .006 radians ($\approx .35°$) and .13 radians/second ($\approx 7.4°$/second), the peak errors being caused by the input disturbance torque of 150 inch-lbf applied to the caudal fin as shown in Figure 3-13. The position and velocity errors are shown in Figure 3-16. Control effort signals are shown in Figure 3-18; the noise definitely affects the signals, but does not greatly affect the outputs. The overall control effort shows some effect from the noise also, but not a significant amount (Figure 3-18). To explore the worst

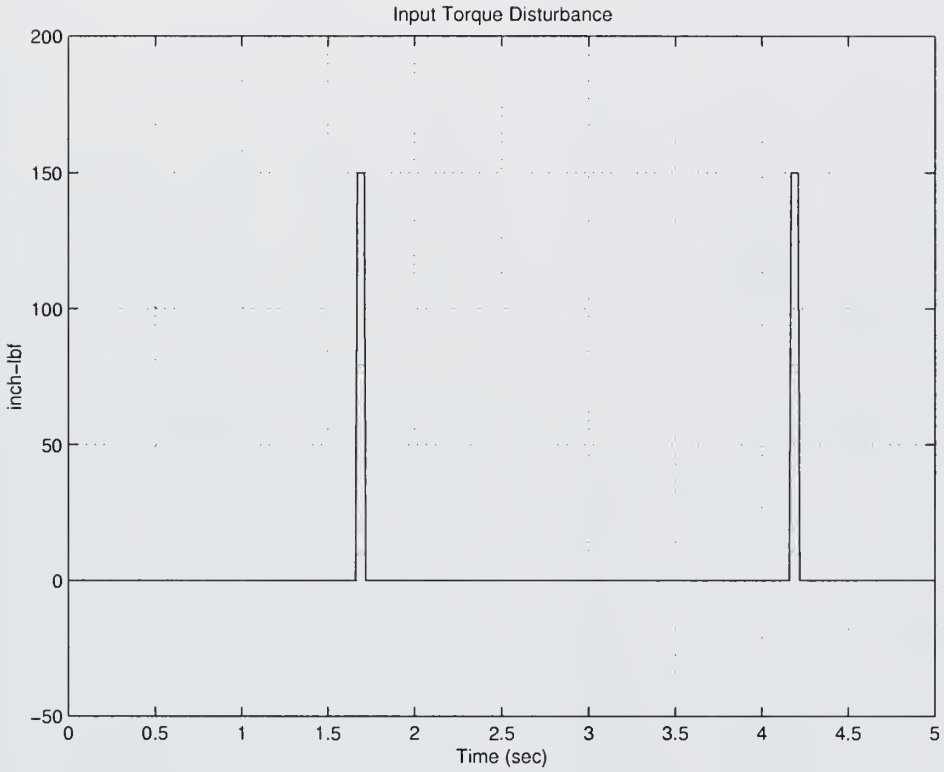

Figure 3-13: Input Disturbance Applied to Computed Torque Control System

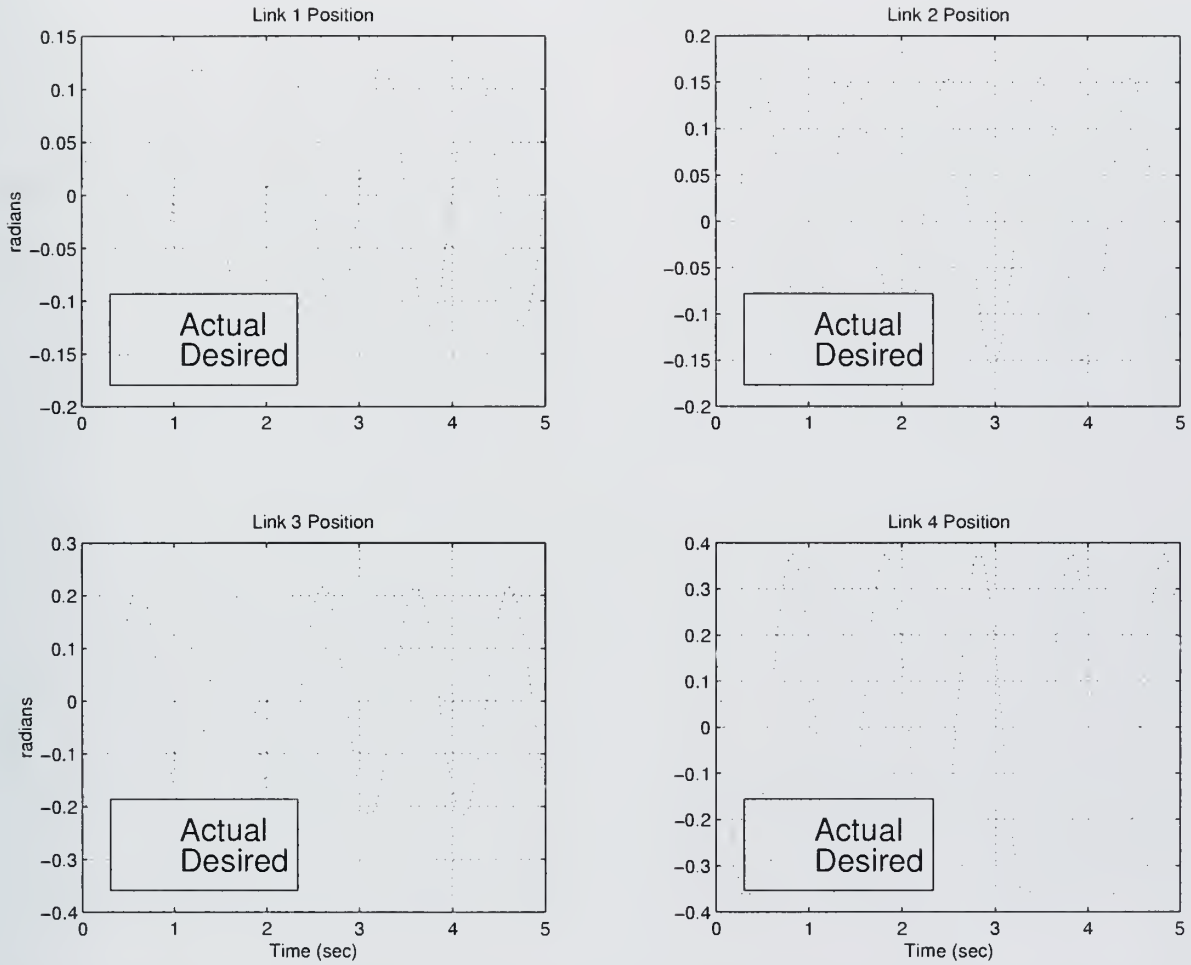

Figure 3-14: Desired and Actual Positions of Links in the Presence of Noise and Input Disturbance

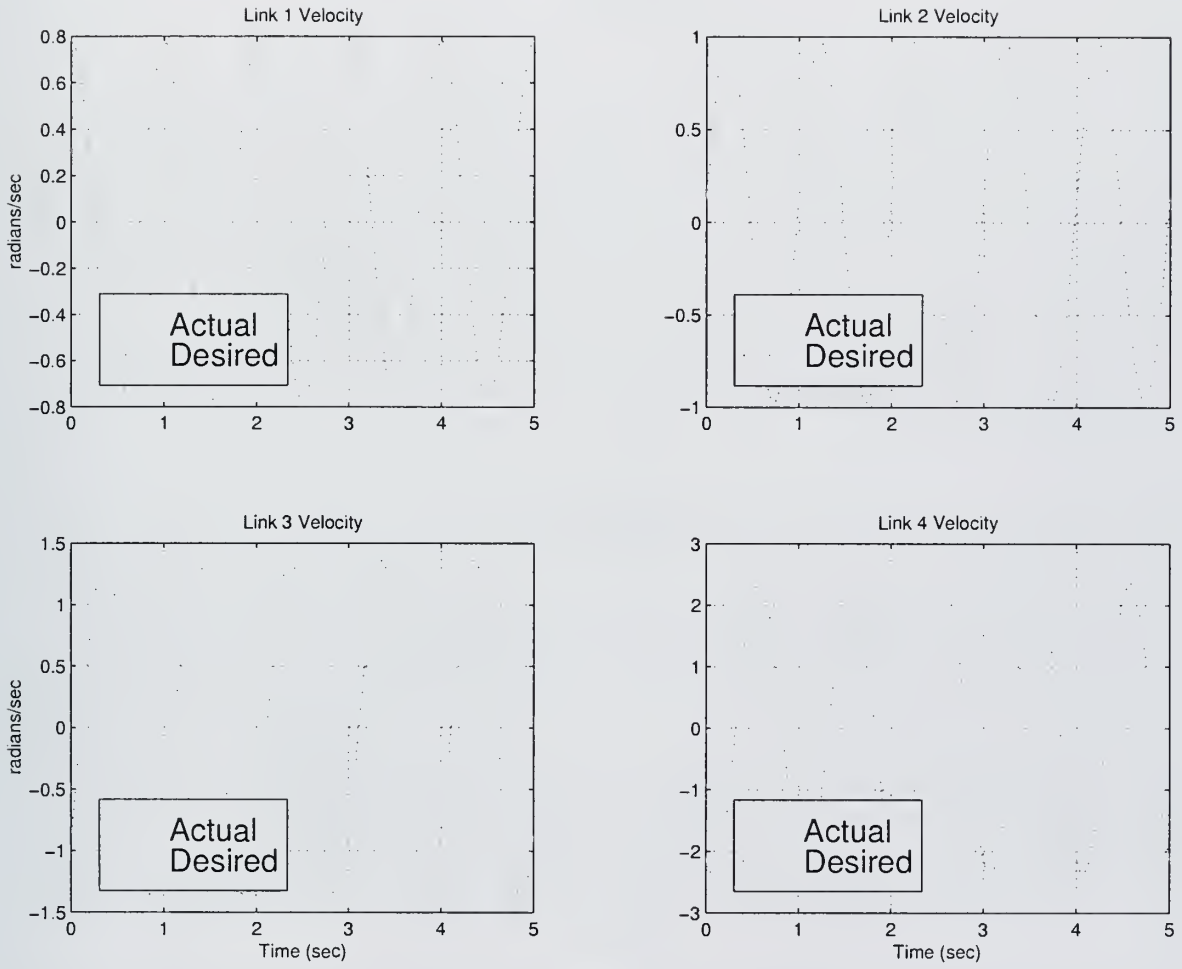

Figure 3-15: Desired and Actual Velocities of Links in the Presence of Noise and Input Disturbance

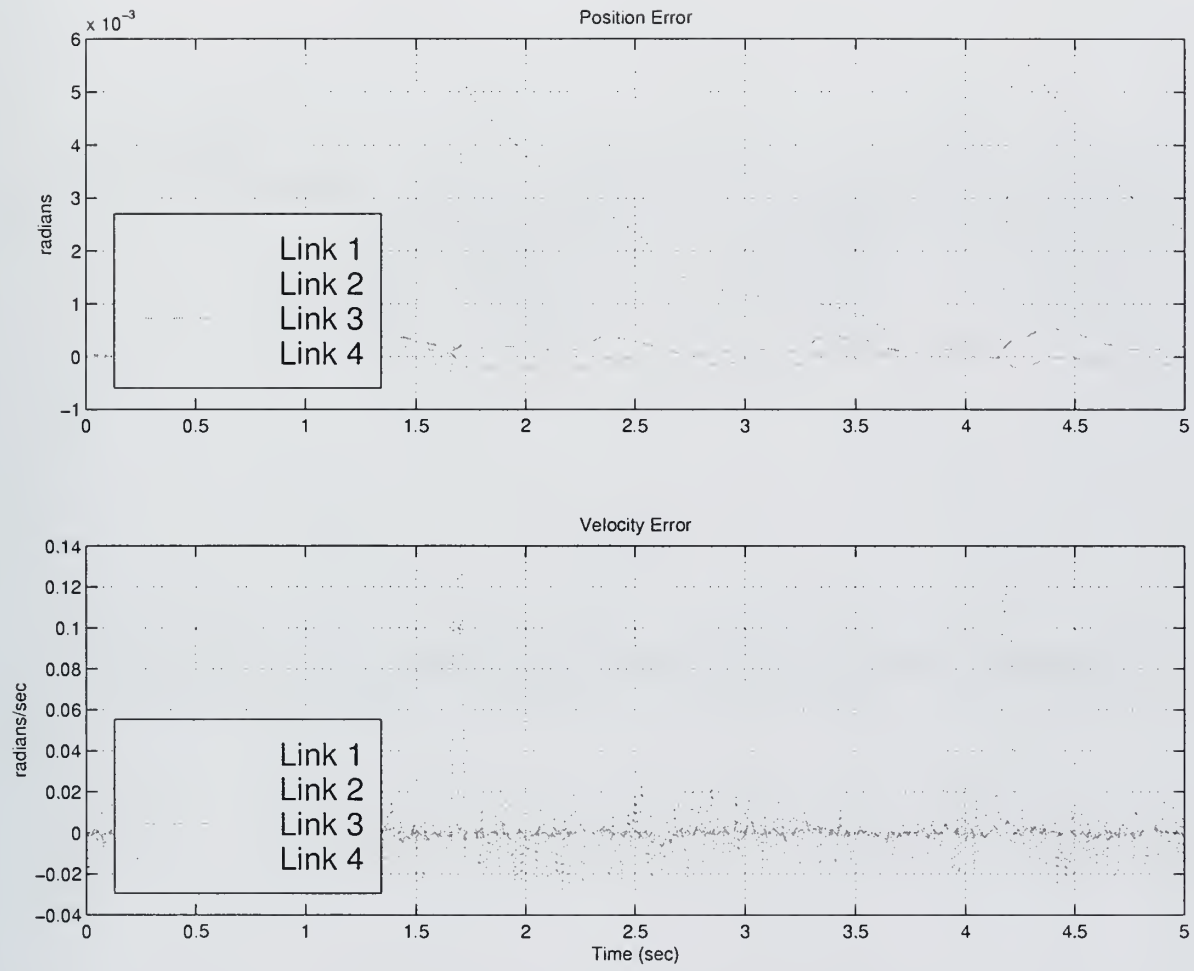

Figure 3-16: Position and Velocity Errors of the System in the Presence of Noise and Input Disturbance

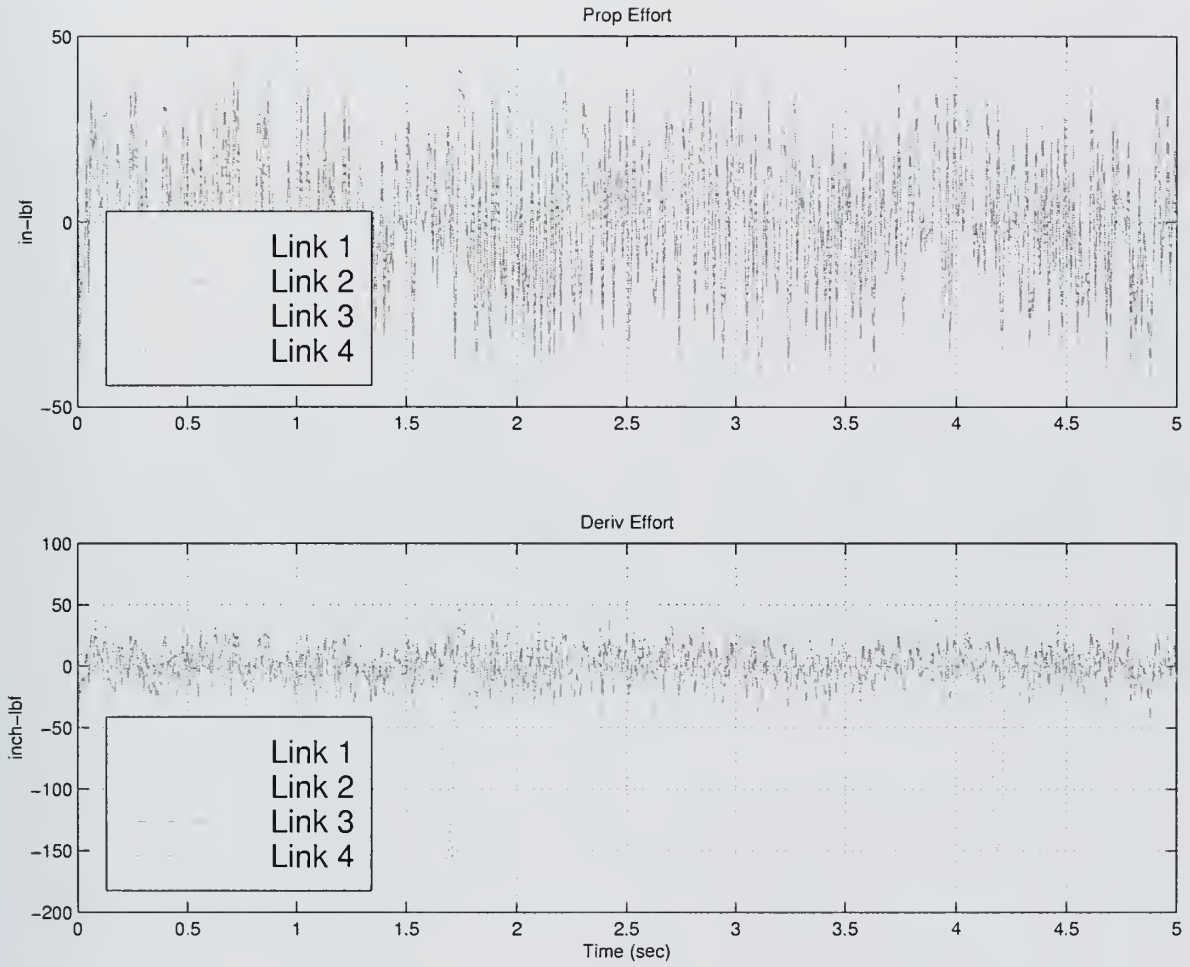

Figure 3-17: Proportional and Derivative Control Effort Signals in the Presence of Noise and Input Disturbances

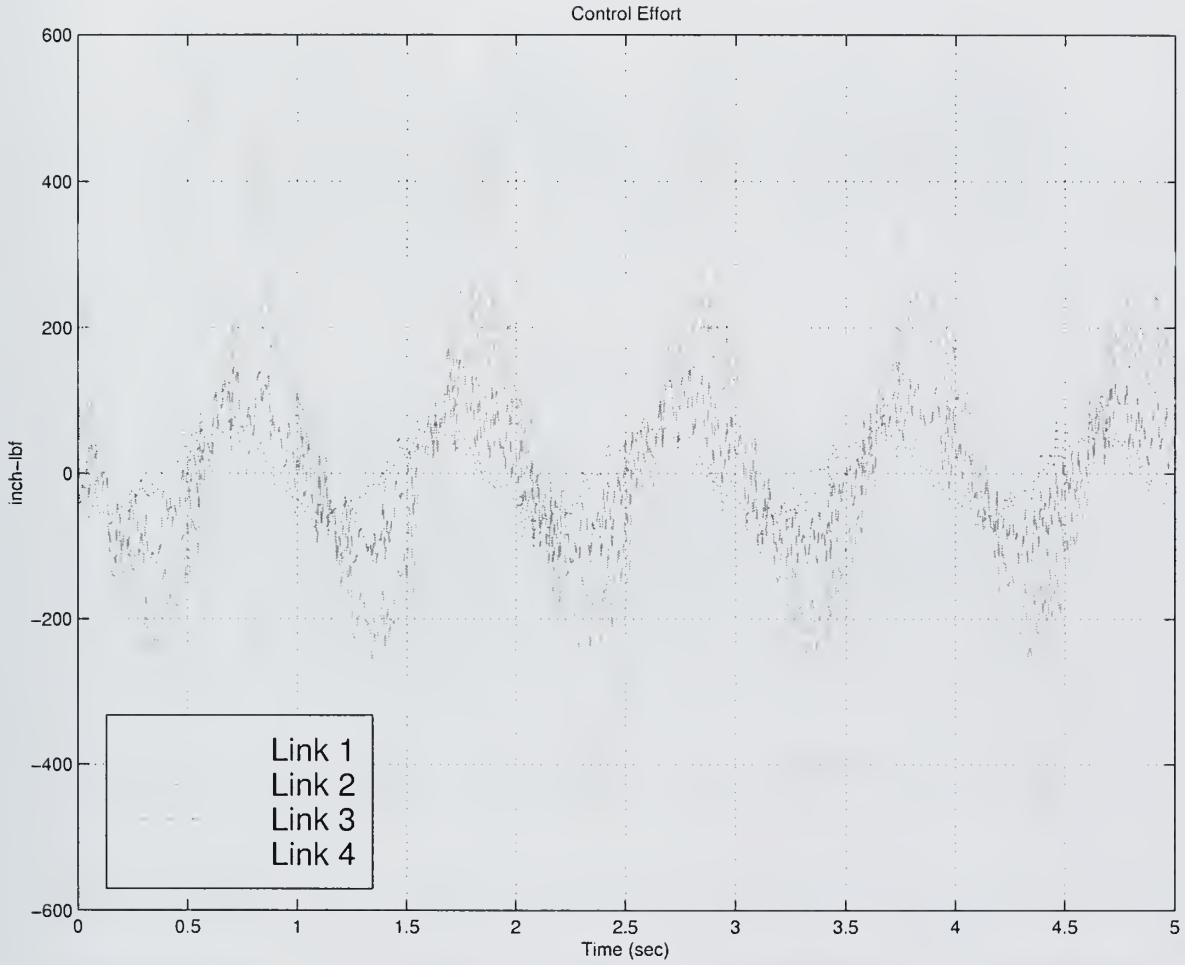

Figure 3-18: Total Control Effort Signal in the Presence of Noise and Input Disturbances

case for noise, I increased the noise levels at the position sensor and the velocity sensor to .02 radians and .2 radians/second, respectively (see Figure 3-19). The same input disturbance is still applied, but not shown here. The system performance begins to degrade appreciably at this point, as can be seen in Figures 3-20 and 3-21.

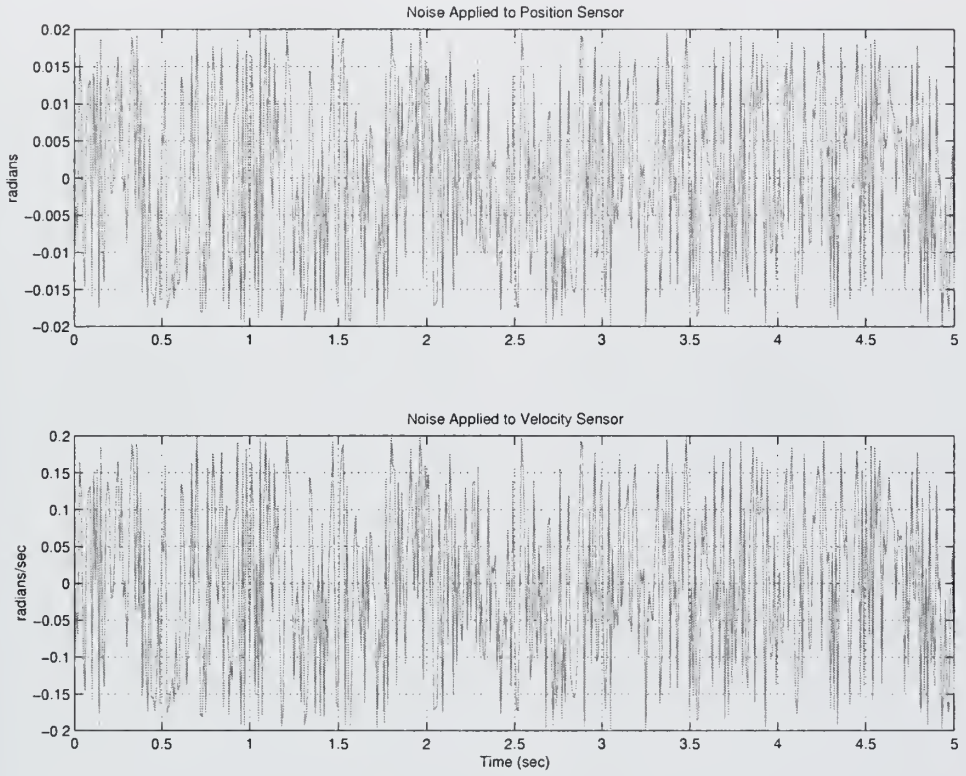

Figure 3-19: Noise Applied to the Position Sensor, top, and Velocity Sensor, bottom

Thus, the system will be subject to a noisy environment, but the noise input here is 0.02 radians ($\approx 1°$) and .2 radians/second ($\approx 10°$/second) which is extremely large and unlikely to be present at any time.

3.6.2 Model Error Sensitivity

To test the sensitivity of my system to model errors, I varied the values of the matrices in my dynamics equations by $\pm 25\%$ to see how well the system tracked the desired

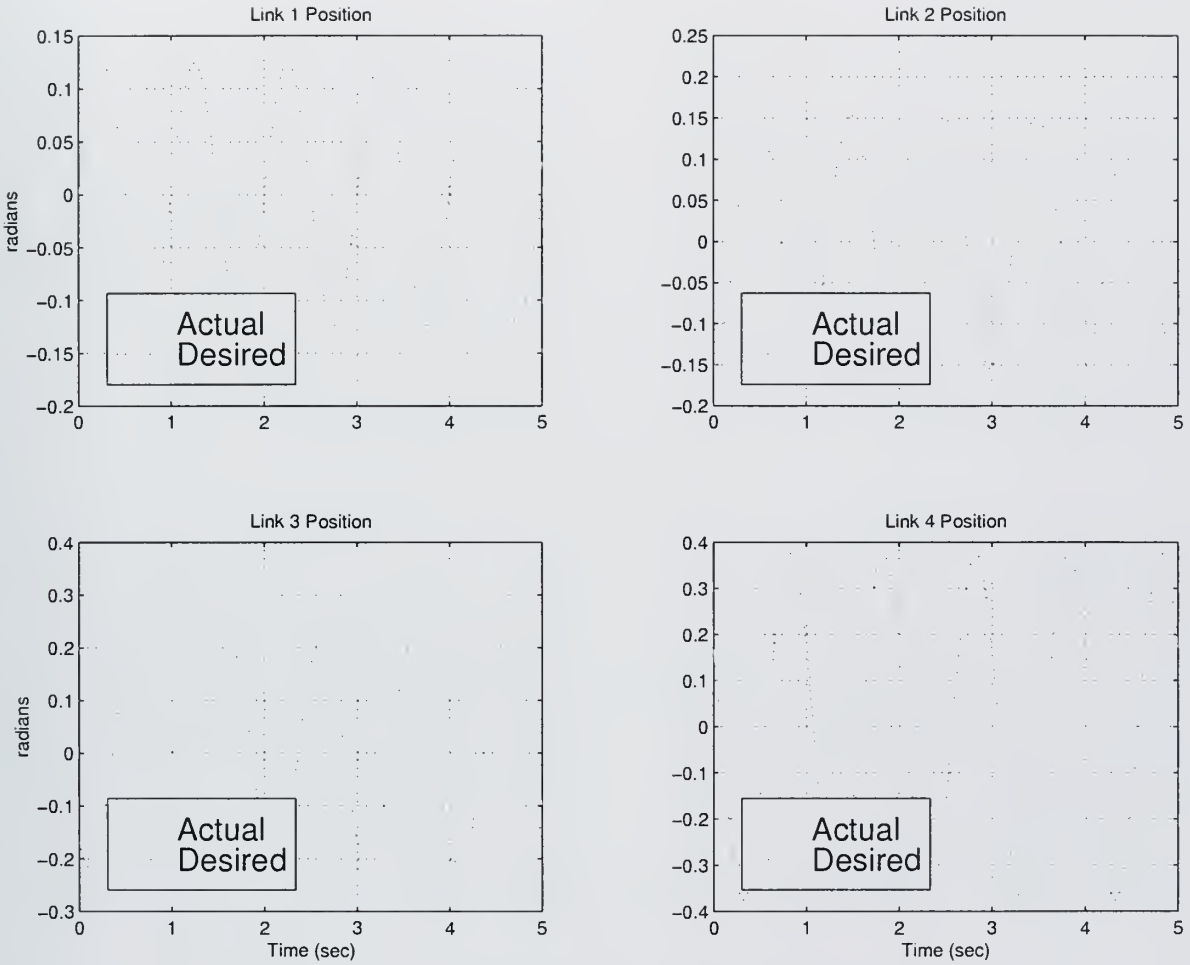

Figure 3-20: Desired and Actual Positions of Links in the Presence of Increased Noise

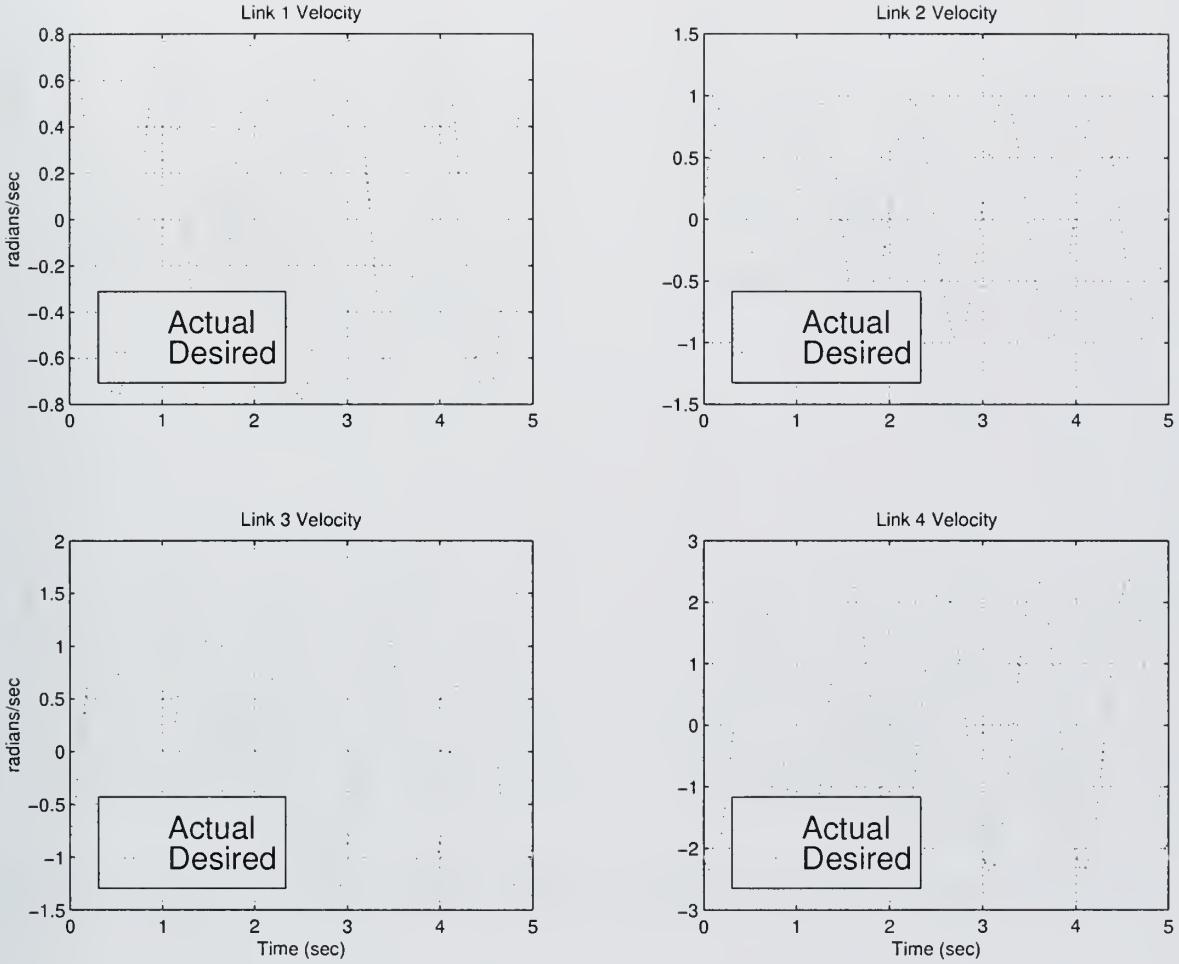

Figure 3-21: Desired and Actual Velocities of Links in the Presence of Increased Noise

sinusoid at 1.0 Hz. First, the model parameters were perturbed −25%. The position and velocity outputs are shown in Figures 3-22 and 3-23. The errors are plotted in Figure 3-24. As can be seen from the errors, the control system is robust enough

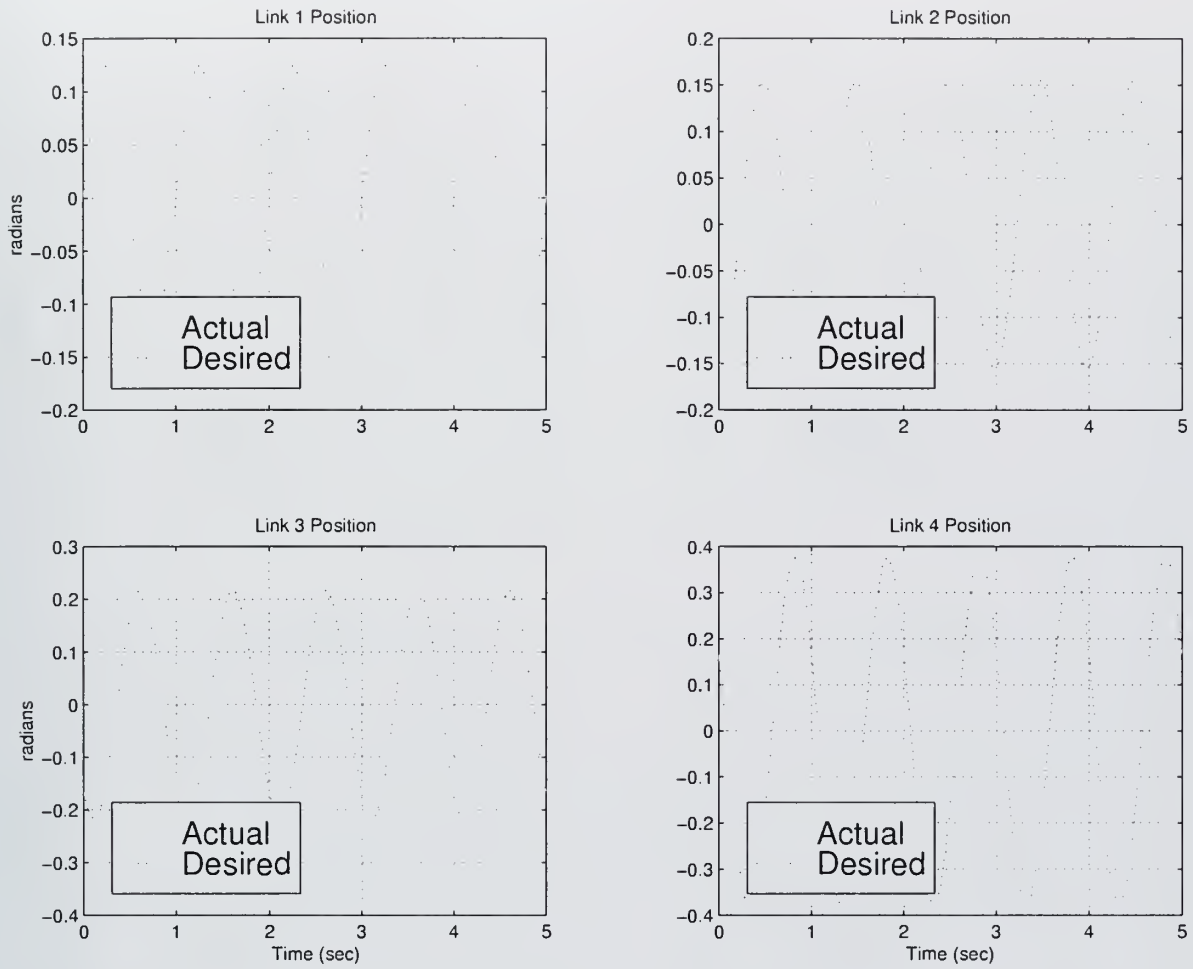

Figure 3-22: Desired and Actual Positions of Links in the Presence of 25% Overestimation of Model Dynamic Parameters

to handle such large model errors. Now, increasing my model parameters 25%, the following trajectories are output (see Figures 3-25 and 3-26). Errors are plotted in Figure 3-27, and again, the errors clearly meet the specification of 1% average.

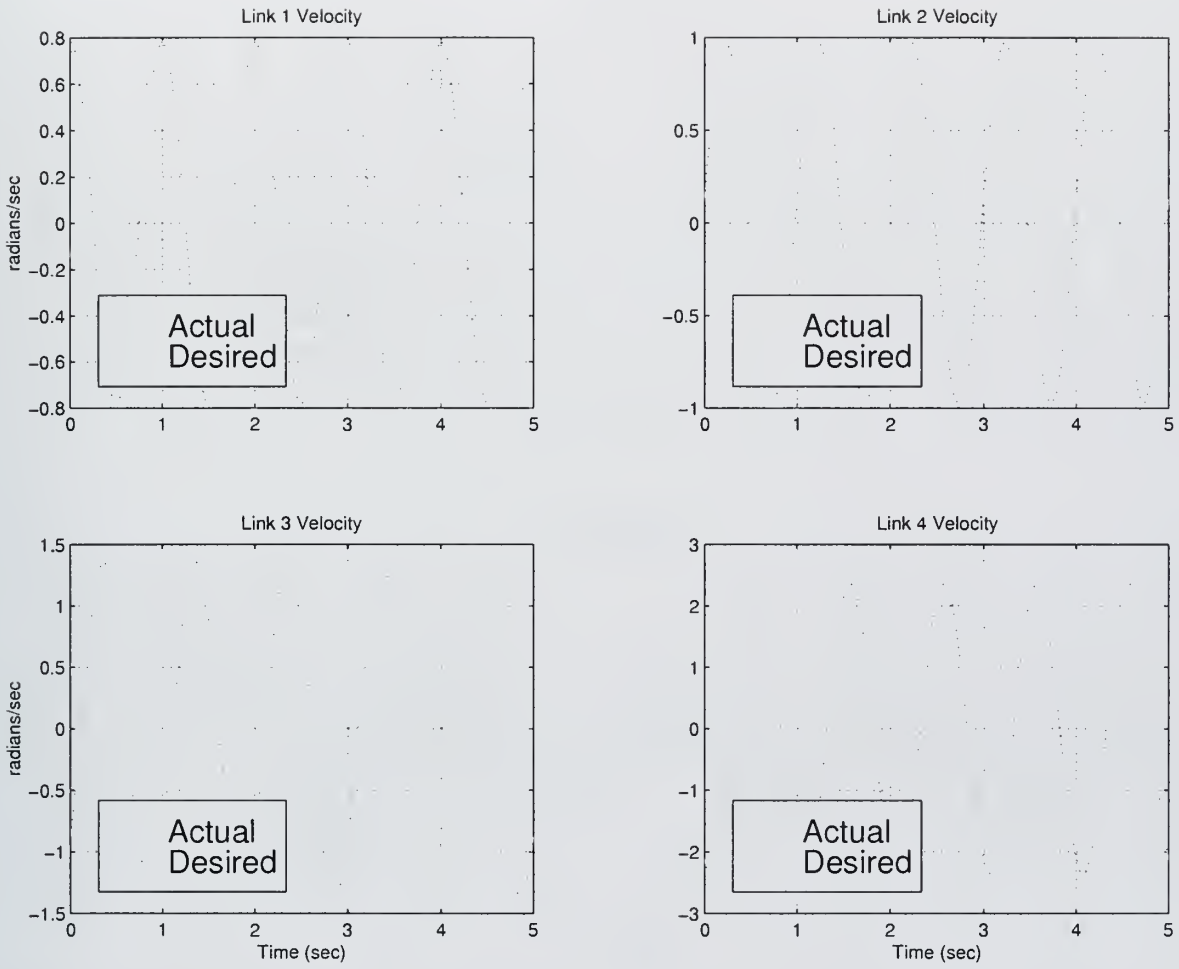

Figure 3-23: Desired and Actual Positions of Links in the Presence of 25% Overestimation of Model Dynamic Parameters

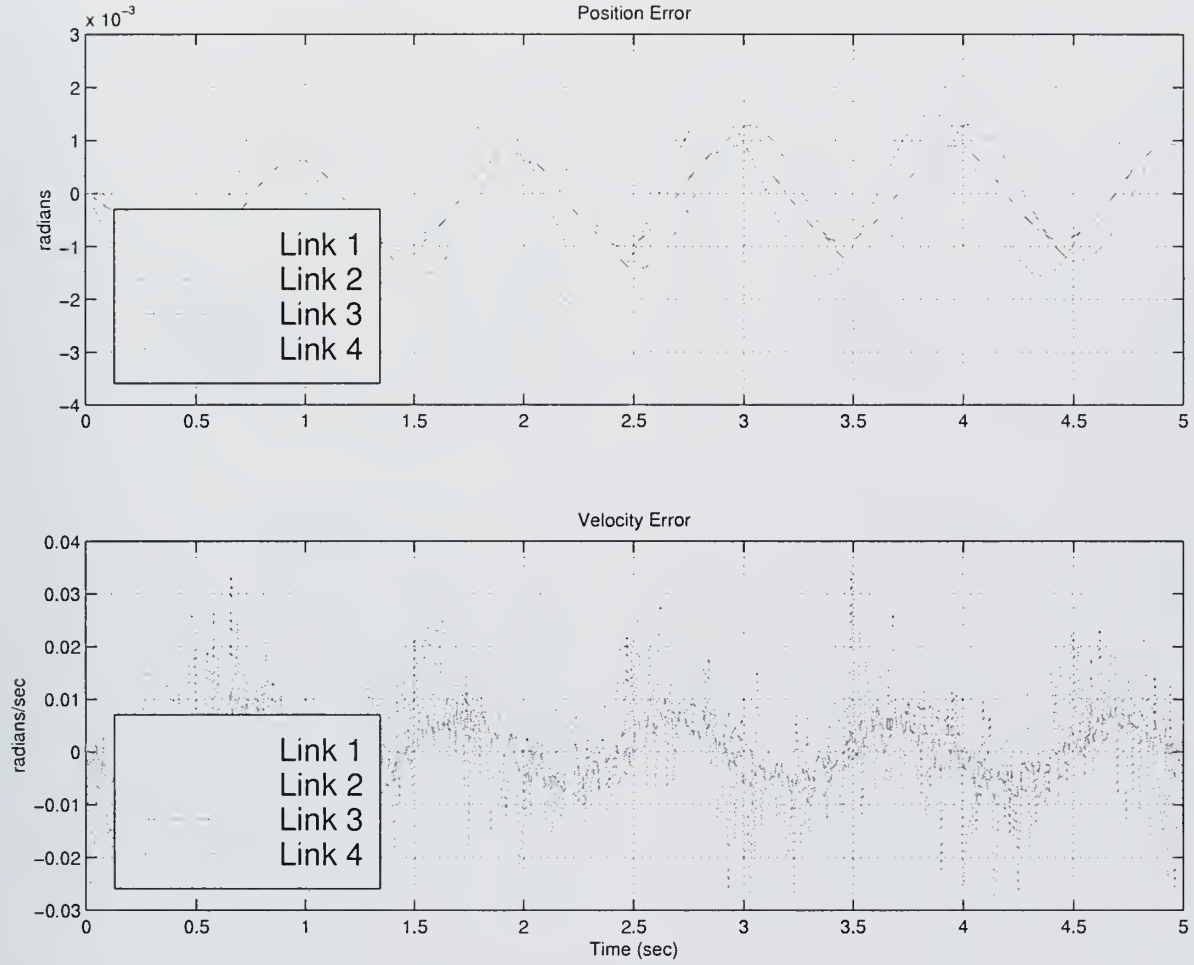

Figure 3-24: Position and Velocity Errors of Links in the Presence of 25% Overestimation of Model Dynamic Parameters

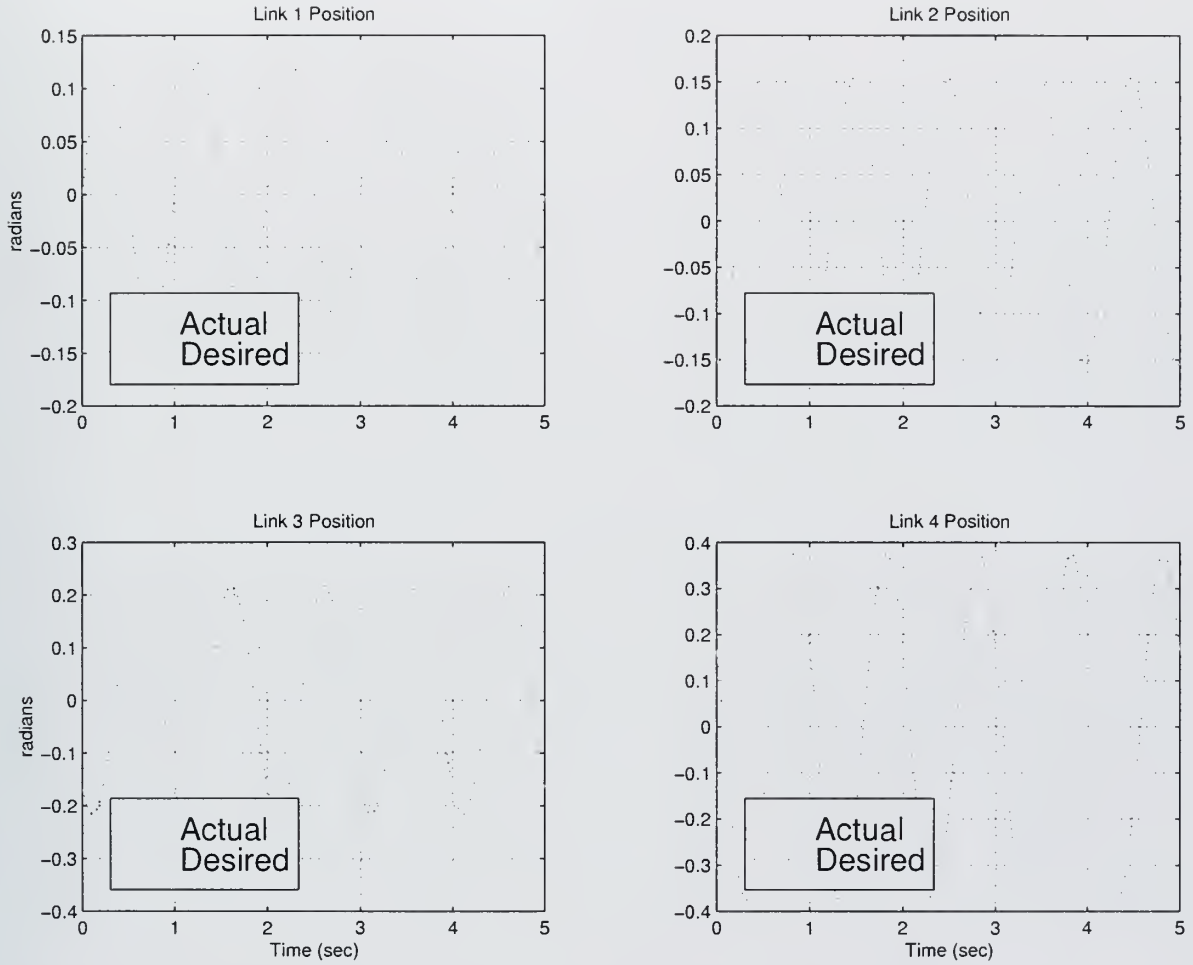

Figure 3-25: Desired and Actual Positions of Links in the Presence of 25% Underestimation of Model Dynamic Parameters

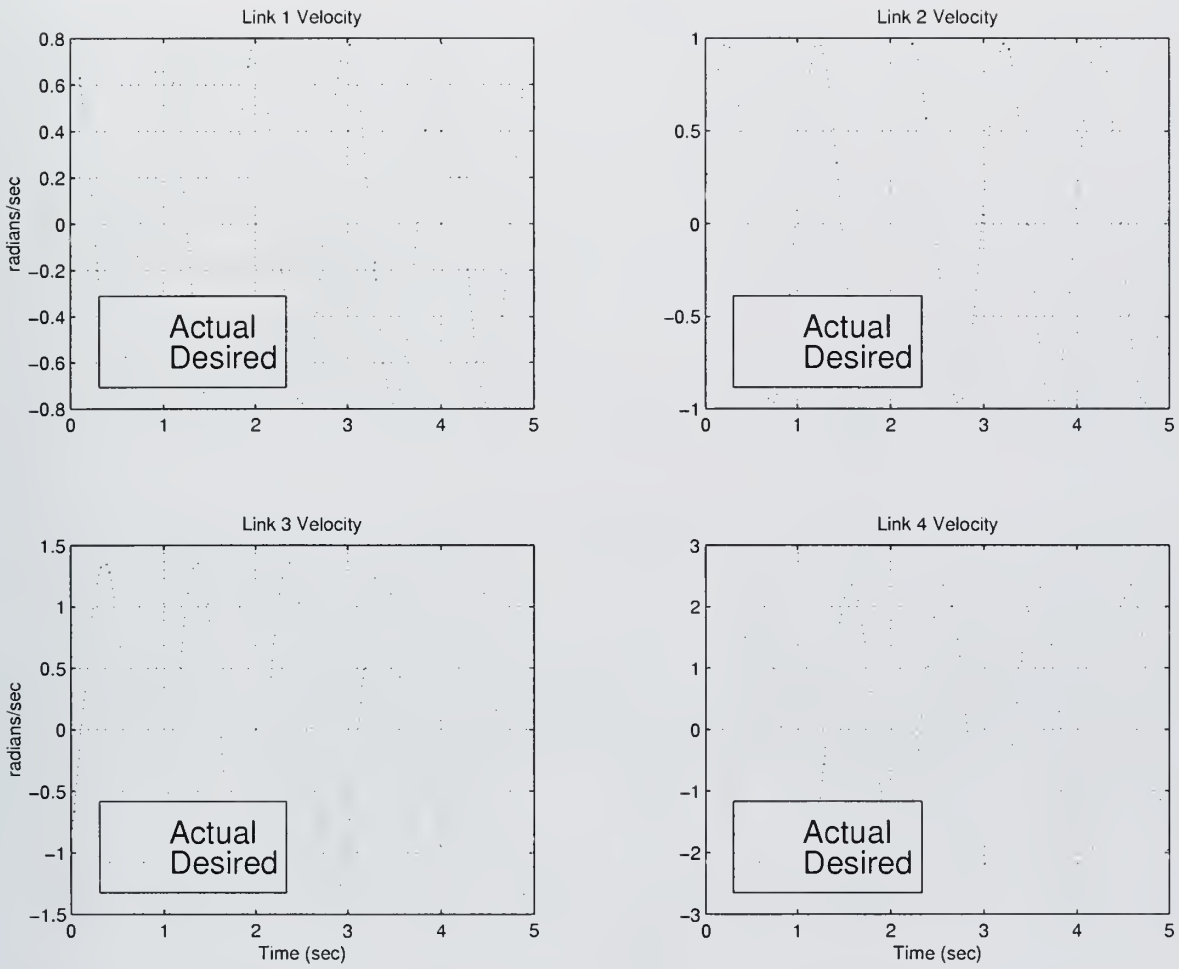

Figure 3-26: Desired and Actual Positions of Links in the Presence of 25% Underestimation of Model Dynamic Parameters

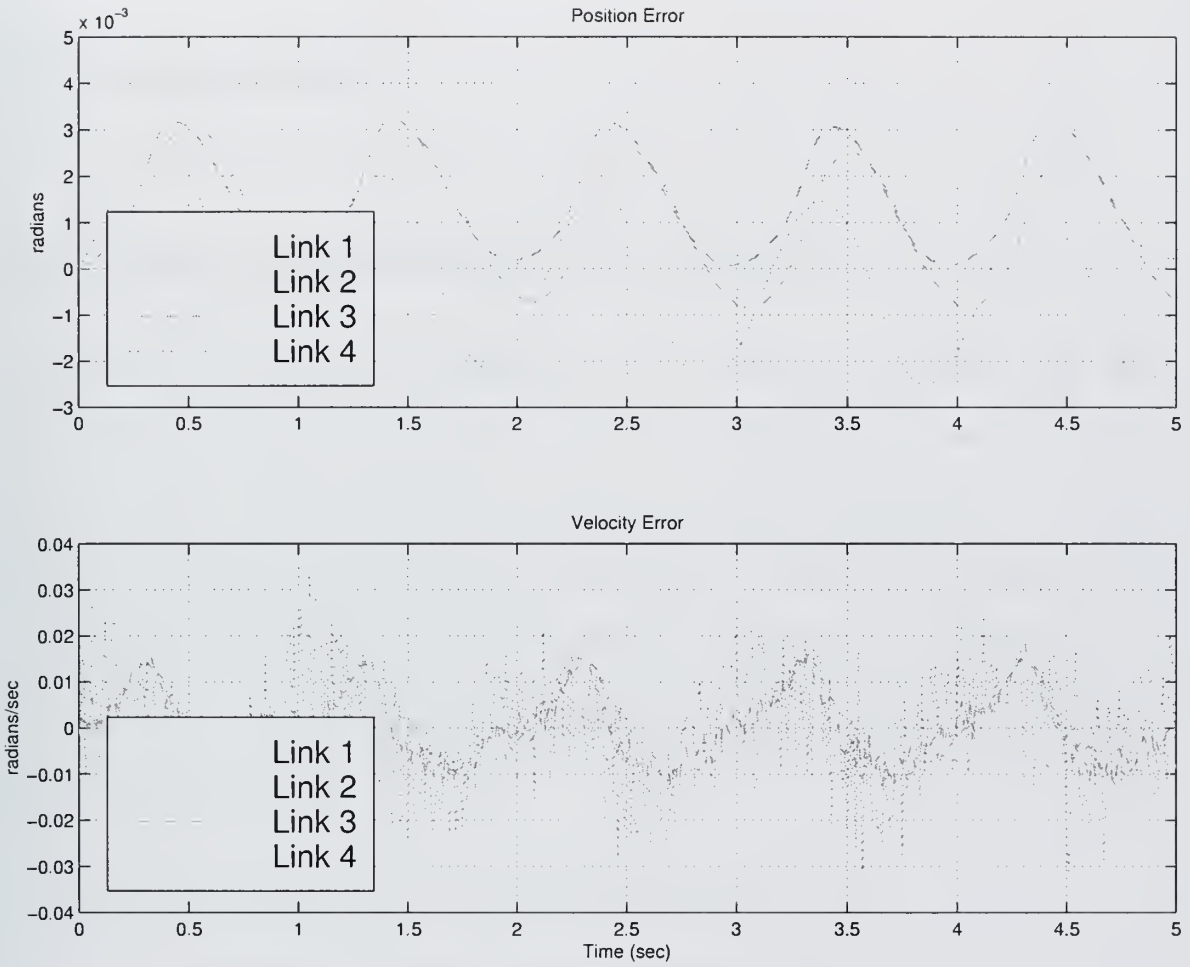

Figure 3-27: Position and Velocity Errors of Links in the Presence of 25% Underestimation of Model Dynamic Parameters

Chapter 4

Conclusions

4.1 Controller Performance and Robustness

Controller performance can be a difficult concept to quantify, especially in this case. For instance, it was shown in Section 3.5 that a controller that does well in step response may not do well in tracking a signal, particularly if the input is at a high frequency relative to the bandwidth of the system. Overall, the computed torque controller performs well in simulation. The system shows good noise and disturbance rejection, and is tolerant to significant model error. In simulation, the control system demonstrated the ability:

- to reject noise that is on the order of 20 quantization levels.
- to reject disturbances on the order of 15% of the input torque.
- to reject model parameter errors of 25%.

These were achieved with less than 1% average error in position and velocity output. The computed torque method is very robust and also very simple to implement in the VCUUV. The torque input can be computed before the start of a data run or mission, and then the states and inputs placed into a look-up table that allows periodic and

indefinite (the ability to repeat the motion by simply returning to the beginning of the lookup table without any discontinuities) access to the trajectory data. Since the estimation of the states is now given in a lookup table, the computations will go much faster than other control methods and there will be no sample delay.

4.2 Summary

There are three major sections of this work, the first being the derivation of Lighthill's EBT for the discrete tail system, the Lagrangian dynamics derivation of the free-flood water, and the controller design. As it turns out, the control method will take care of many approximations and compounding errors, but it is still necessary to have a rough estimate of the loading in order to calculate the input torques. The control method has it's disadvantages also, namely, that it is more difficult to prearrange sudden or special maneuvers, such as starting or turning. Special care has to be taken to ensure that the torque inputs calculated are not above the limitations of the system. This should be easily taken care of in software with saturation, however. Overall, the system model is reasonably accurate and the controller is very robust.

4.3 Future Work

The most obvious task to be performed next is to implement this algorithm in the VCUUV. At the time of this writing, the VCUUV is undergoing initial testing with a decoupled PD controller at the University of New Hampshire, Durham, and time constraints preclude implementing the computed torque controller. One of my original goals when selecting this thesis topic was to develop a heading control for the VCUUV. After considering this possibility at length, it seemed like an extremely high-level task

given the unsteady hydrodynamics are not well understood. When the vehicle is off-course, what command could be given to the undulating motion to bring it back? How is the vehicle commanded to a new heading? Although it was decided that the heading control would be beyond the scope of this thesis, I have recognized possible solutions to this challenging problem:

- Bias the tail motion to "center" around a new $y = 0$ line (see Figure 2-6).
- Bias the caudal fin motion to create a "net" angle of attack through the swimming cycle. This could create a moment about the center of mass to bring the vehicle back to the desired heading.
- Model the VCUUV as a five link arm, treating the rigid forebody as the fifth link in the free-body system. To change heading, command the forebody to a new relative angle. Once the system settles, reset the tail motion center in-line with the forebody.

These suggestions could be looked at, and would be a logical extension of the work I've done.

The final suggestion for future work is to perform a system identification on the VCUUV to determine a very accurate system model. If this can be done, and it should be possible, then the computed torque method will be even more accurate and even more errors can be tolerated from noise in the sensors and analog-to-digital conversion effects.

Appendix A

Development of Dynamics Equations in Maple V

A.1 Define the Linear Jacobian Matrices

$$JL_1 := \begin{bmatrix} -Lc_1 \sin(\theta_1) & 0 & 0 & 0 \\ Lc_1 \cos(\theta_1) & 0 & 0 & 0 \end{bmatrix}$$

$$JL_2 := \begin{bmatrix} -L_1 \sin(\theta_1) - Lc_2 \sin(\%1) & -Lc_2 \sin(\%1) & 0 & 0 \\ L_1 \cos(\theta_1) + Lc_2 \cos(\%1) & Lc_2 \cos(\%1) & 0 & 0 \end{bmatrix}$$

$$\%1 := \theta_1 + \theta_2$$

$$JL_3 :=$$

$$[-L_1 \sin(\theta_1) - L_2 \sin(\%2) - Lc_3 \sin(\%1),\ -L_2 \sin(\%2) - Lc_3 \sin(\%1),\ -Lc_3 \sin(\%1),\ 0]$$

$$[L_1 \cos(\theta_1) + L_2 \cos(\%2) + Lc_3 \cos(\%1),\ L_2 \cos(\%2) + Lc_3 \cos(\%1),\ Lc_3 \cos(\%1),\ 0]$$

$$\%1 := \theta_1 + \theta_2 + \theta_3$$

$$\%2 := \theta_1 + \theta_2$$

$$JL_4 :=$$

$$\Big[-L_1 \sin(\theta_1) - L_2 \sin(\%3) - L_3 \sin(\%2) - Lc_4 \sin(\%1),$$

$$-L_2 \sin(\%3) - L_3 \sin(\%2) - Lc_4 \sin(\%1),\ -L_3 \sin(\%2) - Lc_4 \sin(\%1),\ -Lc_4 \sin(\%1)\Big]$$

$$\Big[L_1\cos(\theta_1) + L_2\cos(\%3) + L_3\cos(\%2) + Lc_4\cos(\%1)\,,$$
$$L_2\cos(\%3) + L_3\cos(\%2) + Lc_4\cos(\%1)\,,\ L_3\cos(\%2) + Lc_4\cos(\%1)\,,\ Lc_4\cos(\%1)\Big]$$
$$\%1 := \theta_1 + \theta_2 + \theta_3 + \theta_4$$
$$\%2 := \theta_1 + \theta_2 + \theta_3$$
$$\%3 := \theta_1 + \theta_2$$

A.2 Define the Angular Jacobian Matrices

$$JA_1 := \begin{bmatrix} 1 & 0 & 0 & 0 \end{bmatrix}$$

$$JA_2 := \begin{bmatrix} 1 & 1 & 0 & 0 \end{bmatrix}$$

$$JA_3 := \begin{bmatrix} 1 & 1 & 1 & 0 \end{bmatrix}$$

$$JA_4 := \begin{bmatrix} 1 & 1 & 1 & 1 \end{bmatrix}$$

A.3 Construct the H Matrix: Inertia Tensor

$$\begin{bmatrix} m_1\,{Lc_1}^2 & 0 & 0 & 0 \\ 0 & 0 & 0 & 0 \\ 0 & 0 & 0 & 0 \\ 0 & 0 & 0 & 0 \end{bmatrix}$$

$$\begin{bmatrix} m_2\,{L_1}^2 + 2\,\%1 + m_2\,{Lc_2}^2 & \%1 + m_2\,{Lc_2}^2 & 0 & 0 \\ \%1 + m_2\,{Lc_2}^2 & m_2\,{Lc_2}^2 & 0 & 0 \\ 0 & 0 & 0 & 0 \\ 0 & 0 & 0 & 0 \end{bmatrix}$$
$$\%1 := m_2\,L_1\,Lc_2\cos(\theta_2)$$

$$\Big[m_3\,{Lc_3}^2 + m_3\,{L_1}^2 + m_3\,{L_2}^2 + 2\,\%4 + 2\,\%3 + 2\,\%2 - 2\,\%1\,,$$
$$m_3\,{Lc_3}^2 + m_3\,{L_2}^2 + 2\,\%4 + \%3 + \%2 - \%1\,,\ m_3\,{Lc_3}^2 + \%4 + \%3 - \%1\,,\ 0\Big]$$
$$\Big[m_3\,{Lc_3}^2 + m_3\,{L_2}^2 + 2\,\%4 + \%3 + \%2 - \%1\,,\ m_3\,{Lc_3}^2 + m_3\,{L_2}^2 + 2\,\%4\,,\ m_3\,{Lc_3}^2 + \%4\,,\ 0\Big]$$

$$\left[m_3\,{Lc_3}^2+\%4+\%3-\%1\,,\ m_3\,{Lc_3}^2+\%4\,,\ m_3\,{Lc_3}^2\,,\ 0\right]$$

$$[0\,,\ 0\,,\ 0\,,\ 0]$$

$$\%1 := m_3\,L_1\,Lc_3\sin(\theta_2)\sin(\theta_3)$$

$$\%2 := m_3\,L_1\,L_2\cos(\theta_2)$$

$$\%3 := m_3\,L_1\,Lc_3\cos(\theta_2)\cos(\theta_3)$$

$$\%4 := m_3\,L_2\,Lc_3\cos(\theta_3)$$

$$\left[-2\,\%11+m_4\,{Lc_4}^2+m_4\,{L_2}^2-2\,\%10+2\,\%9+2\,\%8-2\,\%7-2\,\%6+2\,\%5+2\,\%4\right.$$
$$+m_4\,{L_1}^2-2\,\%3+2\,\%2+m_4\,{L_3}^2+2\,\%1,\ -\%11+m_4\,{Lc_4}^2+m_4\,{L_2}^2-2\,\%10+2\,\%9$$
$$+\%8-\%7-\%6+\%5+2\,\%4-\%3+\%2+m_4\,{L_3}^2+2\,\%1,$$
$$-\%11+m_4\,{Lc_4}^2-\%10+\%9+\%8-\%7-\%6+\%5+\%4-\%3+m_4\,{L_3}^2+2\,\%1\,,$$
$$\left.-\%11+m_4\,{Lc_4}^2-\%10+\%9+\%8-\%7-\%3+\%1\right]$$

$$\left[-\%11+m_4\,{Lc_4}^2+m_4\,{L_2}^2-2\,\%10+2\,\%9+\%8-\%7-\%6+\%5+2\,\%4-\%3+\%2\right.$$
$$\left.+m_4\,{L_3}^2+2\,\%1,\ m_4\,{Lc_4}^2+m_4\,{L_2}^2-2\,\%10+2\,\%9+2\,\%4+m_4\,{L_3}^2+2\,\%1\,,\right.$$
$$\left.m_4\,{Lc_4}^2-\%10+\%9+\%4+m_4\,{L_3}^2+2\,\%1\,,\ m_4\,{Lc_4}^2-\%10+\%9+\%1\right]$$

$$\left[-\%11+m_4\,{Lc_4}^2-\%10+\%9+\%8-\%7-\%6+\%5+\%4-\%3+m_4\,{L_3}^2+2\,\%1\,,\right.$$
$$\left.m_4\,{Lc_4}^2-\%10+\%9+\%4+m_4\,{L_3}^2+2\,\%1\,,\ m_4\,{Lc_4}^2+m_4\,{L_3}^2+2\,\%1\,,\ m_4\,{Lc_4}^2+\%1\right]$$

$$\left[-\%11+m_4\,{Lc_4}^2-\%10+\%9+\%8-\%7-\%3+\%1\,,\ m_4\,{Lc_4}^2-\%10+\%9+\%1\,,\right.$$
$$\left.m_4\,{Lc_4}^2+\%1\,,\ m_4\,{Lc_4}^2\right]$$

$$\%1 := m_4\,L_3\,Lc_4\cos(\theta_4)$$

$$\%2 := m_4\,L_1\,L_2\cos(\theta_2)$$

$$\%3 := m_4\,L_1\,Lc_4\sin(\theta_2)\sin(\theta_3)\cos(\theta_4)$$

$$\%4 := m_4\,L_2\,L_3\cos(\theta_3)$$

$$\%5 := m_4\,L_1\,L_3\cos(\theta_2)\cos(\theta_3)$$

$$\%6 := m_4\,L_1\,L_3\sin(\theta_2)\sin(\theta_3)$$

$$\%7 := m_4\,L_1\,Lc_4\cos(\theta_2)\sin(\theta_3)\sin(\theta_4)$$

$$\%8 := m_4\,L_1\,Lc_4\cos(\theta_2)\cos(\theta_3)\cos(\theta_4)$$

$$\%9 := m_4\,L_2\,Lc_4\cos(\theta_3)\cos(\theta_4)$$

$$\%10 := m_4\,L_2\,Lc_4\sin(\theta_3)\sin(\theta_4)$$

$$\%11 := m_4\,L_1\,Lc_4\sin(\theta_2)\cos(\theta_3)\sin(\theta_4)$$

$$He := \begin{bmatrix} Ic_1 & 0 & 0 & 0 \\ 0 & 0 & 0 & 0 \\ 0 & 0 & 0 & 0 \\ 0 & 0 & 0 & 0 \end{bmatrix}$$

$$Hf := \begin{bmatrix} Ic_2 & Ic_2 & 0 & 0 \\ Ic_2 & Ic_2 & 0 & 0 \\ 0 & 0 & 0 & 0 \\ 0 & 0 & 0 & 0 \end{bmatrix}$$

$$Hg := \begin{bmatrix} Ic_3 & Ic_3 & Ic_3 & 0 \\ Ic_3 & Ic_3 & Ic_3 & 0 \\ Ic_3 & Ic_3 & Ic_3 & 0 \\ 0 & 0 & 0 & 0 \end{bmatrix}$$

$$Hh := \begin{bmatrix} Ic_4 & Ic_4 & Ic_4 & Ic_4 \\ Ic_4 & Ic_4 & Ic_4 & Ic_4 \\ Ic_4 & Ic_4 & Ic_4 & Ic_4 \\ Ic_4 & Ic_4 & Ic_4 & Ic_4 \end{bmatrix}$$

$$H := Ha + Hb + Hc + Hd + He + Hf + Hg + Hh$$

A.4 Construct the h Matrix: Centrifugal and Coriolis Effects

array(1..4, 1..4, 1..4, [

$(1, 1, 1) = 0$

$(1, 1, 2) = -2\,\%16 - 2\,\%12 - 2\,\%15 - 2\,\%13 - 2\,\%6 - 2\,\%7 + 2\,\%4 - 2\,\%10 - 2\,\%11$
$- 2\,\%5 - 2\,\%14$

$(1, 1, 3) = -2\,\%9 - 2\,\%13 - 2\,\%12 + 2\,\%4 - 2\,\%2 - 2\,\%3 - 2\,\%5 - 2\,\%6 - 2\,\%11$
$- 2\,\%10 - 2\,\%8 - 2\,\%7$

$(1, 1, 4) = -2\,\%7 - 2\,\%3 - 2\,\%2 - 2\,\%6 - 2\,\%5 + 2\,\%4 - 2\,\%1$

$(1, 2, 1) = 0$

$$(1,\,2,\,2) = -\%16 - \%12 - \%15 - \%13 - \%6 - \%7 + \%4 - \%10 - \%11 - \%5 - \%14$$

$$(1,\,2,\,3) =$$

$$-2\,\%9 - \%13 - \%12 + \%4 - 2\,\%2 - 2\,\%3 - \%5 - \%6 - \%11 - \%10 - 2\,\%8 - \%7$$

$$(1,\,2,\,4) = -\%7 - 2\,\%3 - 2\,\%2 - \%6 - \%5 + \%4 - 2\,\%1$$

$$(1,\,3,\,1) = 0$$

$$(1,\,3,\,2) = -\%12 - \%13 - \%6 - \%7 + \%4 - \%10 - \%11 - \%5$$

$$(1,\,3,\,3) = -\%9 - \%13 - \%12 + \%4 - \%2 - \%3 - \%5 - \%6 - \%11 - \%10 - \%8 - \%7$$

$$(1,\,3,\,4) = -\%7 - \%3 - \%2 - \%6 - \%5 + \%4 - 2\,\%1$$

$$(1,\,4,\,1) = 0$$

$$(1,\,4,\,2) = -\%6 - \%7 + \%4 - \%5$$

$$(1,\,4,\,3) = \%4 - \%2 - \%3 - \%5 - \%6 - \%7$$

$$(1,\,4,\,4) = -\%7 - \%3 - \%2 - \%6 - \%5 + \%4 - \%1$$

$$(2,\,1,\,1) = \%16 + \%12 + \%15 + \%13 + \%6 + \%7 - \%4 + \%10 + \%11 + \%5 + \%14$$

$$(2,\,1,\,2) = -\frac{1}{2}\%16 - \frac{1}{2}\%12 - \frac{1}{2}\%15 - \frac{1}{2}\%13 - \frac{1}{2}\%6 - \frac{1}{2}\%7 + \frac{1}{2}\%4 - \frac{1}{2}\%10 - \frac{1}{2}\%11 - \frac{1}{2}\%5 - \frac{1}{2}\%14$$

$$(2,\,1,\,3) = -2\,\%9 - \frac{1}{2}\%13 - \frac{1}{2}\%12 + \frac{1}{2}\%4 - 2\,\%2 - 2\,\%3 - \frac{1}{2}\%5 - \frac{1}{2}\%6 - \frac{1}{2}\%11 - \frac{1}{2}\%10 - 2\,\%8 - \frac{1}{2}\%7$$

$$(2,\,1,\,4) = -\frac{1}{2}\%7 - 2\,\%3 - 2\,\%2 - \frac{1}{2}\%6 - \frac{1}{2}\%5 + \frac{1}{2}\%4 - 2\,\%1$$

$$(2,\,2,\,1) = \frac{1}{2}\%16 + \frac{1}{2}\%12 + \frac{1}{2}\%15 + \frac{1}{2}\%13 + \frac{1}{2}\%6 + \frac{1}{2}\%7 - \frac{1}{2}\%4 + \frac{1}{2}\%10 + \frac{1}{2}\%11 + \frac{1}{2}\%5 + \frac{1}{2}\%14$$

$$(2,\,2,\,2) = 0$$

$$(2,\,2,\,3) = -2\,\%9 - 2\,\%2 - 2\,\%3 - 2\,\%8$$

$$(2,\,2,\,4) = -2\,\%3 - 2\,\%2 - 2\,\%1$$

$$(2,\,3,\,1) = \frac{1}{2}\%12 + \frac{1}{2}\%13 + \frac{1}{2}\%6 + \frac{1}{2}\%7 - \frac{1}{2}\%4 + \frac{1}{2}\%10 + \frac{1}{2}\%11 + \frac{1}{2}\%5$$

$$(2,\,3,\,2) = 0$$

$$(2,\,3,\,3) = -\%9 - \%2 - \%3 - \%8$$

$$(2,\,3,\,4) = -\%3 - \%2 - 2\,\%1$$

$$(2,\,4,\,1) = \frac{1}{2}\%6 + \frac{1}{2}\%7 - \frac{1}{2}\%4 + \frac{1}{2}\%5$$

$$(2,\,4,\,2) = 0$$

$$(2,\,4,\,3) = -\%2 - \%3$$

$$(2,\,4,\,4) = -\%3 - \%2 - \%1$$

$$(3,\,1,\,1) = \%9 + \%13 + \%12 - \%4 + \%2 + \%3 + \%5 + \%6 + \%11 + \%10 + \%8 + \%7$$

$$(3,\,1,\,2) = -\frac{1}{2}\%12 - \frac{1}{2}\%13 + \%9 - \frac{1}{2}\%6 - \frac{1}{2}\%7 + \frac{1}{2}\%4 - \frac{1}{2}\%10 - \frac{1}{2}\%11 - \frac{1}{2}\%5 + \%2 + \%3 + \%8$$

$$(3,\,1,\,3) = -\frac{1}{2}\%9 - \frac{1}{2}\%3 - \frac{1}{2}\%8 - \frac{1}{2}\%2 - \frac{1}{2}\%12 - \frac{1}{2}\%13 - \frac{1}{2}\%6 - \frac{1}{2}\%7 + \frac{1}{2}\%4 - \frac{1}{2}\%10 - \frac{1}{2}\%11 - \frac{1}{2}\%5$$

$$(3,\,1,\,4) = -\frac{1}{2}\%7 - \frac{1}{2}\%3 - \frac{1}{2}\%2 - \frac{1}{2}\%6 - \frac{1}{2}\%5 + \frac{1}{2}\%4 - 2\%1$$

$$(3,\,2,\,1) =$$

$$\%9 + \frac{1}{2}\%13 + \frac{1}{2}\%12 - \frac{1}{2}\%4 + \%2 + \%3 + \frac{1}{2}\%5 + \frac{1}{2}\%6 + \frac{1}{2}\%11 + \frac{1}{2}\%10 + \%8 + \frac{1}{2}\%7$$

$$(3,\,2,\,2) = \%9 + \%2 + \%3 + \%8$$

$$(3,\,2,\,3) = -\frac{1}{2}\%9 - \frac{1}{2}\%2 - \frac{1}{2}\%3 - \frac{1}{2}\%8$$

$$(3,\,2,\,4) = -\frac{1}{2}\%3 - \frac{1}{2}\%2 - 2\%1$$

$$(3,\,3,\,1) = \frac{1}{2}\%9 + \frac{1}{2}\%13 + \frac{1}{2}\%12 - \frac{1}{2}\%4 + \frac{1}{2}\%2 + \frac{1}{2}\%3 + \frac{1}{2}\%5 + \frac{1}{2}\%6 + \frac{1}{2}\%11 + \frac{1}{2}\%10 + \frac{1}{2}\%8 + \frac{1}{2}\%7$$

$$(3,\,3,\,2) = \frac{1}{2}\%9 + \frac{1}{2}\%2 + \frac{1}{2}\%3 + \frac{1}{2}\%8$$

$$(3,\,3,\,3) = 0$$

$$(3,\,3,\,4) = -2\%1$$

$$(3,\,4,\,1) = -\frac{1}{2}\%4 + \frac{1}{2}\%2 + \frac{1}{2}\%3 + \frac{1}{2}\%5 + \frac{1}{2}\%6 + \frac{1}{2}\%7$$

$$(3,\,4,\,2) = \frac{1}{2}\%2 + \frac{1}{2}\%3$$

$$(3,\,4,\,3) = 0$$

$$(3,\,4,\,4) = -\%1$$

$$(4,\,1,\,1) = \%7 + \%3 + \%2 + \%6 + \%5 - \%4 + \%1$$

$$(4,\,1,\,2) = -\frac{1}{2}\%6 - \frac{1}{2}\%7 + \frac{1}{2}\%4 - \frac{1}{2}\%5 + \%3 + \%2 + \%1$$

$$(4,\,1,\,3) = \frac{1}{2}\%4 - \frac{1}{2}\%2 - \frac{1}{2}\%3 - \frac{1}{2}\%5 - \frac{1}{2}\%6 - \frac{1}{2}\%7 + \%1$$

$$(4,\,1,\,4) = -\frac{1}{2}\%7 - \frac{1}{2}\%3 - \frac{1}{2}\%2 - \frac{1}{2}\%6 - \frac{1}{2}\%5 + \frac{1}{2}\%4 - \frac{1}{2}\%1$$

$$(4,\,2,\,1) = \frac{1}{2}\%7 + \%3 + \%2 + \frac{1}{2}\%6 + \frac{1}{2}\%5 - \frac{1}{2}\%4 + \%1$$

$$(4,\ 2,\ 2) = \%3 + \%2 + \%1$$

$$(4,\ 2,\ 3) = -\frac{1}{2}\,\%2 - \frac{1}{2}\,\%3 + \%1$$

$$(4,\ 2,\ 4) = -\frac{1}{2}\,\%3 - \frac{1}{2}\,\%2 - \frac{1}{2}\,\%1$$

$$(4,\ 3,\ 1) = \frac{1}{2}\,\%7 + \frac{1}{2}\,\%3 + \frac{1}{2}\,\%2 + \frac{1}{2}\,\%6 + \frac{1}{2}\,\%5 - \frac{1}{2}\,\%4 + \%1$$

$$(4,\ 3,\ 2) = \frac{1}{2}\,\%3 + \frac{1}{2}\,\%2 + \%1$$

$$(4,\ 3,\ 3) = \%1$$

$$(4,\ 3,\ 4) = -\frac{1}{2}\,\%1$$

$$(4,\ 4,\ 1) = \frac{1}{2}\,\%7 + \frac{1}{2}\,\%3 + \frac{1}{2}\,\%2 + \frac{1}{2}\,\%6 + \frac{1}{2}\,\%5 - \frac{1}{2}\,\%4 + \frac{1}{2}\,\%1$$

$$(4,\ 4,\ 2) = \frac{1}{2}\,\%3 + \frac{1}{2}\,\%2 + \frac{1}{2}\,\%1$$

$$(4,\ 4,\ 3) = \frac{1}{2}\,\%1$$

$$(4,\ 4,\ 4) = 0$$

])

$$\%1 := m_4\, L_3\, Lc_4 \sin(\theta_4)$$

$$\%2 := m_4\, L_2\, Lc_4 \cos(\theta_3) \sin(\theta_4)$$

$$\%3 := m_4\, L_2\, Lc_4 \sin(\theta_3) \cos(\theta_4)$$

$$\%4 := m_4\, L_1\, Lc_4 \sin(\theta_2) \sin(\theta_3) \sin(\theta_4)$$

$$\%5 := m_4\, L_1\, Lc_4 \cos(\theta_2) \sin(\theta_3) \cos(\theta_4)$$

$$\%6 := m_4\, L_1\, Lc_4 \cos(\theta_2) \cos(\theta_3) \sin(\theta_4)$$

$$\%7 := m_4\, L_1\, Lc_4 \sin(\theta_2) \cos(\theta_3) \cos(\theta_4)$$

$$\%8 := m_4\, L_2\, L_3 \sin(\theta_3)$$

$$\%9 := m_3\, L_2\, Lc_3 \sin(\theta_3)$$

$$\%10 := m_4\, L_1\, L_3 \cos(\theta_2) \sin(\theta_3)$$

$$\%11 := m_4\, L_1\, L_3 \sin(\theta_2) \cos(\theta_3)$$

$$\%12 := m_3\, L_1\, Lc_3 \sin(\theta_2) \cos(\theta_3)$$

$$\%13 := m_3\, L_1\, Lc_3 \cos(\theta_2) \sin(\theta_3)$$

$$\%14 := m_4\, L_1\, L_2 \sin(\theta_2)$$

$$\%15 := m_3\, L_1\, L_2 \sin(\theta_2)$$

$$\%16 := m_2\, L_1\, Lc_2 \sin(\theta_2)$$

Appendix B

Lighthill EBT Derivation in Maple V

B.1 Define the Arrays.

$$y := \text{array}(1..4, [])$$

$$\theta(t) := [?_1, ?_2, ?_3, ?_4]$$

$$q := \text{array}(1..4, [])$$

$$l := \text{array}(1..4, [])$$

$$m\_a := \text{array}(1..4, [])$$

$$m\_22 := \text{array}(1..4, [])$$

$$m\_26 := \text{array}(1..4, [])$$

$$m\_66 := \text{array}(1..4, [])$$

$$dtau := \text{array}(1..4, [])$$

$$Y := \text{array}(0..4, [])$$

B.2 Define the Geometry of the Linkage.

$$\theta_1(t) := q_1(t)$$

$$\theta_2(t) := q_1(t) + q_2(t)$$

$$\theta_3(t) := q_1(t) + q_2(t) + q_3(t)$$

$$\theta_4(t) := q_1(t) + q_2(t) + q_3(t) + q_4(t)$$

$$Y_0(t) := 0$$

$$Y_1(t) := q_1(t)\, l_1$$

$$Y_2(t) := q_1(t)\, l_1 + (q_1(t) + q_2(t))\, l_2$$

$$Y_3(t) := q_1(t)\, l_1 + (q_1(t) + q_2(t))\, l_2 + (q_1(t) + q_2(t) + q_3(t))\, l_3$$

$$Y_4(t) := q_1(t)\, l_1 + (q_1(t) + q_2(t))\, l_2 + (q_1(t) + q_2(t) + q_3(t))\, l_3 + (q_1(t) + q_2(t) + q_3(t) + q_4(t))\, l_4$$

B.3 Displacement of Links 1 Through 4.

$$y_1(x_1,\, t) := q_1(t)\, x_1$$

$$\omega_1(x_1,\, t) := (\frac{\partial}{\partial t}\, q_1(t))\, x_1 + U\, q_1(t)$$

$$mom_1(x_1,\, t) := m\_a_1(x_1)\, ((\frac{\partial}{\partial t}\, q_1(t))\, x_1 + U\, q_1(t))$$

$$dF_1(x_1,\, t) := (m\_a_1(x_1)\, ((\frac{\partial^2}{\partial t^2}\, q_1(t))\, x_1 + U\, (\frac{\partial}{\partial t}\, q_1(t)))$$
$$+ U\, ((\frac{\partial}{\partial x_1}\, m\_a_1(x_1))\, ((\frac{\partial}{\partial t}\, q_1(t))\, x_1 + U\, q_1(t)) + m\_a_1(x_1)\, (\frac{\partial}{\partial t}\, q_1(t))))dx$$

$$dF_1(x_1,\, t) := (m\_a_1(x_1)\, (\frac{\partial^2}{\partial t^2}\, q_1(t))\, x_1 + 2\, m\_a_1(x_1)\, U\, (\frac{\partial}{\partial t}\, q_1(t))$$
$$+ U\, (\frac{\partial}{\partial x_1}\, m\_a_1(x_1))\, (\frac{\partial}{\partial t}\, q_1(t))\, x_1 + (\frac{\partial}{\partial x_1}\, m\_a_1(x_1))\, U^2\, q_1(t))dx$$

$$y_2(x_2,\, t) := (q_1(t) + q_2(t))\, x_2 + q_1(t)\, l_1$$

$$\omega_2(x_2,\, t) := ((\frac{\partial}{\partial t}\, q_1(t)) + (\frac{\partial}{\partial t}\, q_2(t)))\, x_2 + (\frac{\partial}{\partial t}\, q_1(t))\, l_1 + U\, (q_1(t) + q_2(t))$$

$$mom_2(x_2,\, t) := m\_a_2(x_2)\, (((\frac{\partial}{\partial t}\, q_1(t)) + (\frac{\partial}{\partial t}\, q_2(t)))\, x_2 + (\frac{\partial}{\partial t}\, q_1(t))\, l_1 + U\, (q_1(t) + q_2(t)))$$

$$dF_2(x_2,\, t) := (m\_a_2(x_2)\, (((\frac{\partial^2}{\partial t^2}\, q_1(t)) + (\frac{\partial^2}{\partial t^2}\, q_2(t)))\, x_2 + (\frac{\partial^2}{\partial t^2}\, q_1(t))\, l_1 + U\, \%1)$$
$$+ U\, ((\frac{\partial}{\partial x_2}\, m\_a_2(x_2))\, (\%1\, x_2 + (\frac{\partial}{\partial t}\, q_1(t))\, l_1 + U\, (q_1(t) + q_2(t))) + m\_a_2(x_2)\, \%1))dx$$

$$\%1 := (\frac{\partial}{\partial t}\, q_1(t)) + (\frac{\partial}{\partial t}\, q_2(t))$$

$$dF_2(x_2,\, t) := (m\_a_2(x_2)\, x_2\, (\frac{\partial^2}{\partial t^2}\, q_1(t)) + m\_a_2(x_2)\, x_2\, (\frac{\partial^2}{\partial t^2}\, q_2(t)) + m\_a_2(x_2)\, (\frac{\partial^2}{\partial t^2}\, q_1(t))\, l_1$$
$$+ 2\, m\_a_2(x_2)\, U\, (\frac{\partial}{\partial t}\, q_1(t)) + 2\, m\_a_2(x_2)\, U\, (\frac{\partial}{\partial t}\, q_2(t)) + U\, \%1\, x_2\, (\frac{\partial}{\partial t}\, q_1(t))$$
$$+ U\, \%1\, x_2\, (\frac{\partial}{\partial t}\, q_2(t)) + U\, \%1\, (\frac{\partial}{\partial t}\, q_1(t))\, l_1 + \%1\, U^2\, q_1(t) + \%1\, U^2\, q_2(t))\, dx$$
$$\%1 := \frac{\partial}{\partial x_2}\, m\_a_2(x_2)$$

$$y_3(x_3,\, t) := (q_1(t) + q_2(t) + q_3(t))\, x_3 + q_1(t)\, l_1 + (q_1(t) + q_2(t))\, l_2$$

$$\omega_3(x_3,\, t) := ((\frac{\partial}{\partial t}\, q_1(t)) + (\frac{\partial}{\partial t}\, q_2(t)) + (\frac{\partial}{\partial t}\, q_3(t)))\, x_3 + (\frac{\partial}{\partial t}\, q_1(t))\, l_1 + ((\frac{\partial}{\partial t}\, q_1(t)) + (\frac{\partial}{\partial t}\, q_2(t)))\, l_2$$
$$+ U\, (q_1(t) + q_2(t) + q_3(t))$$

$$mom_3(x_3,\, t) := m\_a_3(x_3)(((\frac{\partial}{\partial t}\, q_1(t)) + (\frac{\partial}{\partial t}\, q_2(t)) + (\frac{\partial}{\partial t}\, q_3(t)))\, x_3 + (\frac{\partial}{\partial t}\, q_1(t))\, l_1$$
$$+ ((\frac{\partial}{\partial t}\, q_1(t)) + (\frac{\partial}{\partial t}\, q_2(t)))\, l_2 + U\, (q_1(t) + q_2(t) + q_3(t)))$$

$$dF_3(x_3,\, t) := (m\_a_3(x_3)($$
$$((\frac{\partial^2}{\partial t^2}\, q_1(t)) + (\frac{\partial^2}{\partial t^2}\, q_2(t)) + (\frac{\partial^2}{\partial t^2}\, q_3(t)))\, x_3 + (\frac{\partial^2}{\partial t^2}\, q_1(t))\, l_1 + ((\frac{\partial^2}{\partial t^2}\, q_1(t)) + (\frac{\partial^2}{\partial t^2}\, q_2(t)))\, l_2 + U\, \%1)$$
$$+ U($$
$$(\frac{\partial}{\partial x_3}\, m\_a_3(x_3))\, (\%1\, x_3 + (\frac{\partial}{\partial t}\, q_1(t))\, l_1 + ((\frac{\partial}{\partial t}\, q_1(t)) + (\frac{\partial}{\partial t}\, q_2(t)))\, l_2 + U\, (q_1(t) + q_2(t) + q_3(t)))$$
$$+ m\_a_3(x_3)\, \%1))\, dx$$
$$\%1 := (\frac{\partial}{\partial t}\, q_1(t)) + (\frac{\partial}{\partial t}\, q_2(t)) + (\frac{\partial}{\partial t}\, q_3(t))$$

$$dF_3(x_3,\, t) := (m\_a_3(x_3)\, x_3\, (\frac{\partial^2}{\partial t^2}\, q_1(t)) + m\_a_3(x_3)\, x_3\, (\frac{\partial^2}{\partial t^2}\, q_2(t)) + m\_a_3(x_3)\, x_3\, (\frac{\partial^2}{\partial t^2}\, q_3(t))$$
$$+ m\_a_3(x_3)\, (\frac{\partial^2}{\partial t^2}\, q_1(t))\, l_1 + m\_a_3(x_3)\, l_2\, (\frac{\partial^2}{\partial t^2}\, q_1(t)) + m\_a_3(x_3)\, l_2\, (\frac{\partial^2}{\partial t^2}\, q_2(t))$$
$$+ 2\, m\_a_3(x_3)\, U\, (\frac{\partial}{\partial t}\, q_1(t)) + 2\, m\_a_3(x_3)\, U\, (\frac{\partial}{\partial t}\, q_2(t)) + 2\, m\_a_3(x_3)\, U\, (\frac{\partial}{\partial t}\, q_3(t))$$
$$+ U\, \%1\, x_3\, (\frac{\partial}{\partial t}\, q_1(t)) + U\, \%1\, x_3\, (\frac{\partial}{\partial t}\, q_2(t)) + U\, \%1\, x_3\, (\frac{\partial}{\partial t}\, q_3(t)) + U\, \%1\, (\frac{\partial}{\partial t}\, q_1(t))\, l_1$$
$$+ U\, \%1\, l_2\, (\frac{\partial}{\partial t}\, q_1(t)) + U\, \%1\, l_2\, (\frac{\partial}{\partial t}\, q_2(t)) + \%1\, U^2\, q_1(t) + \%1\, U^2\, q_2(t) + \%1\, U^2\, q_3(t))\, dx$$

$$\%1 := \frac{\partial}{\partial x_3}\, m\_a_3(x_3)$$

$$y_4(x_4,\, t) :=$$
$$(q_1(t) + q_2(t) + q_3(t) + q_4(t))\, x_4 + q_1(t)\, l_1 + (q_1(t) + q_2(t))\, l_2 + (q_1(t) + q_2(t) + q_3(t))\, l_3$$

$$\omega_4(x_4,\, t) := ((\frac{\partial}{\partial t}\, q_1(t)) + (\frac{\partial}{\partial t}\, q_2(t)) + (\frac{\partial}{\partial t}\, q_3(t)) + (\frac{\partial}{\partial t}\, q_4(t)))\, x_4 + (\frac{\partial}{\partial t}\, q_1(t))\, l_1$$
$$+ ((\frac{\partial}{\partial t}\, q_1(t)) + (\frac{\partial}{\partial t}\, q_2(t)))\, l_2 + ((\frac{\partial}{\partial t}\, q_1(t)) + (\frac{\partial}{\partial t}\, q_2(t)) + (\frac{\partial}{\partial t}\, q_3(t)))\, l_3$$
$$+ U\, (q_1(t) + q_2(t) + q_3(t) + q_4(t))$$

$$mom_4(x_4,\, t) := m\_a_4(x_4)(((\frac{\partial}{\partial t}\, q_1(t)) + (\frac{\partial}{\partial t}\, q_2(t)) + (\frac{\partial}{\partial t}\, q_3(t)) + (\frac{\partial}{\partial t}\, q_4(t)))\, x_4 + (\frac{\partial}{\partial t}\, q_1(t))\, l_1$$
$$+ ((\frac{\partial}{\partial t}\, q_1(t)) + (\frac{\partial}{\partial t}\, q_2(t)))\, l_2 + ((\frac{\partial}{\partial t}\, q_1(t)) + (\frac{\partial}{\partial t}\, q_2(t)) + (\frac{\partial}{\partial t}\, q_3(t)))\, l_3$$
$$+ U\, (q_1(t) + q_2(t) + q_3(t) + q_4(t)))$$

$$dF_4(x_4,\, t) := (m\_a_4(x_4)((\%2 + (\frac{\partial^2}{\partial t^2}\, q_2(t)) + (\frac{\partial^2}{\partial t^2}\, q_3(t)) + (\frac{\partial^2}{\partial t^2}\, q_4(t)))\, x_4 + \%2\, l_1$$
$$+ (\%2 + (\frac{\partial^2}{\partial t^2}\, q_2(t)))\, l_2 + (\%2 + (\frac{\partial^2}{\partial t^2}\, q_2(t)) + (\frac{\partial^2}{\partial t^2}\, q_3(t)))\, l_3 + U\, \%1) + U((\frac{\partial}{\partial x_4}\, m\_a_4(x_4))($$
$$\%1\, x_4 + (\frac{\partial}{\partial t}\, q_1(t))\, l_1 + ((\frac{\partial}{\partial t}\, q_1(t)) + (\frac{\partial}{\partial t}\, q_2(t)))\, l_2 + ((\frac{\partial}{\partial t}\, q_1(t)) + (\frac{\partial}{\partial t}\, q_2(t)) + (\frac{\partial}{\partial t}\, q_3(t)))\, l_3$$
$$+ U\, (q_1(t) + q_2(t) + q_3(t) + q_4(t))) + m\_a_4(x_4)\, \%1))\, dx$$
$$\%1 := (\frac{\partial}{\partial t}\, q_1(t)) + (\frac{\partial}{\partial t}\, q_2(t)) + (\frac{\partial}{\partial t}\, q_3(t)) + (\frac{\partial}{\partial t}\, q_4(t))$$
$$\%2 := \frac{\partial^2}{\partial t^2}\, q_1(t)$$

$$dF_4(x_4,\, t) := (2\, m\_a_4(x_4)\, U\, (\frac{\partial}{\partial t}\, q_3(t)) + m\_a_4(x_4)\, l_3\, (\frac{\partial^2}{\partial t^2}\, q_3(t)) + \%1\, U^2\, q_1(t) + \%1\, U^2\, q_2(t)$$
$$+ \%1\, U^2\, q_3(t) + \%1\, U^2\, q_4(t) + m\_a_4(x_4)\, x_4\, \%2 + m\_a_4(x_4)\, x_4\, (\frac{\partial^2}{\partial t^2}\, q_2(t))$$
$$+ m\_a_4(x_4)\, x_4\, (\frac{\partial^2}{\partial t^2}\, q_3(t)) + m\_a_4(x_4)\, x_4\, (\frac{\partial^2}{\partial t^2}\, q_4(t)) + m\_a_4(x_4)\, \%2\, l_1 + m\_a_4(x_4)\, l_2\, \%2$$
$$+ m\_a_4(x_4)\, l_2\, (\frac{\partial^2}{\partial t^2}\, q_2(t)) + m\_a_4(x_4)\, l_3\, \%2 + m\_a_4(x_4)\, l_3\, (\frac{\partial^2}{\partial t^2}\, q_2(t)) + 2\, m\_a_4(x_4)\, U\, (\frac{\partial}{\partial t}\, q_1(t))$$
$$+ 2\, m\_a_4(x_4)\, U\, (\frac{\partial}{\partial t}\, q_2(t)) + 2\, m\_a_4(x_4)\, U\, (\frac{\partial}{\partial t}\, q_4(t)) + U\, \%1\, x_4\, (\frac{\partial}{\partial t}\, q_1(t))$$
$$+ U\, \%1\, x_4\, (\frac{\partial}{\partial t}\, q_2(t)) + U\, \%1\, x_4\, (\frac{\partial}{\partial t}\, q_3(t)) + U\, \%1\, x_4\, (\frac{\partial}{\partial t}\, q_4(t)) + U\, \%1\, (\frac{\partial}{\partial t}\, q_1(t))\, l_1$$

$$+ U\,\%1\,l_2\,(\frac{\partial}{\partial t}\,q_1(t)) + U\,\%1\,l_2\,(\frac{\partial}{\partial t}\,q_2(t)) + U\,\%1\,l_3\,(\frac{\partial}{\partial t}\,q_1(t)) + U\,\%1\,l_3\,(\frac{\partial}{\partial t}\,q_2(t))$$
$$+ U\,\%1\,l_3\,(\frac{\partial}{\partial t}\,q_3(t)))dx$$
$$\%1 := \frac{\partial}{\partial x_4}\,m\_a_4(x_4)$$
$$\%2 := \frac{\partial^2}{\partial t^2}\,q_1(t)$$

B.4 Torque for Link 1

$$dtau_1(t) := x_1(m\_a_1(x_1)\,\%3\,x_1 + 2\,m\_a_1(x_1)\,U\,(\frac{\partial}{\partial t}\,q_1(t)) + U\,(\frac{\partial}{\partial x_1}\,m\_a_1(x_1))\,(\frac{\partial}{\partial t}\,q_1(t))\,x_1$$
$$+ (\frac{\partial}{\partial x_1}\,m\_a_1(x_1))\,U^2\,q_1(t))dx + (x_2 + l_1)(m\_a_2(x_2)\,x_2\,\%3 + m\_a_2(x_2)\,x_2\,\%2$$
$$+ m\_a_2(x_2)\,\%3\,l_1 + 2\,m\_a_2(x_2)\,U\,(\frac{\partial}{\partial t}\,q_1(t)) + 2\,m\_a_2(x_2)\,U\,(\frac{\partial}{\partial t}\,q_2(t)) + U\,\%5\,x_2\,(\frac{\partial}{\partial t}\,q_1(t))$$
$$+ U\,\%5\,x_2\,(\frac{\partial}{\partial t}\,q_2(t)) + U\,\%5\,(\frac{\partial}{\partial t}\,q_1(t))\,l_1 + \%5\,U^2\,q_1(t) + \%5\,U^2\,q_2(t))dx + (x_3 + l_1 + l_2)($$
$$m\_a_3(x_3)\,x_3\,\%3 + m\_a_3(x_3)\,x_3\,\%2 + m\_a_3(x_3)\,x_3\,(\frac{\partial^2}{\partial t^2}\,q_3(t)) + m\_a_3(x_3)\,\%3\,l_1$$
$$+ m\_a_3(x_3)\,l_2\,\%3 + m\_a_3(x_3)\,l_2\,\%2 + 2\,m\_a_3(x_3)\,U\,(\frac{\partial}{\partial t}\,q_1(t)) + 2\,m\_a_3(x_3)\,U\,(\frac{\partial}{\partial t}\,q_2(t))$$
$$+ 2\,m\_a_3(x_3)\,U\,(\frac{\partial}{\partial t}\,q_3(t)) + U\,\%4\,x_3\,(\frac{\partial}{\partial t}\,q_1(t)) + U\,\%4\,x_3\,(\frac{\partial}{\partial t}\,q_2(t)) + U\,\%4\,x_3\,(\frac{\partial}{\partial t}\,q_3(t))$$
$$+ U\,\%4\,(\frac{\partial}{\partial t}\,q_1(t))\,l_1 + U\,\%4\,l_2\,(\frac{\partial}{\partial t}\,q_1(t)) + U\,\%4\,l_2\,(\frac{\partial}{\partial t}\,q_2(t)) + \%4\,U^2\,q_1(t) + \%4\,U^2\,q_2(t)$$
$$+ \%4\,U^2\,q_3(t))dx + (x_4 + l_1 + l_2 + l_3)(2\,m\_a_4(x_4)\,U\,(\frac{\partial}{\partial t}\,q_3(t)) + m\_a_4(x_4)\,l_3\,(\frac{\partial^2}{\partial t^2}\,q_3(t))$$
$$+ \%1\,U^2\,q_1(t) + \%1\,U^2\,q_2(t) + \%1\,U^2\,q_3(t) + \%1\,U^2\,q_4(t) + m\_a_4(x_4)\,x_4\,\%3$$
$$+ m\_a_4(x_4)\,x_4\,\%2 + m\_a_4(x_4)\,x_4\,(\frac{\partial^2}{\partial t^2}\,q_3(t)) + m\_a_4(x_4)\,x_4\,(\frac{\partial^2}{\partial t^2}\,q_4(t)) + m\_a_4(x_4)\,\%3\,l_1$$
$$+ m\_a_4(x_4)\,l_2\,\%3 + m\_a_4(x_4)\,l_2\,\%2 + m\_a_4(x_4)\,l_3\,\%3 + m\_a_4(x_4)\,l_3\,\%2$$
$$+ 2\,m\_a_4(x_4)\,U\,(\frac{\partial}{\partial t}\,q_1(t)) + 2\,m\_a_4(x_4)\,U\,(\frac{\partial}{\partial t}\,q_2(t)) + 2\,m\_a_4(x_4)\,U\,(\frac{\partial}{\partial t}\,q_4(t))$$
$$+ U\,\%1\,x_4\,(\frac{\partial}{\partial t}\,q_1(t)) + U\,\%1\,x_4\,(\frac{\partial}{\partial t}\,q_2(t)) + U\,\%1\,x_4\,(\frac{\partial}{\partial t}\,q_3(t)) + U\,\%1\,x_4\,(\frac{\partial}{\partial t}\,q_4(t))$$
$$+ U\,\%1\,(\frac{\partial}{\partial t}\,q_1(t))\,l_1 + U\,\%1\,l_2\,(\frac{\partial}{\partial t}\,q_1(t)) + U\,\%1\,l_2\,(\frac{\partial}{\partial t}\,q_2(t)) + U\,\%1\,l_3\,(\frac{\partial}{\partial t}\,q_1(t))$$
$$+ U\,\%1\,l_3\,(\frac{\partial}{\partial t}\,q_2(t)) + U\,\%1\,l_3\,(\frac{\partial}{\partial t}\,q_3(t)))dx$$
$$\%1 := \frac{\partial}{\partial x_4}\,m\_a_4(x_4)$$

$$\%2 := \frac{\partial^2}{\partial t^2}\, q_2(t)$$
$$\%3 := \frac{\partial^2}{\partial t^2}\, q_1(t)$$
$$\%4 := \frac{\partial}{\partial x_3}\, m\_a_3(x_3)$$
$$\%5 := \frac{\partial}{\partial x_2}\, m\_a_2(x_2)$$

$$\begin{aligned}
&(x_1\,(\frac{\partial}{\partial x_1}\, m_a_1(x_1))\,U^2\,dx + (x_2 + l_1)\,\%6\,U^2\,dx + \%4\,\%5\,U^2\,dx + \%1\,\%3\,U^2\,dx)\,q_1(t) + (\\
&\quad x_1\,(2\,m_a_1(x_1)\,U + U\,(\frac{\partial}{\partial x_1}\, m_a_1(x_1))\,x_1)\,dx\\
&\quad + (x_2 + l_1)\,(2\,m_a_2(x_2)\,U + U\,\%6\,x_2 + U\,\%6\,l_1)\,dx\\
&\quad + \%4\,(U\,\%5\,x_3 + U\,\%5\,l_2 + 2\,m_a_3(x_3)\,U + U\,\%5\,l_1)\,dx\\
&\quad + \%1\,(U\,\%3\,x_4 + U\,\%3\,l_2 + 2\,\%2 + U\,\%3\,l_3 + U\,\%3\,l_1)\,dx)(\frac{\partial}{\partial t}\, q_1(t)) + (m_a_1(x_1)\,{x_1}^2\,dx\\
&\quad + (x_2 + l_1)\,(m_a_2(x_2)\,l_1 + m_a_2(x_2)\,x_2)\,dx\\
&\quad + \%4\,(m_a_3(x_3)\,x_3 + m_a_3(x_3)\,l_1 + m_a_3(x_3)\,l_2)\,dx\\
&\quad + \%1\,(m_a_4(x_4)\,x_4 + m_a_4(x_4)\,l_1 + m_a_4(x_4)\,l_2 + m_a_4(x_4)\,l_3)\,dx)(\frac{\partial^2}{\partial t^2}\, q_1(t))\\
&\quad + ((x_2 + l_1)\,\%6\,U^2\,dx + \%4\,\%5\,U^2\,dx + \%1\,\%3\,U^2\,dx)\,q_2(t) + (\\
&\quad (x_2 + l_1)\,(U\,\%6\,x_2 + 2\,m_a_2(x_2)\,U)\,dx + \%4\,(U\,\%5\,x_3 + 2\,m_a_3(x_3)\,U + U\,\%5\,l_2)\,dx\\
&\quad + \%1\,(U\,\%3\,l_3 + U\,\%3\,x_4 + U\,\%3\,l_2 + 2\,\%2)\,dx)(\frac{\partial}{\partial t}\, q_2(t)) + ((x_2 + l_1)\,m_a_2(x_2)\,x_2\,dx\\
&\quad + \%4\,(m_a_3(x_3)\,x_3 + m_a_3(x_3)\,l_2)\,dx + \%1\,(m_a_4(x_4)\,x_4 + m_a_4(x_4)\,l_2 + m_a_4(x_4)\,l_3)\,dx)\\
&\quad (\frac{\partial^2}{\partial t^2}\, q_2(t)) + (\%4\,\%5\,U^2\,dx + \%1\,\%3\,U^2\,dx)\,q_3(t)\\
&\quad + (\%4\,(2\,m_a_3(x_3)\,U + U\,\%5\,x_3)\,dx + \%1\,(U\,\%3\,l_3 + U\,\%3\,x_4 + 2\,\%2)\,dx)\,(\frac{\partial}{\partial t}\, q_3(t))\\
&\quad + (\%4\,m_a_3(x_3)\,x_3\,dx + \%1\,(m_a_4(x_4)\,l_3 + m_a_4(x_4)\,x_4)\,dx)\,(\frac{\partial^2}{\partial t^2}\, q_3(t)) + \%1\,\%3\,U^2\,dx\,q_4(t)\\
&\quad + \%1\,(U\,\%3\,x_4 + 2\,\%2)\,dx\,(\frac{\partial}{\partial t}\, q_4(t)) + \%1\,m_a_4(x_4)\,x_4\,(\frac{\partial^2}{\partial t^2}\, q_4(t))\,dx
\end{aligned}$$
$$\%1 := x_4 + l_1 + l_2 + l_3$$
$$\%2 := m\_a_4(x_4)\,U$$
$$\%3 := \frac{\partial}{\partial x_4}\, m\_a_4(x_4)$$
$$\%4 := x_3 + l_1 + l_2$$
$$\%5 := \frac{\partial}{\partial x_3}\, m\_a_3(x_3)$$

$$\%6 := \frac{\partial}{\partial x_2}\, m\_a_2(x_2)$$

B.5 Torque for Link 2

$$dtau_2(t) := x_2(m\_a_2(x_2)\, x_2\, \%3 + m\_a_2(x_2)\, x_2\, \%2 + m\_a_2(x_2)\, \%3\, l_1 + 2\, m\_a_2(x_2)\, U\, (\frac{\partial}{\partial t}\, q_1(t))$$
$$+ 2\, m\_a_2(x_2)\, U\, (\frac{\partial}{\partial t}\, q_2(t)) + U\, \%5\, x_2\, (\frac{\partial}{\partial t}\, q_1(t)) + U\, \%5\, x_2\, (\frac{\partial}{\partial t}\, q_2(t)) + U\, \%5\, (\frac{\partial}{\partial t}\, q_1(t))\, l_1$$
$$+ \%5\, U^2\, q_1(t) + \%5\, U^2\, q_2(t))\, dx + (x_3 + l_2)(m\_a_3(x_3)\, x_3\, \%3 + m\_a_3(x_3)\, x_3\, \%2$$
$$+ m\_a_3(x_3)\, x_3\, (\frac{\partial^2}{\partial t^2}\, q_3(t)) + m\_a_3(x_3)\, \%3\, l_1 + m\_a_3(x_3)\, l_2\, \%3 + m\_a_3(x_3)\, l_2\, \%2$$
$$+ 2\, m\_a_3(x_3)\, U\, (\frac{\partial}{\partial t}\, q_1(t)) + 2\, m\_a_3(x_3)\, U\, (\frac{\partial}{\partial t}\, q_2(t)) + 2\, m\_a_3(x_3)\, U\, (\frac{\partial}{\partial t}\, q_3(t))$$
$$+ U\, \%4\, x_3\, (\frac{\partial}{\partial t}\, q_1(t)) + U\, \%4\, x_3\, (\frac{\partial}{\partial t}\, q_2(t)) + U\, \%4\, x_3\, (\frac{\partial}{\partial t}\, q_3(t)) + U\, \%4\, (\frac{\partial}{\partial t}\, q_1(t))\, l_1$$
$$+ U\, \%4\, l_2\, (\frac{\partial}{\partial t}\, q_1(t)) + U\, \%4\, l_2\, (\frac{\partial}{\partial t}\, q_2(t)) + \%4\, U^2\, q_1(t) + \%4\, U^2\, q_2(t) + \%4\, U^2\, q_3(t))\, dx +$$
$$(x_4 + l_2 + l_3)(2\, m\_a_4(x_4)\, U\, (\frac{\partial}{\partial t}\, q_3(t)) + m\_a_4(x_4)\, l_3\, (\frac{\partial^2}{\partial t^2}\, q_3(t)) + \%1\, U^2\, q_1(t) + \%1\, U^2\, q_2(t)$$
$$+ \%1\, U^2\, q_3(t) + \%1\, U^2\, q_4(t) + m\_a_4(x_4)\, x_4\, \%3 + m\_a_4(x_4)\, x_4\, \%2 + m\_a_4(x_4)\, x_4\, (\frac{\partial^2}{\partial t^2}\, q_3(t))$$
$$+ m\_a_4(x_4)\, x_4\, (\frac{\partial^2}{\partial t^2}\, q_4(t)) + m\_a_4(x_4)\, \%3\, l_1 + m\_a_4(x_4)\, l_2\, \%3 + m\_a_4(x_4)\, l_2\, \%2$$
$$+ m\_a_4(x_4)\, l_3\, \%3 + m\_a_4(x_4)\, l_3\, \%2 + 2\, m\_a_4(x_4)\, U\, (\frac{\partial}{\partial t}\, q_1(t)) + 2\, m\_a_4(x_4)\, U\, (\frac{\partial}{\partial t}\, q_2(t))$$
$$+ 2\, m\_a_4(x_4)\, U\, (\frac{\partial}{\partial t}\, q_4(t)) + U\, \%1\, x_4\, (\frac{\partial}{\partial t}\, q_1(t)) + U\, \%1\, x_4\, (\frac{\partial}{\partial t}\, q_2(t)) + U\, \%1\, x_4\, (\frac{\partial}{\partial t}\, q_3(t))$$
$$+ U\, \%1\, x_4\, (\frac{\partial}{\partial t}\, q_4(t)) + U\, \%1\, (\frac{\partial}{\partial t}\, q_1(t))\, l_1 + U\, \%1\, l_2\, (\frac{\partial}{\partial t}\, q_1(t)) + U\, \%1\, l_2\, (\frac{\partial}{\partial t}\, q_2(t))$$
$$+ U\, \%1\, l_3\, (\frac{\partial}{\partial t}\, q_1(t)) + U\, \%1\, l_3\, (\frac{\partial}{\partial t}\, q_2(t)) + U\, \%1\, l_3\, (\frac{\partial}{\partial t}\, q_3(t)))\, dx$$
$$\%1 := \frac{\partial}{\partial x_4}\, m\_a_4(x_4)$$
$$\%2 := \frac{\partial^2}{\partial t^2}\, q_2(t)$$
$$\%3 := \frac{\partial^2}{\partial t^2}\, q_1(t)$$
$$\%4 := \frac{\partial}{\partial x_3}\, m\_a_3(x_3)$$
$$\%5 := \frac{\partial}{\partial x_2}\, m\_a_2(x_2)$$

$$
\begin{aligned}
&(x_2\,\%5\,U^2\,dx + (x_3 + l_2)\,\%4\,U^2\,dx + \%1\,\%3\,U^2\,dx)\,q_1(t) + (\\
&\quad x_2\,(2\,m\_a_2(x_2)\,U + U\,\%5\,x_2 + U\,\%5\,l_1)\,dx\\
&\quad + (x_3 + l_2)\,(U\,\%4\,x_3 + U\,\%4\,l_2 + 2\,m\_a_3(x_3)\,U + U\,\%4\,l_1)\,dx\\
&\quad + \%1\,(U\,\%3\,x_4 + U\,\%3\,l_2 + 2\,\%2 + U\,\%3\,l_3 + U\,\%3\,l_1)\,dx)(\frac{\partial}{\partial t}\,q_1(t)) + (\\
&\quad x_2\,(m\_a_2(x_2)\,l_1 + m\_a_2(x_2)\,x_2)\,dx + (x_3 + l_2)\,(m\_a_3(x_3)\,x_3 + m\_a_3(x_3)\,l_1 + m\_a_3(x_3)\,l_2)\,dx\\
&\quad + \%1\,(m\_a_4(x_4)\,x_4 + m\_a_4(x_4)\,l_1 + m\_a_4(x_4)\,l_2 + m\_a_4(x_4)\,l_3)\,dx)(\frac{\partial^2}{\partial t^2}\,q_1(t))\\
&\quad + (x_2\,\%5\,U^2\,dx + (x_3 + l_2)\,\%4\,U^2\,dx + \%1\,\%3\,U^2\,dx)\,q_2(t) + (\\
&\quad x_2\,(U\,\%5\,x_2 + 2\,m\_a_2(x_2)\,U)\,dx + (x_3 + l_2)\,(U\,\%4\,x_3 + 2\,m\_a_3(x_3)\,U + U\,\%4\,l_2)\,dx\\
&\quad + \%1\,(U\,\%3\,l_3 + U\,\%3\,x_4 + U\,\%3\,l_2 + 2\,\%2)\,dx)(\frac{\partial}{\partial t}\,q_2(t)) + (m\_a_2(x_2)\,{x_2}^2\,dx\\
&\quad + (x_3 + l_2)\,(m\_a_3(x_3)\,x_3 + m\_a_3(x_3)\,l_2)\,dx\\
&\quad + \%1\,(m\_a_4(x_4)\,x_4 + m\_a_4(x_4)\,l_2 + m\_a_4(x_4)\,l_3)\,dx)(\frac{\partial^2}{\partial t^2}\,q_2(t))\\
&\quad + ((x_3 + l_2)\,\%4\,U^2\,dx + \%1\,\%3\,U^2\,dx)\,q_3(t)\\
&\quad + ((x_3 + l_2)\,(2\,m\_a_3(x_3)\,U + U\,\%4\,x_3)\,dx + \%1\,(U\,\%3\,l_3 + U\,\%3\,x_4 + 2\,\%2)\,dx)\,(\frac{\partial}{\partial t}\,q_3(t))\\
&\quad + ((x_3 + l_2)\,m\_a_3(x_3)\,x_3\,dx + \%1\,(m\_a_4(x_4)\,l_3 + m\_a_4(x_4)\,x_4)\,dx)\,(\frac{\partial^2}{\partial t^2}\,q_3(t))\\
&\quad + \%1\,\%3\,U^2\,dx\,q_4(t) + \%1\,(U\,\%3\,x_4 + 2\,\%2)\,dx\,(\frac{\partial}{\partial t}\,q_4(t)) + \%1\,m\_a_4(x_4)\,x_4\,(\frac{\partial^2}{\partial t^2}\,q_4(t))\,dx\\
&\quad \%1 := x_4 + l_2 + l_3\\
&\quad \%2 := m\_a_4(x_4)\,U\\
&\quad \%3 := \frac{\partial}{\partial x_4}\,m\_a_4(x_4)\\
&\quad \%4 := \frac{\partial}{\partial x_3}\,m\_a_3(x_3)\\
&\quad \%5 := \frac{\partial}{\partial x_2}\,m\_a_2(x_2)
\end{aligned}
$$

B.6 Torque for Link 3

$$
\begin{aligned}
&dtau_3(t) := x_3(m\_a_3(x_3)\,x_3\,\%3 + m\_a_3(x_3)\,x_3\,\%2 + m\_a_3(x_3)\,x_3\,(\frac{\partial^2}{\partial t^2}\,q_3(t)) + m\_a_3(x_3)\,\%3\,l_1\\
&\quad + m\_a_3(x_3)\,l_2\,\%3 + m\_a_3(x_3)\,l_2\,\%2 + 2\,m\_a_3(x_3)\,U\,(\frac{\partial}{\partial t}\,q_1(t)) + 2\,m\_a_3(x_3)\,U\,(\frac{\partial}{\partial t}\,q_2(t))\\
&\quad + 2\,m\_a_3(x_3)\,U\,(\frac{\partial}{\partial t}\,q_3(t)) + U\,\%4\,x_3\,(\frac{\partial}{\partial t}\,q_1(t)) + U\,\%4\,x_3\,(\frac{\partial}{\partial t}\,q_2(t)) + U\,\%4\,x_3\,(\frac{\partial}{\partial t}\,q_3(t))\\
&\quad + U\,\%4\,(\frac{\partial}{\partial t}\,q_1(t))\,l_1 + U\,\%4\,l_2\,(\frac{\partial}{\partial t}\,q_1(t)) + U\,\%4\,l_2\,(\frac{\partial}{\partial t}\,q_2(t)) + \%4\,U^2\,q_1(t) + \%4\,U^2\,q_2(t)
\end{aligned}
$$

$$
\begin{aligned}
&+ \%4\,U^2\,q_3(t))\,dx + (x_4 + l_3)(2\,m\_a_4(x_4)\,U\,(\frac{\partial}{\partial t}\,q_3(t)) + m\_a_4(x_4)\,l_3\,(\frac{\partial^2}{\partial t^2}\,q_3(t))\\
&+ \%1\,U^2\,q_1(t) + \%1\,U^2\,q_2(t) + \%1\,U^2\,q_3(t) + \%1\,U^2\,q_4(t) + m\_a_4(x_4)\,x_4\,\%3\\
&+ m\_a_4(x_4)\,x_4\,\%2 + m\_a_4(x_4)\,x_4\,(\frac{\partial^2}{\partial t^2}\,q_3(t)) + m\_a_4(x_4)\,x_4\,(\frac{\partial^2}{\partial t^2}\,q_4(t)) + m\_a_4(x_4)\,\%3\,l_1\\
&+ m\_a_4(x_4)\,l_2\,\%3 + m\_a_4(x_4)\,l_2\,\%2 + m\_a_4(x_4)\,l_3\,\%3 + m\_a_4(x_4)\,l_3\,\%2\\
&+ 2\,m\_a_4(x_4)\,U\,(\frac{\partial}{\partial t}\,q_1(t)) + 2\,m\_a_4(x_4)\,U\,(\frac{\partial}{\partial t}\,q_2(t)) + 2\,m\_a_4(x_4)\,U\,(\frac{\partial}{\partial t}\,q_4(t))\\
&+ U\,\%1\,x_4\,(\frac{\partial}{\partial t}\,q_1(t)) + U\,\%1\,x_4\,(\frac{\partial}{\partial t}\,q_2(t)) + U\,\%1\,x_4\,(\frac{\partial}{\partial t}\,q_3(t)) + U\,\%1\,x_4\,(\frac{\partial}{\partial t}\,q_4(t))\\
&+ U\,\%1\,(\frac{\partial}{\partial t}\,q_1(t))\,l_1 + U\,\%1\,l_2\,(\frac{\partial}{\partial t}\,q_1(t)) + U\,\%1\,l_2\,(\frac{\partial}{\partial t}\,q_2(t)) + U\,\%1\,l_3\,(\frac{\partial}{\partial t}\,q_1(t))\\
&+ U\,\%1\,l_3\,(\frac{\partial}{\partial t}\,q_2(t)) + U\,\%1\,l_3\,(\frac{\partial}{\partial t}\,q_3(t)))\,dx\\
\%1 &:= \frac{\partial}{\partial x_4}\,m\_a_4(x_4)\\
\%2 &:= \frac{\partial^2}{\partial t^2}\,q_2(t)\\
\%3 &:= \frac{\partial^2}{\partial t^2}\,q_1(t)\\
\%4 &:= \frac{\partial}{\partial x_3}\,m\_a_3(x_3)
\end{aligned}
$$

$$
\begin{aligned}
&\%4\,q_1(t) + (x_3\,(U\,\%3\,x_3 + U\,\%3\,l_2 + 2\,m\_a_3(x_3)\,U + U\,\%3\,l_1)\,dx\\
&+ (x_4 + l_3)\,(U\,\%2\,x_4 + U\,\%2\,l_2 + 2\,\%1 + U\,\%2\,l_3 + U\,\%2\,l_1)\,dx)(\frac{\partial}{\partial t}\,q_1(t)) + (\\
&x_3\,(m\_a_3(x_3)\,x_3 + m\_a_3(x_3)\,l_1 + m\_a_3(x_3)\,l_2)\,dx\\
&+ (x_4 + l_3)\,(m\_a_4(x_4)\,x_4 + m\_a_4(x_4)\,l_1 + m\_a_4(x_4)\,l_2 + m\_a_4(x_4)\,l_3)\,dx)(\frac{\partial^2}{\partial t^2}\,q_1(t)) + \%4\,q_2(t)\\
&+ (x_3\,(U\,\%3\,x_3 + 2\,m\_a_3(x_3)\,U + U\,\%3\,l_2)\,dx\\
&+ (x_4 + l_3)\,(U\,\%2\,l_3 + U\,\%2\,x_4 + U\,\%2\,l_2 + 2\,\%1)\,dx)(\frac{\partial}{\partial t}\,q_2(t)) +\\
&(x_3\,(m\_a_3(x_3)\,x_3 + m\_a_3(x_3)\,l_2)\,dx + (x_4 + l_3)\,(m\_a_4(x_4)\,x_4 + m\_a_4(x_4)\,l_2 + m\_a_4(x_4)\,l_3)\,dx)\\
&(\frac{\partial^2}{\partial t^2}\,q_2(t)) + \%4\,q_3(t)\\
&+ (x_3\,(2\,m\_a_3(x_3)\,U + U\,\%3\,x_3)\,dx + (x_4 + l_3)\,(U\,\%2\,l_3 + U\,\%2\,x_4 + 2\,\%1)\,dx)\,(\frac{\partial}{\partial t}\,q_3(t))\\
&+ (m\_a_3(x_3)\,{x_3}^2\,dx + (x_4 + l_3)\,(m\_a_4(x_4)\,l_3 + m\_a_4(x_4)\,x_4)\,dx)\,(\frac{\partial^2}{\partial t^2}\,q_3(t))\\
&+ (x_4 + l_3)\,\%2\,U^2\,dx\,q_4(t) + (x_4 + l_3)\,(U\,\%2\,x_4 + 2\,\%1)\,dx\,(\frac{\partial}{\partial t}\,q_4(t))\\
&+ (x_4 + l_3)\,m\_a_4(x_4)\,x_4\,(\frac{\partial^2}{\partial t^2}\,q_4(t))\,dx
\end{aligned}
$$

$$\%1 := m\_a_4(x_4)\,U$$
$$\%2 := \frac{\partial}{\partial x_4}\, m\_a_4(x_4)$$
$$\%3 := \frac{\partial}{\partial x_3}\, m\_a_3(x_3)$$
$$\%4 := x_3\,\%3\,U^2\,dx + (x_4 + l_3)\,\%2\,U^2\,dx$$

B.7 Torque for Link 4.

$$\begin{aligned}
dtau_4(t) := {} & x_4(2\,m_a_4(x_4)\,U\,(\frac{\partial}{\partial t}\,q_3(t)) + m_a_4(x_4)\,l_3\,(\frac{\partial^2}{\partial t^2}\,q_3(t)) + \%1\,U^2\,q_1(t) + \%1\,U^2\,q_2(t) \\
& + \%1\,U^2\,q_3(t) + \%1\,U^2\,q_4(t) + m_a_4(x_4)\,x_4\,\%2 + m_a_4(x_4)\,x_4\,(\frac{\partial^2}{\partial t^2}\,q_2(t)) \\
& + m_a_4(x_4)\,x_4\,(\frac{\partial^2}{\partial t^2}\,q_3(t)) + m_a_4(x_4)\,x_4\,(\frac{\partial^2}{\partial t^2}\,q_4(t)) + m_a_4(x_4)\,\%2\,l_1 + m_a_4(x_4)\,l_2\,\%2 \\
& + m_a_4(x_4)\,l_2\,(\frac{\partial^2}{\partial t^2}\,q_2(t)) + m_a_4(x_4)\,l_3\,\%2 + m_a_4(x_4)\,l_3\,(\frac{\partial^2}{\partial t^2}\,q_2(t)) + 2\,m_a_4(x_4)\,U\,(\frac{\partial}{\partial t}\,q_1(t)) \\
& + 2\,m_a_4(x_4)\,U\,(\frac{\partial}{\partial t}\,q_2(t)) + 2\,m_a_4(x_4)\,U\,(\frac{\partial}{\partial t}\,q_4(t)) + U\,\%1\,x_4\,(\frac{\partial}{\partial t}\,q_1(t)) \\
& + U\,\%1\,x_4\,(\frac{\partial}{\partial t}\,q_2(t)) + U\,\%1\,x_4\,(\frac{\partial}{\partial t}\,q_3(t)) + U\,\%1\,x_4\,(\frac{\partial}{\partial t}\,q_4(t)) + U\,\%1\,(\frac{\partial}{\partial t}\,q_1(t))\,l_1 \\
& + U\,\%1\,l_2\,(\frac{\partial}{\partial t}\,q_1(t)) + U\,\%1\,l_2\,(\frac{\partial}{\partial t}\,q_2(t)) + U\,\%1\,l_3\,(\frac{\partial}{\partial t}\,q_1(t)) + U\,\%1\,l_3\,(\frac{\partial}{\partial t}\,q_2(t)) \\
& + U\,\%1\,l_3\,(\frac{\partial}{\partial t}\,q_3(t)))\,dx
\end{aligned}$$
$$\%1 := \frac{\partial}{\partial x_4}\, m\_a_4(x_4)$$
$$\%2 := \frac{\partial^2}{\partial t^2}\, q_1(t)$$

$$\begin{aligned}
& dx\,x_4\,\%2\,U^2\,q_1(t) + x_4\,(U\,\%2\,x_4 + U\,\%2\,l_2 + 2\,\%1 + U\,\%2\,l_3 + U\,\%2\,l_1)\,dx\,(\frac{\partial}{\partial t}\,q_1(t)) \\
& + x_4\,(m_a_4(x_4)\,x_4 + m_a_4(x_4)\,l_1 + m_a_4(x_4)\,l_2 + m_a_4(x_4)\,l_3)\,dx\,(\frac{\partial^2}{\partial t^2}\,q_1(t)) \\
& + dx\,x_4\,\%2\,U^2\,q_2(t) + x_4\,(U\,\%2\,l_3 + U\,\%2\,x_4 + U\,\%2\,l_2 + 2\,\%1)\,dx\,(\frac{\partial}{\partial t}\,q_2(t)) \\
& + x_4\,(m_a_4(x_4)\,x_4 + m_a_4(x_4)\,l_2 + m_a_4(x_4)\,l_3)\,dx\,(\frac{\partial^2}{\partial t^2}\,q_2(t)) + dx\,x_4\,\%2\,U^2\,q_3(t) \\
& + x_4\,(U\,\%2\,l_3 + U\,\%2\,x_4 + 2\,\%1)\,dx\,(\frac{\partial}{\partial t}\,q_3(t)) \\
& + x_4\,(m_a_4(x_4)\,l_3 + m_a_4(x_4)\,x_4)\,dx\,(\frac{\partial^2}{\partial t^2}\,q_3(t)) + dx\,x_4\,\%2\,U^2\,q_4(t)
\end{aligned}$$

$$+ x_4\,(U\,\%2\,x_4 + 2\,\%1)\,dx\,(\frac{\partial}{\partial t}\,q_4(t)) + dx\,m\_a_4(x_4)\,{x_4}^2\,(\frac{\partial^2}{\partial t^2}\,q_4(t))$$

$$\%1 := m\_a_4(x_4)\,U$$

$$\%2 := \frac{\partial}{\partial x_4}\,m\_a_4(x_4)$$

Appendix C

VCUUV Hydraulic Propulsion Plant Simulation

C.1 Introduction

The Vorticity Controlled Unmanned Undersea Vehicle (VCUUV) Project at Draper Laboratories is an effort to design and build the first free-swimming fish-like UUV. The initial stage of this project involved a feasibility study for various propulsion plants; this paper deals with only the hydraulic plant feasibility study and simulation.

The simulation was performed using MATLAB to calculate the hydraulic and motive power over a time period of swimming motion using the estimated torques and angular motions at each of four body joints as input.

C.2 Component Selection

Although the VCUUV prototype is expected to be over 6 feet in length, it will require minimum size components to achieve neutral buoyancy and to allow room for other propulsion, processing components and possibly a payload. Oildyne Corporation manufactures compact hydraulic cylinders that are suitable for this use that also

Vendor	Component	Use	Specifications	Cost	Weight	Comments
Oildyne	Hydraulic Cylinders	Force Actuators	0.5" up to 2.0" diameters. 0.5" has up to 9" stroke length. 5000 psi maximum pressure.	$850 each with position sensors $200 without position sensors	2.5 lbs each	Has many options for position sensing (Linear Resistance Transducer) and mounting styles. Price varies widely. Waterproof connectors are available.
Oildyne	Hydraulic Pump	System Hydraulic Power Source	Model HP2500 0.4 gpm @ 350 psi and 2000 rpm η_m = 78% 3000 psi max continuous	$303	2.10 lbs	Many different pump sizes available.
York Industries	High Pressure Accumulator	Surge Energy Storage	Dependent on final size required	$435	3.20 lbs	
HR Textron	Hydroelectric Servovalves	Cylinder Control	2000 psi maximum pressure. 50 mA gives 0.4 gpm flowrate @ 1000 psi	4@$1050 = $4200	.78 lbs each	Higher capacity servovalves available; 0.9, 1.8 and 3.5 gpm.

Table C.1: Hydraulic Plant Concept Component Summary

carry the option of position sensing integral with the actuator. The cylinder stroke length can also be specified, which can further allow minimization of the size of these components. HR Textron manufactures hydroelectric servovalves that offer a very linear response and this has been confirmed by actual manufacturer's engineering data plots. The smallest model available would be suitable for the VCUUV, and offers a 0.4 gpm flowrate at 50mA control current. Oildyne also makes a very compact hydraulic pump capable of supplying the system's average flowrate. Due to the large pressure surges caused by the nature of the VCUUV's motion, a high pressure accumulator will be required to act as an energy storage device. A summary of the components is provided in Table C.1.

C.3 Development of the Model

The approach for the numerical solution was to reproduce the simulate the body joints' positions and torques over a time period with sufficiently small time increments to give the desired graphical resolution and solution accuracy.

First, the joint angular displacements were translated into hydraulic piston linear position by taking the sine of the maximum angular deflection and multiplying it

by an estimated moment arm of the piston actuator. The size of the moment arm available for the hydraulic piston is limited by the actual half-width of the VCUUV body at each joint, and the distance used for the calculation was estimated from the VCUUV's transverse offsets at the longitudinal position of each joint. This was done assuming the hydraulic pistons will be placed in such a way that they move parallel to the spine, except for the tail joint, where there is an extremely small moment arm available and a relatively high torque required. For this reason, the tail joint was given a moment arm larger than the half-width of the body. The mechanical arrangement of the tail actuator will have to be designed to allow a moment arm at the tail joint of approximately 2 inches, probably a forward extension into the body with the piston motion perpendicular to the spine. The maximum force required for each linear actuator was derived from the maximum moment required divided by the moment arm. To reproduce the swimming motion, each successive joint has a 30 degree phase lag, which can be seen in the graphical output titled "Piston Displacement and Velocity" in Figure C-1. I assumed a tail beat frequency of 0.5 Hz.

Next, the pressure required to produce the forces at each joint were calculated by dividing force by the area of the piston at each successive time step. There is a very obvious nonlinearity in the pressure input, which can be seen in the plot titled "Pressure Drop Across Servovalve and Piston" in Figure C-2. This abrupt change in pressure required is due to the difference in area on each side of the hydraulic piston, due to the reduced effective area of the tailrod side of the piston. Likewise, the hydraulic fluid flowrate through each cylinder is a function of the piston area (multiplied by velocity) and also exhibits this nonlinearity. I used standard cylinder sizes and the areas given for each side of the piston from Oildyne's catalog of small

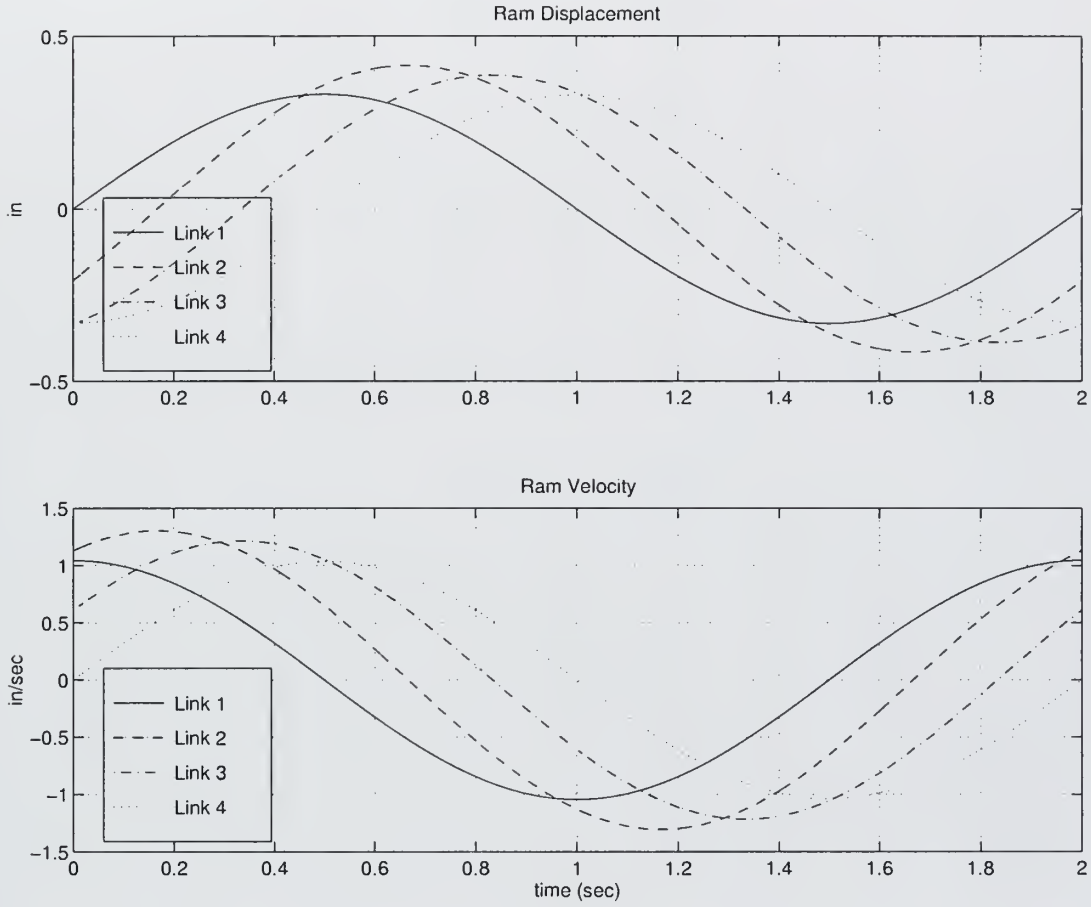

Figure C-1: Piston Displacement And Velocity

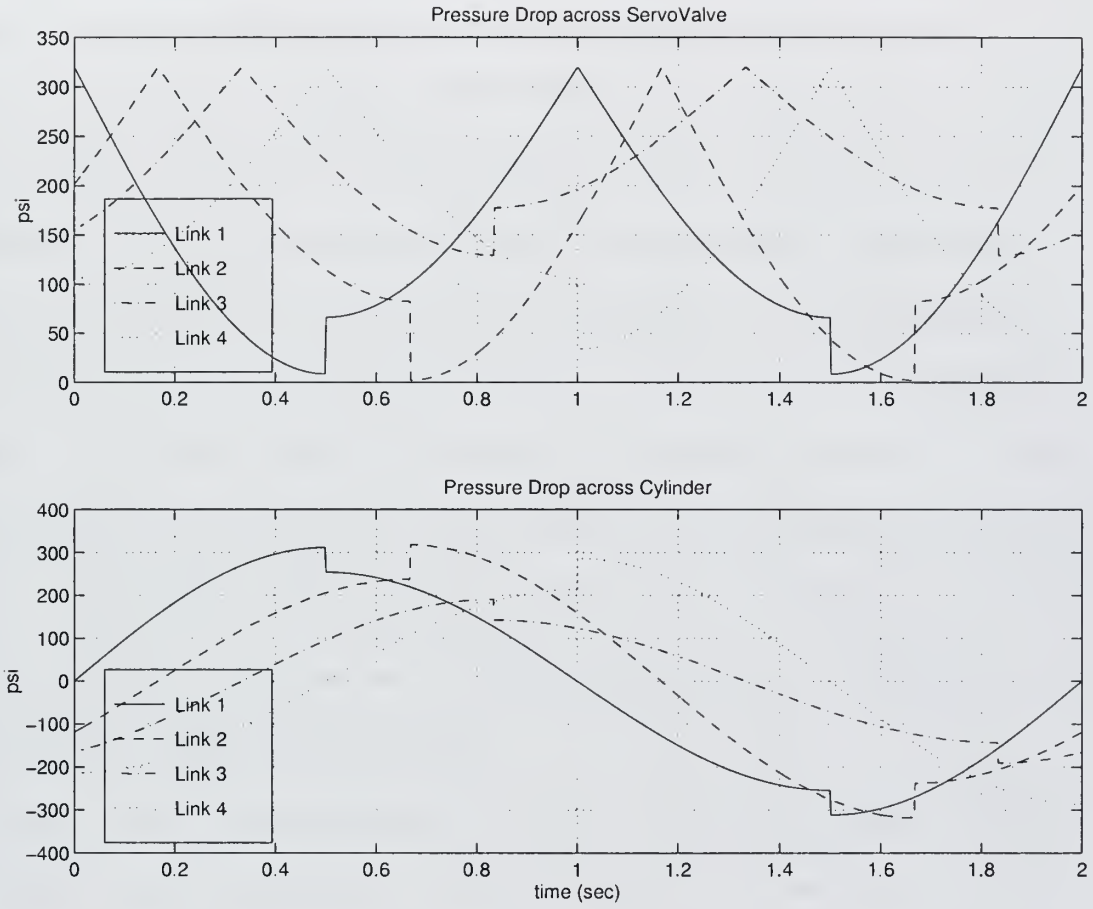

Figure C-2: Pressure Drop Across Servovalve and Piston

cylinders. I included several different standard sizes in my simulation to experiment with the model. As can be seen in the graphs in Figure C-2, the pressure drop across the piston and the pressure drop across the servovalve add up to the main header pressure from the pump. These two components give the total pressure drop across the system. The servovalve control current to produce the instantaneous flowrate required is calculated from the linear gain relationship given by the manufacturer, and is adjusted using Darcy's formula; namely that flowrate is proportional to the square root of pressure differential. The dual nonlinear effect of the piston area difference on flowrate and pressure required is reflected in the servovalve control current, as can be seen in Figure C-3. After some experimentation, it became apparent that the nonlinear effect of the difference in piston areas was the cause of large total pressure peaks and flowrates in the system. It is possible, and desirable, to reverse the direction of 2 of the 4 pistons, so the system is acting on half the full area sides of the actuators and half of the tailrod sides of the actuators, which evens the system peaks considerably. I incorporated the ability to model this in the MATLAB file, and my final output utilizes this arrangement.

Finally, efficiency is calculated from the total power input; hydraulic header pressure times total flowrate (shown in Figure C-6, and total power output; which is calculated as the sum of the piston forces times their respective velocities. Graphical output of the instantaneous efficiency is given in Figure C-5.

C.4 Development of the System

Initially, I chose the smallest of the Oildyne cylinders, which are 0.5 inches in diameter, with a 0.243 inch tailrod diameter. Using the estimated torques and maximum

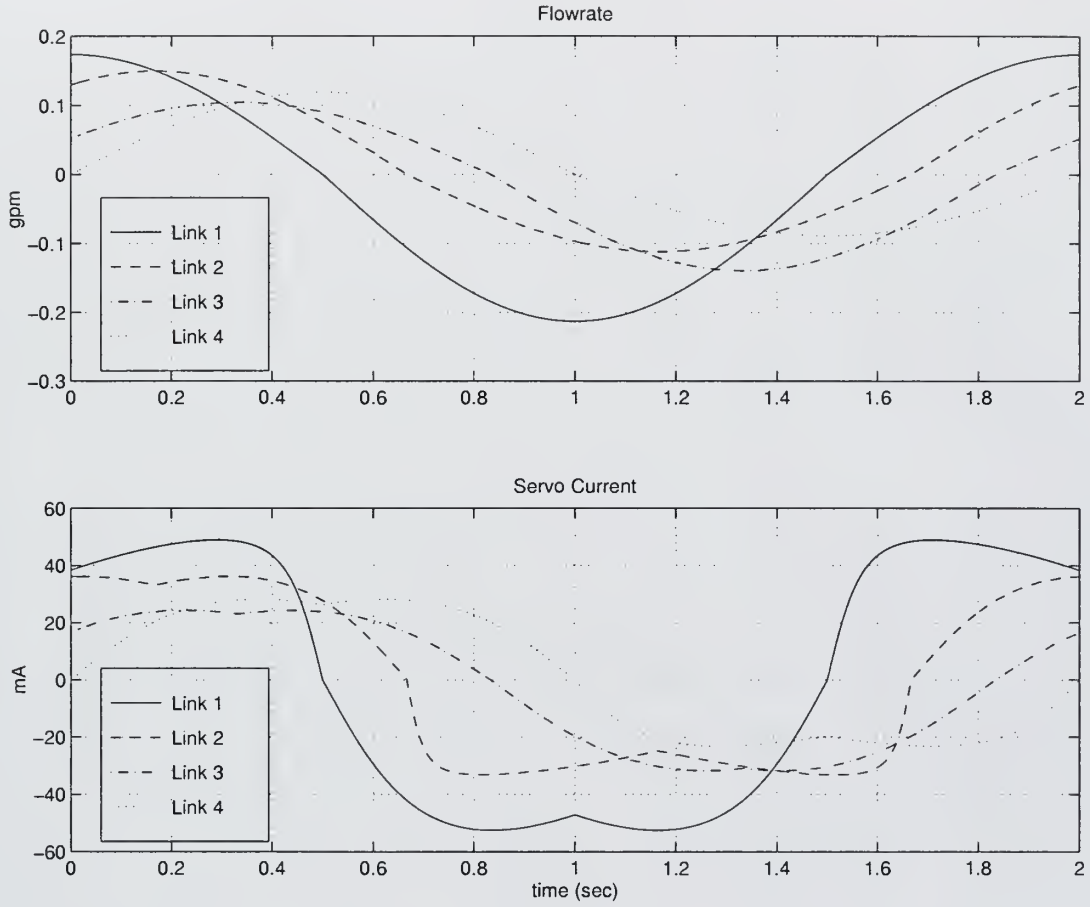

Figure C-3: Fluid Flow And Servovalve Current

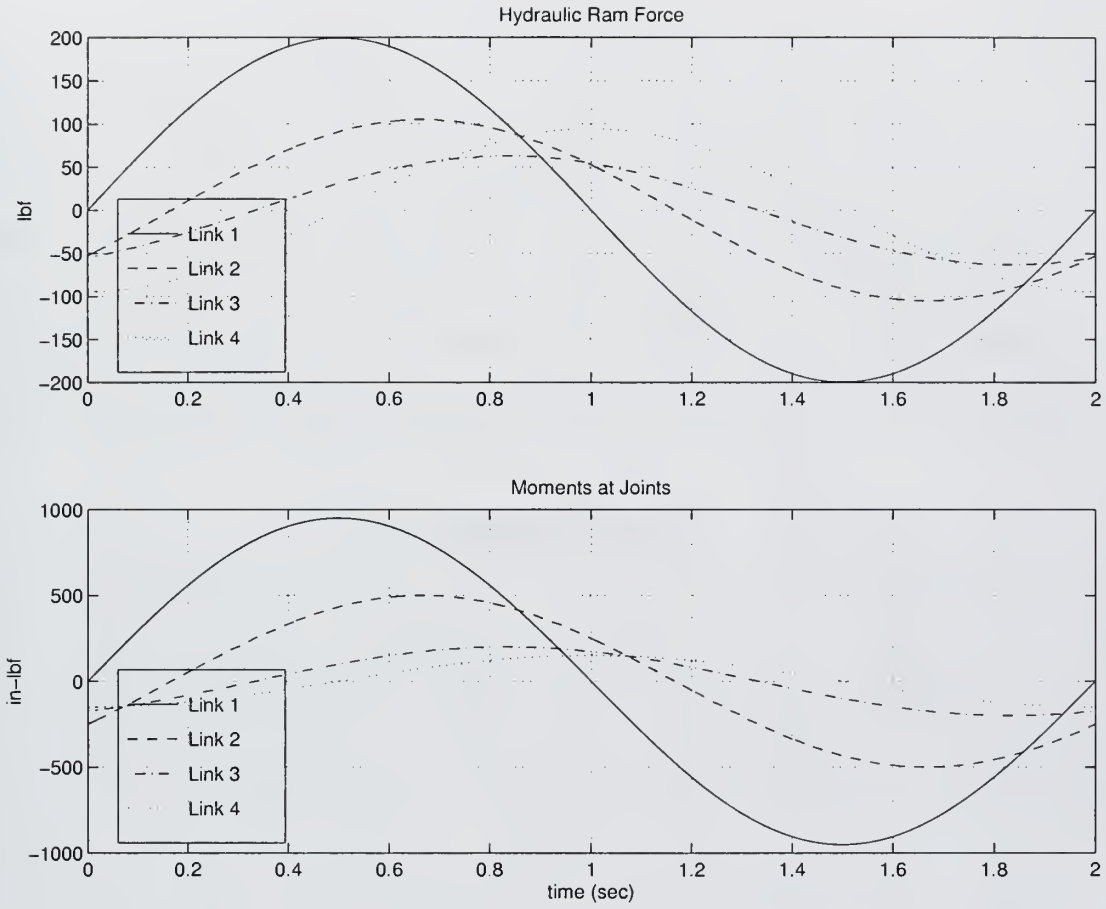

Figure C-4: Piston Force And Joint Moment

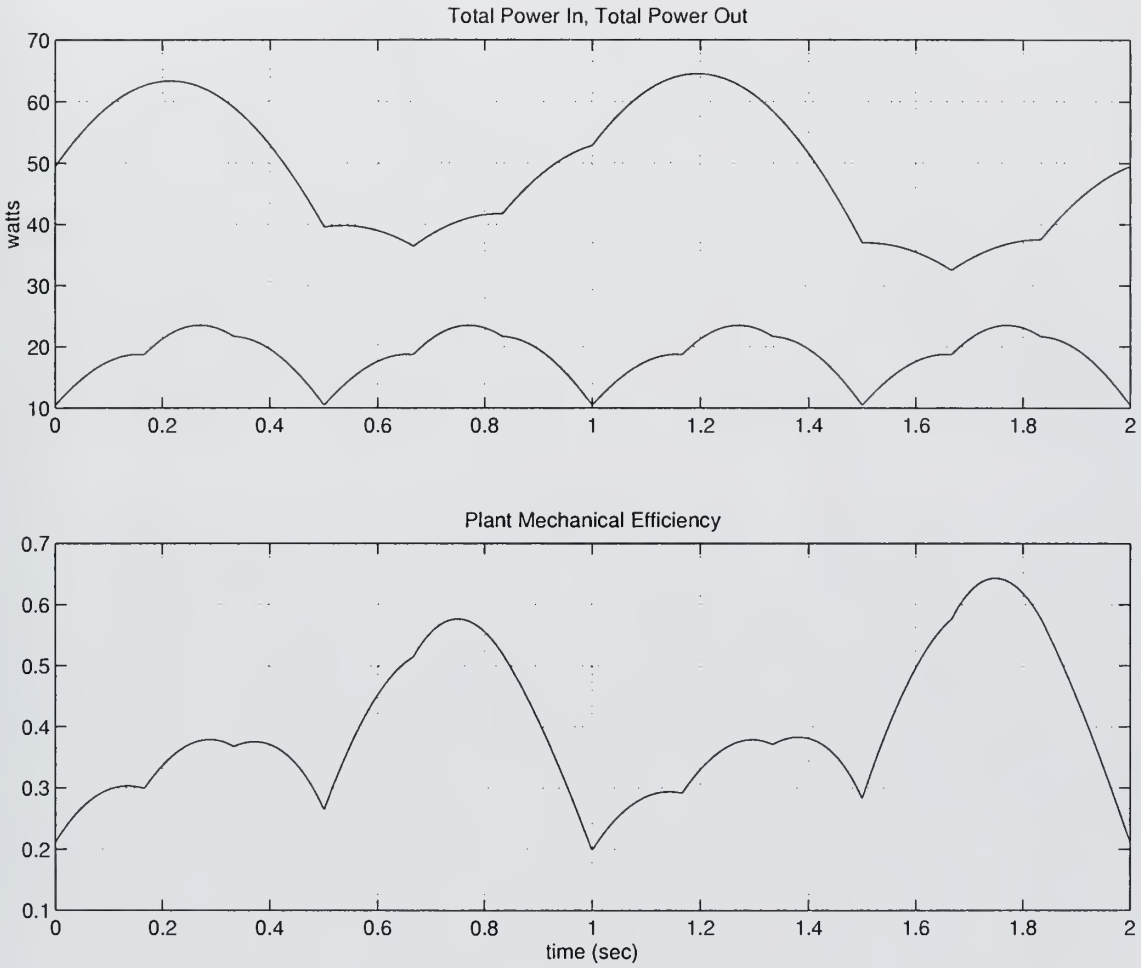

Figure C-5: Total System Power And Efficiency

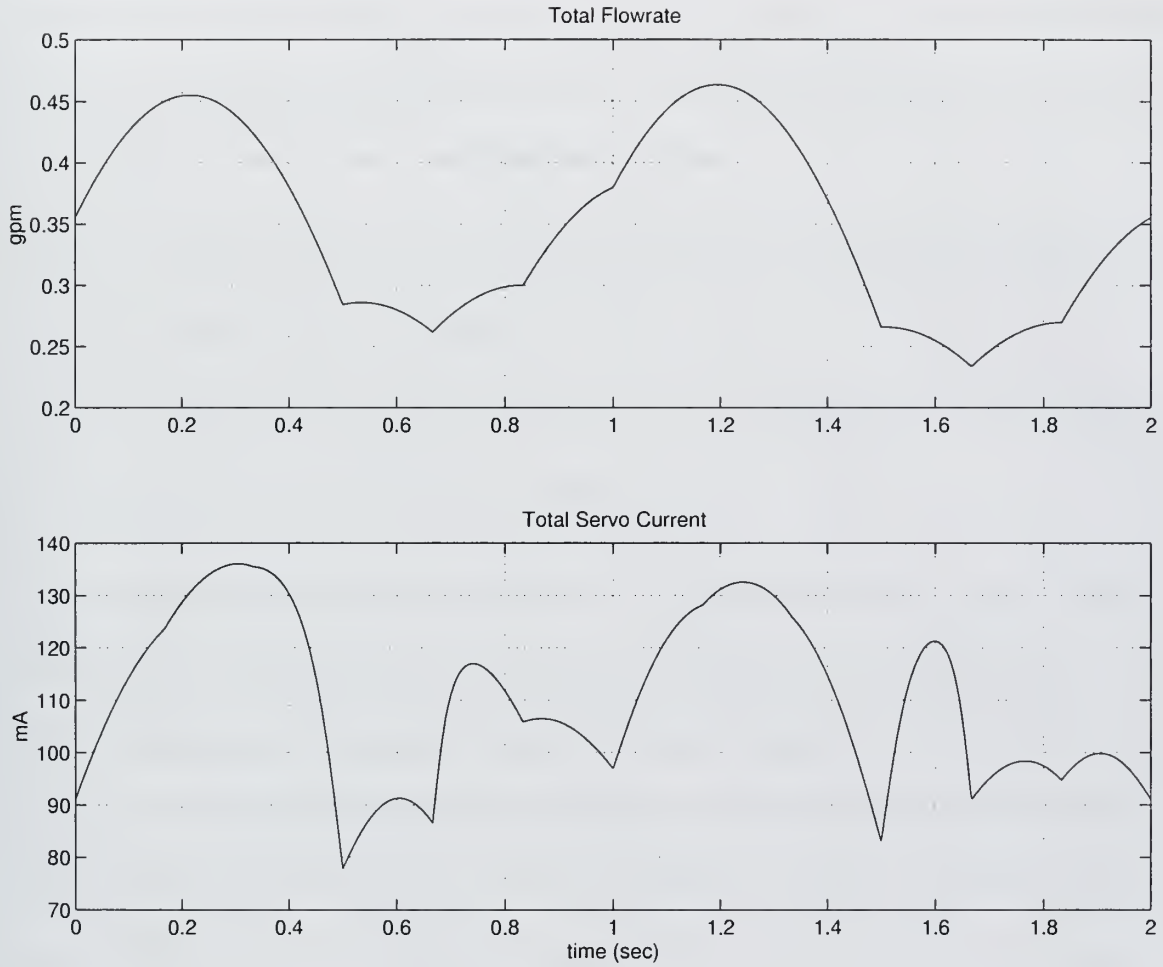

Figure C-6: Total Flowrate and Total Servovalve Current

angular positions. I ran the model and observed that, due to the small cylinders, a high system pressure was required to drive the hip joint, which has a maximum torque of 950 in-lbf. For the remaining lower torque cylinders, there was a lower pressure required and a corresponding large pressure drop realized across their associated servovalves. This translates into low efficiency, since the pressure drop across the servovalve can be considered wasted energy. The solution was to increase the hip joint and second joint cylinder sizes to allow lower system pressure to produce the required force. This produced two beneficial results:

- greater efficiency due to a lower percentage of the pressure drop occurring across the servovalve where it is wasted
- lower system pressure, which is better from a practical standpoint to minimize system hydraulic seal tightness requirements, etc.

Eventually, this led to greater cylinder sizes for all cylinders, up to 1 inch diameter cylinder for the hip joint and 0.75 inch diameter for the remaining cylinders. The limit for increasing cylinder size was the servovalve current ($\approx 50mA$) and flowrate limitations versus dramatically increased flowrate ($\propto D^2$) required to drive the pistons. It should be noted that HR Textron has higher capacity servovalves available which could be used to reduce system pressure even more, with a minor increase in efficiency at the expense of increased electrical current required.

C.5 Conclusions

The system pressure, efficiency, cylinder sizes, and servovalve sizes rely heavily on the tail beat frequency of the system (system flowrate) and the maximum torque (system

pressure). The control system can be designed to optimize efficiency by adjusting system pressure for different operating conditions or for simplicity, the system can be optimized for a single predominant operating point. The final optimized system is shown in Table C.5

Number of Joints	4 (including tail)
Cylinder Diameters	hip joint: 1" remaining joints: 0.75"
Cylinder Arrangement	alternating orientation
Avg System Efficiency	39%
Input Power	64.5 Watts peak 48.7 Watts average
Output Power	23.5 Watts peak 18.7 Watts average
Maximum Torques	950 in-lbf (hip) 500 in-lbf (#2) 200 in-lbf (#3) 150 in-lbf (tail)
Moment Arms	4.76" (hip) 4.76" (#2) 3.18" (#3) 1.59" (tail)
System Flowrate	.46 gpm max .35 gpm average
System Pressure	320 psi
Tail Beat Frequency	0.5 Hz
Control Current	136 mA peak 110 mA average

Table C.2: Hydraulic Plant Final Summary

Bibliography

[1] Haruhiko Asada and Jean-Jacques E. Slotine. *Robot Analysis and Control.* John Wiley & Sons, Inc., New York, 1986.

[2] David S. Barrett. *Propulsive Efficiency of a Flexible Hull Underwater Vehicle.* PhD thesis, Massachusetts Institute of Technology, 1996.

[3] J. E. Bobrow et al. Adaptive, high bandwidth control of a hydraulic actuator. *Transactions of the ASME*, 118:714–720, 1996.

[4] C.M. Breder. The locomotion of fishes. *Zoologica (N.Y.)*, 4:159–256, 1926.

[5] Heidi Dewar and Jeffrey B. Graham. Studies of tropical tuna swimming performance in a large water tunnel. *J. exp. Biol.*, 192:45–59, 1994.

[6] Powell Franklin and Workman. *Digital Control of Dynamic Systems.* Addison-Wesley, 1991.

[7] Sir James Gray. Studies in animal locomotion: The propulsive powers of the dolphin. *Journal of Experimental Biology*, XIII(2):192–199, 1936.

[8] D. M. Lane et al. Motion planning and contact control for a tele-assisted hydraulic underwater robot. Kluwer Academic Publishers, 1996.

[9] M. J. Lighthill. Aquatic animal propulsion of high hydrodynamic efficiency. *Journal of Fluid Mechanics*, 44:265–301, 1970.

[10] J.N. Newman. *Marine Hydrodynamics.* MIT Press, 1977.

[11] Jean-Jacques E. Slotine and Weiping Li. *Applied Nonlinear Control.* Prentice Hall, 1991.

[12] Michael S. Triantafyllou and George S. Triantafyllou. An efficient swimming machine. *Scientific American*, 272(3):64–70, March 1995.

[13] M.S. Triantafyllou. Maneuvering and control of surface and undersea vehicles. Class Notes, MIT Course 13.49.

[14] Steven Vogel. *Life in Moving Fluids.* Princeton University Press, 2 edition, 1994.